The Synthesis and Characterization of Novel High-Silica Zeolites

Thesis by

Raul F. Lobo

In Partial Fulfillment of the Requirements

for the Degree of

Doctor of Philosophy

California Institute of Technology

Pasadena, California

1995

(Submitted November 28, 1994)

ii

To my parents

Acknowledgments

I wish to express my most sincere and deep appreciation to my advisor Prof. Mark E. Davis. His constant support, thoughtfulness, guidance and the freedom of work that he gave me are an indispensable ingredient of the results presented here.

The collaboration with Dr. S.I. Zones was tremendously productive, rewarding and enjoyable. I also thank the other members of my committee, Professors Andrew G. Myers and George Gavalas for their time, interest and encouragement during the course of this work.

All the members of the Davis's group have collaborated in one way or another to the ideas and results presented here, and have made the work in the lab always lively and interesting. I am particularly thankful to H.X. Li and C.Y. Chen who taught me most of what I know about zeolite synthesis and characterization.

I need to thank many people outside the Institute who have help me to go around many difficult corners found along the path of a long process such as a Ph.D. Special thanks are for Dr. Y. Nakagawa, Dr. M. Pan, Dr. J. B. Higgins and Dr. I. Chan. I am grateful to Dr. Antonio Redondo for allowing me to carry out the computer simulations at Los Alamos. Inside the Institute, I have profited constantly from the help of its capable staff who have made a lot easier my research work. Specially I want to thank Tom Dunn, Larry Henling, Adria McMilan, April Olson, Ruth Pineda, Rich Gerhard for their help.

Finally I want to thank my family; without their encouragement and support this work would not have been carried out.

Abstract

The synthesis and characterization of high-silica molecular sieves is reviewed using molecular recognition phenomena and structure-direction as the unifying themes. A comparative analysis between the synthesis conditions employed and the zeolite structures formed is carried out starting with the synthesis of clathrasils or 0-dimensional zeolites, and extending to one-dimensional, multi-dimensional zeosils. The review finishes with the analysis of the combined effects of heteroatoms (Al, B and Zn) and organic structure-directing agents in zeolite product selectivity and thermodynamic stability.

Structure-direction phenomena is further investigated using the synthesis and characterization of the pure-silica zeolite SSZ-24, prepared using the chiral molecule N(16)methylsparteinium hydroxide as the structure-directing agent. The material is characterized using X-ray powder diffraction (XRD), scanning electron microscopy (SEM), solid-state NMR spectroscopy, fourier transform IR spectroscopy (FTIR) and physical adsorption experiments. The B-substituted SSZ-24 prepared here is the first example where the isomorphous substitution of B for Si in the SSZ-24 framework is accomplished during synthesis using sodium borate as the source of B. The B can be easily substituted by Al. The Al-substituted SSZ-24 is an active catalyst for the cracking of alkanes and may be potentially useful in refinery and chemical processes.

The structure solutions and a detailed structural characterizations of the disordered zeolites SSZ-26 and SSZ-33 is presented. These two materials are the first synthetic zeolites with intersecting open 10- and 12-ring pore systems. SSZ-26 and SSZ-33 are expected to show a combination of reaction activity, selectivity and stability unique among known zeolites. SSZ-26 and SSZ-33 may be very useful for catalytic applications in the petrochemical and refining industries. The feasibility of synthesizing a zeolite whose pore

structure has been designed a priori is demonstrated with the zeolite SSZ-26 and its structure-directing agent.

The synthesis of a new borosilicate, CIT-1, is described. The proposed structure of CIT-1 is confirmed by a Rietveld refinement of the synchrotron XRD pattern. CIT-1 is demonstrated to be an ordered polymorph of the SSZ-33 zeolites. The catalytic properties of CIT-1 are compared to the catalytic properties of known high-silica zeolites (ZSM-5 and zeolite beta) and CIT-1 is shown to be a very active catalyst for the cracking of n-butane. The synthesis of CIT-1 supports the idea that the chiral polymorph A of zeolite beta can be synthesized using the appropriate structure-directing agent.

A combination of molecular modeling and ^{1}H MAS NMR spectroscopy are used to characterize the interactions of structure-directing agents with the zeolite framework. The results indicate that to simulate correctly the energetic interaction and motional properties of structure-directing agents in zeolites, short-range and long-range forces, water molecules, silanol groups and defects need to be considered simultaneously.

Objectives

The objective of this work is to understand the energetic and geometric relationships between organic structure-directing agents and high-silica molecular sieves. Structure-direction is viewed here as a process of molecular recognition in which the geometrical characteristics of the organic structure-directing agent are imprinted into the shape and size of the zeolite pores.

Chapter One is a general overview of the synthesis of high-silica zeolites. Here the effect of the different synthesis variables on the structure of the zeolite formed are investigated. Emphasis is given to how the size and shape of the organic structure-directing agent change the size and shape of the pores and cages of zeolites and clathrasils. The important structural effects that small mounts of trivalent (B, Al, Ga) and divalent cations (Zn) on the structure of the zeolite formed are analyzed.

Chapter One indicates that one of the aspects of molecular recognition that have not been accomplished is the formation of a chiral zeolite using a chiral structure-directing agent. The results of the synthesis using a chiral molecule as structure-directing agent are presented in Chapter Two. The zeolite formed (SSZ-24) is not chiral, and this result is explained as a consequence of the rapid rotation of the organic molecule inside the zeolite pores (Chapter Six).

Chapters Three and Four present the structure solution and structural characterization of the zeolites SSZ-26 and the related SSZ-33. The organic structure-directing agent used for the synthesis of SSZ-26 was carefully designed such that it would direct the formation of a zeolite with an intersecting pore system. To investigate whether there is a complementarity between the geometry of the polycyclic structure-directing agent and the zeolite pores it was necessary to solve the structures and fully characterize these

novel zeolites. The complementarity between the zeolite pores and the geometry of he structure directing agent is investigated using energy minimization calculations.

SSZ-26 and SSZ-33 are disordered zeolites which are formed by the stacking of layers in two different sequences. In Chapter Five, the concepts of structure-direction are extended to show how an organic structure-directing agent can be used to control the stacking sequence of zeolite layers. This chapter gives a complete characterization of a novel zeolite, CIT-1, which is an ordered polymorph of SSZ-26 and SSZ-33. The reasons that allow the organic structure-directing agent of CIT-1 to direct the formation of only one of the stacking sequences are investigated by comparison to the organic structure-directing agent that forms the disordered material SSZ-33.

Chapter Six characterizes the interaction between organic structure-directing agents and zeolite frameworks using energy minimization calculations and ^{1}H MAS NMR spectroscopy. Despite the large amount of information available on the structural characterization of the calcined form of high-silica zeolites, very little work has been carried out on the as-synthesized materials. In this chapter, the differences between the as-synthesized and calcined materials are investigated in particular to high-light the effect that these differences may have on the phenomenon of structure-direction.

Table of Contents

List of Figures

Chapter One

Chapter Six

List of Tables

Chapter Three

Chapter Four

Chapter Five

Chapter Six

Chapter One

Structure-Direction in Zeolite Synthesis

Structure-Direction in Zeolite Synthesis

Raul F. Lobo, Stacey I. Zones[†] and Mark E. Davis

Chemical Engineering, California Institute of Technology, Pasadena, CA 91125

[†]*Chevron Research and Technology Company, Richmond, CA 94802-0627*

Abstract

The concepts of structure-direction in the synthesis of clathrasils and high-silica molecular sieves are reviewed. The effects of size, geometry and chemical nature of the organic structure-directing agent on the crystalline structures that are formed are discussed beginning with clathrasils (0-dimensional pore systems) and ending with 12-ring zeolites with tridimensional pore systems. Emphasis is focused on the energetic interactions between the organic guest and the inorganic framework. The energetic stability of porous frameworks is compared to the stability of dense pure-silica phases and the effects of trivalent (Al, B) and divalent (Zn) tetrahedral heteroatoms on the structure of zeolites formed is reviewed. The application of structure-directing concepts are described using the syntheses of ZSM-18 and SSZ-26 as examples, and the control over long-range order in zeolites by structure-directing effects is illustrated by the purposeful variation of the stacking probability of SSZ-33–CIT-1 and FAU–EMT intergrowths.

1.1 Introduction

Zeolites and molecular sieves are important industrial materials that have a broad range of applications. Many zeolites with different structures and compositions are commercially available and used in refining and chemical processing as catalysts, adsorption materials and drying agents as well as in ion exchange operations[1,2]. Zeolites and molecular sieves show a strikingly close relationship between their microscopic structure and macroscopic properties. This relationship is particularly clear in their ability to sieve organic and inorganic molecules based on size. Also, the rigorous steric control that zeolite frameworks offer on the chemical reactions occurring inside their pores is directly related to their microscopic structure.

The relationships between the microscopic structure and macroscopic properties have been large driving forces for the synthesis of new materials with novel pore architectures and crystal compositions. It is expected that molecular sieves with new pore structures will show catalytic properties not observed before. Although over 89 different structures are known[3], this is just a small fraction of all the hypothetical structures that have been proposed[4,5].

In this review we will focus on the relationships between the geometrical and chemical properties of the organic molecules used to direct the crystallization of a particular zeolite structure, and the geometry and characteristics of the cages and pores of the zeolites in which the organic molecules have been occluded. Additionally, we will look at the effects of alkali-metal ions and trivalent and divalent tetrahedral atoms on the zeolites structures formed and how these effects are coupled to the actions of the organic structure-directing agent.

We will emphasize high-silica materials because these molecular sieves are the ones that offer the greatest possibility of control through the use of organic molecules in the synthesis gel. Many new microporous aluminophosphates ($AlPO_4$) and metal-substituted alumino-phosphates (MAPO) have been and are continuing to be reported. However, the connection between synthesis conditions and the structures of these molecular sieves is very poorly understood. In these materials, the crystal structure of the final product often depends on the presence of a particular organic molecule in the synthesis gel. However, the relationship between the organic molecules and the pores or cages is very loose, and sometimes the organic molecule is not even present inside the pores of the molecular sieves as is the case for VPI-5 [6,7]. Also, aluminosilicates and borosilicates with low ratios of SiO_2/M_2O_3 will not be covered because the structure of these hydrophilic and highly anionic framework materials is mostly dependent on interactions with the inorganic cations of the synthesis gel.

In addition to an enhanced interaction with organic structure-directing agents, materials formed mostly from silicate tetrahedra (T) have the advantage over $AlPO_4$'s and aluminosilicates in that the T—O—T angle with only Si as the T atoms is much more flexible than other T—O—T angles [8,9]. This is an indication that, in principle, more frameworks should be attainable. Also, high-silica materials can have among their structural building units rings with odd and even number of tetrahedral atoms, which are not found in $AlPO_4$'s because of the rigorous aluminum-phosphorous alternation.

We begin our discussions with an introduction to the concepts of structure-direction by illustrating the synthesis of clathrasils. Next we describe recent findings on the relative energetic stability of different pure-silica framework structures and discuss different factors that may affect the crystallization kinetics of zeolites. In the following section, we return to explore more complex zeolite synthesis in which the structure-directing effects not only depend upon the organic structure-directing agent, but also are influenced by the presence

of different alkali-metal cations and trivalent and divalent T atoms —such as aluminum and zinc— in the synthesis gel.

The three-letter code of the International Zeolite Association will be used throughout the review [3] and some familiarity with zeolites and zeolite synthesis will be assumed on the part of the reader. Previous reviews and articles related to the material covered here can be found in the references [10-14].

1.2   Clathrasils

Clathrasils are a group of tectosilicates formed of polyhedra (cages) that enclose relatively small organic or inorganic molecules. The clathrasils can be considered as zeolites with pores of 0-dimension. The different cages found in the known clathrasils are illustrated in Table 1.1 and many of the structure-directing agents used for the synthesis of these tectosilicates can be found in ref. 13.

Gies and Marler [15] have carried out the synthesis of clathrasils using the simple reaction system SiO_2/structure-directing agent/H_2O, by systematically changing the nature of the structure-directing agent. The advantage of this simple gel composition is that changes in the clathrate structure can be unambiguously attributed to the effect of the structure-directing agent. Gies and Marler found that 61 molecules varying from noble gases such as Kr and Xe to large amines such as 1-aminoadamantane can be used to control the structure of the clathrasil formed.

Guest molecules of similar size and shape were found to direct the crystallization of the same product, regardless of differences in chemical properties. The following series of molecules formed the MTN structure in all cases:

I **II** **III** **IV** **V**
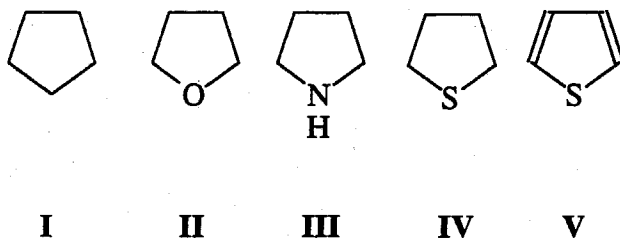
Although the structure is independent of the chemical properties, they found that the kinetics of crystallization are very dependent on the basicity of the organic molecule [16]. The most basic molecule (**III**) gave the highest rate of crystallization and the least basic (**I**) gave the slowest.

Several guest molecules formed different frameworks under different synthesis conditions, and a strong dependence of the structure type on synthesis temperature was observed. For example, 1-aminoadamantane was found to form DDR, SGT, DOH and deca-docedasil 3H as the temperature was increased from 140 to 200 °C. In general, the smaller cage was found at the lower synthesis temperatures. Although large molecules form crystals with larger cages, some relatively small molecules —like 2-methylpyrrolidine— were found in the large $[5^{12}6^8]$ cage of DOH.

The relation between the geometry of the organic molecule and the geometry of the cage is limited for clathrasils. For example, the following molecules can be used to synthesize DOH:

VI **VII** **VIII** **IX** **X**
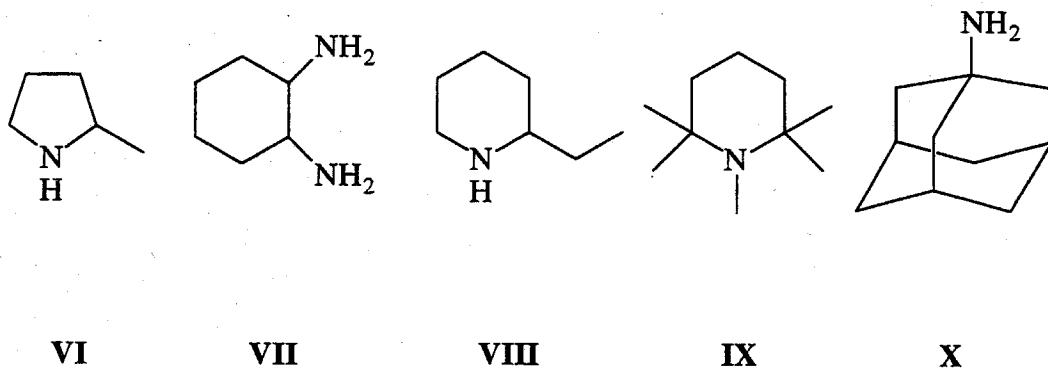
These results when viewed in combination with the effect of the temperature on the size of the cage suggest that the thermal motion of the molecule in the crystallization gel may inhibit the imprinting of the detailed geometry of the molecule, and that the silicate gel 'senses' only the geometry of the volume of revolution of the structure-directing molecule.

We carried out a set of experiments similar to the ones reported by Gies and Marler in which the only components of the gel were the structure-directing agent, the silica source (Cab-O-Sil, M5) and water. The results of these experiments (Table 2) are roughly in agreement with those reported by Gies and Marler. Large molecules form clathrasils with large cages and smaller molecules form crystals with smaller cages.

Clathrasils can be also prepared using non-hydrothermal synthesis conditions, e.g., using an organic solvent. The synthesis of SOD was first reported in this manner by Bibby and Dale [17] and ethylene glycol was used as solvent and as the structure-directing agent. Originally, this result was intriguing because the sodalite structure is the only pure-silica clathrasil —besides AST— that contains only even-membered rings in the structure. The remainder of the clathrasils contain a large fraction of 5-rings as it is generally observed for high-silica zeolites. The molecules of ethylene glycol are found inside the sodalite cages and are necessary for the synthesis of the material. However, recently, Post and coworkers [18] and Chen [19] reported the synthesis of pure-silica SOD under hydrothermal conditions using trioxane and ethylenediamine as structure-directing agents, respectively.

Although, there have been proposals suggesting that there is a relationship between the symmetry of the organic molecule and the symmetry of the cage[20,21], the results reported by Gies and Marler and those presented in Table 1.2 suggest that the relationships found between the point group of the molecule and the point group of the cage are probably accidental. Molecules with no symmetry —except the identity operation— are capable of

directing the formation of cages with very high symmetry (compare Tables 1.1 and 1.2). As suggested above, it seems that the thermal motion of the organic molecule may average out the geometrical differences between the molecules. Definitive prove of the rapid motion of guest molecules inside the cages of clathrasils was recently provided by Gies [14] using static ^{13}C solid-state NMR. Gies showed that organic molecules inside the cages of MTN, DOH and NON are rotating on a time scale that is smaller than the time scale of the NMR experiment. The rapid rotation of organic molecules inside the pores and cages of zeolites has also been reported by Hong and coworkers [22,23]. Using solid-state NMR with and without magic-angle spinning (MAS), they show that adamantane and naphthalene undergo rapid motion inside the pores of zeolite Na-Y. Although these molecules were adsorbed inside the zeolite pores after the zeolite synthesis, similar results have been obtained for 15-crown-5 and 18-crown-6 that were used as structure-directing agents in the synthesis of FAU and EMT [24]. These results indicate that rapid motion of the structure-directing agents in the clathrasil cages is likely to be the 'normal' state of the organic molecule at synthesis temperatures.

Clathrasils have several types of cages in each framework structure (Table 1). How are these voids stabilized? Are any of them empty? Crystallographic studies of clathrasils show that the organic structure-directing molecules are found inside the large cages and small molecules are usually located inside the small cages. Dinitrogen and Kr are occluded inside the $[5^{12}]$ and in the $[5^{12}6^2]$ cages of MEP [25], dinitrogen and ammonia are found inside the $[5^{12}]$ and the $[4^35^46^3]$ cages of DOH [26,27] and dinitrogen is also located in the $[5^{12}]$ cages of MTN and DDR [28,29]. Note that the occluded N_2 was not purposely added to the synthesis, but was 'captured' from the small amount of atmospheric air trapped inside the silica-glass tubes used for the synthesis[26]. Cages smaller than the $[5^{12}]$ cage are probably not filled with any molecules because the available void is too small to be occupied by guest species. It is interesting to speculate whether these materials

could be synthesized in the absence of any small guest molecules that could fill these small cages, especially in the light of what is observed for other aluminous zeolite polymorphs. The small cages of many aluminous zeolites such as CAN, GME, OFF, SOD, etc., are invariably occupied by an alkali-metal cation which stabilizes the cage. Therefore, it seems that in general, with zeolites and clathrasils, small cages are only formed when small guest molecules are present as stabilizing agents.

These crystallographic studies have shown that frequently the point group of the organic structure-directing agent is a subgroup of the point group of the cage. However, the axis of symmetry of the molecules and the cages often do not coincide with each other. 1-Aminoadamantane in the $[5^{12}6^8]$ cage of SGT [30,31] is disordered and the axis of the molecule in the dominant conformation does not correspond to the axis of the cage. Also, the axis of 1–aminoadamantane in the $[5^{12}6^8]$ cage of DOH [24], where the cage belongs to the same point group as the organic molecule, is rotated about 20° with respect to the six fold axis of symmetry of the cage. On the other hand, the axis of 1-aminoadamantane was found to coincide with the three-fold axis of symmetry of the $[4^35^{12}6^18^3]$ cage of DDR[29]. These studies have been carried out at room temperature, and as indicated above, it is likely that the organic molecule at synthesis temperatures (140 °C – 200 °C) is rapidly rotating. The results described above must be carefully interpreted when extrapolating to synthesis mechanisms.

Amines and quaternary ammonium ions are the organic molecules used most frequently in the synthesis of clathrasils and molecular sieves. The hydrophobicity of pure–silica frameworks suggests that the positive charge of the organic cation is balanced by a negative charge formed by a defect in the framework that could be illustrated as follows:

R^+

  —Si—OH Si—O⁻

(structure diagram of a silicate ring with Si–OH and Si–O⁻ groups, R⁺ cation)
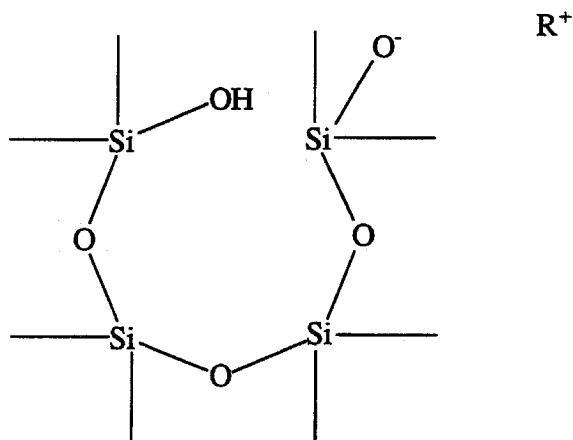
We investigated the possibility that defects such as these could balance the charge of the quaternary ammonium ions by obtaining ^{29}Si MAS NMR on two pure-silica samples of nonasil (NON) synthesized with cyclohexylamine and a quaternary ammonium ion as structure-directing agents (Figure 1.1). The sample synthesized with a quaternary ammonium cation (Fig. 1.1A) shows two peaks that can be assigned to the presence of both Q^3 and Q^4 silicon atoms(Q^i: $Si(OSi)_i O^-_{4-i}$). The presence of Q^3 and Q^4 suggests that the charge of the structure-directing agent is balanced by a defect (deprotonated silanol group) in the zeolite structure. Similar results have been reported for a sample of pure-silica AFI [32] and for high-silica MFI [33] synthesized with quaternary ammonium ions as structure-directing agents. The resolution of the MAS NMR spectrum of the sample synthesized with the amine (Fig. 1.1B) is enhanced to the point of recognition of most of the different tetrahedral environments present in NON [3]. The increase in resolution of ^{29}Si MAS NMR spectrum has been linked to the absence of defects in the framework [34,35] and suggests that the amine is not protonated inside the NON cages. These results are in agreement with the idea that the charge of quaternary ammonium cations in high-silica zeolites is often balanced by deprotonated silanol groups in the structure. The infrared spectra of these two samples only show weak evidence to suggest the presence of the O—

H stretching band (expected at approximately 3300 cm^{-1}), indicating instead that the structure of the defects is closer to the following illustration:

$$R^+ \qquad\qquad\qquad\qquad\qquad\qquad R^+$$

$$
\begin{array}{ccc}
O^- & & O^- \\
\diagdown & | \qquad\qquad | & \diagup \\
{-}Si & & Si{-} \\
& \diagdown \qquad\qquad \diagup & \\
& O \qquad\qquad O & \\
& \diagdown \qquad\qquad \diagup & \\
{-}Si & {-}O{-} & Si{-} \\
| & & |
\end{array}
$$
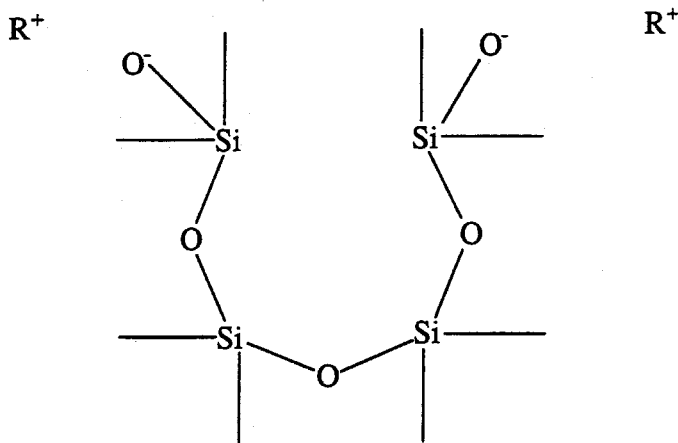
In this second alternative, two positive charges are balanced for each defect. If defects are energetically destabilizing, then it is expected that the structure will crystallize such that the least number of defects are formed to balance the positive charge of the organic guest molecule. This is accomplished by a mechanism best represented by the second illustration. However, this model does not necessarily exclude the formation of defects with protonated silanol groups. From the perspective of structure-direction, this is important because it suggests that molecules with large charge/volume ratio —tetramethylammonium, for example— are not good alternatives for the synthesis of clathrasils. It also indicates that materials with a large void fraction require organic guests with a very low charge/volume ratio for the defects to have a small impact on the stability of the organic-inorganic composite.

The above discussions illustrate several important issues on the synthesis of clathrasils and pure–silica molecular sieves. The conditions at which an organic guest will best form a clathrasil have been summarized by Gerke, Gies and Liebau [cited in ref. 36] and are as follows:

1. The molecule should have sufficient room within a particular cage or pore.

2. The molecule must be stable under the synthesis conditions.

3. The molecule should fit the inner surface of the cage with as many van der Waals contacts as possible, but with the least deformation.

4. The guest molecule should have only a weak tendency to form complexes with the solvent.

5. More rigid molecules will tend to form clathrasils easier than flexible molecules.

6. The tendency to form a clathrasil will increase with the basicity or polarizability of the guest molecule.

From the molecular point of view, the first condition indicates that if the organic molecule is bigger than the polyhedral cage, steric forces inhibit the formation of the clathrasil. The second point suggests that molecules that can react under basic, hydrothermal synthesis conditions will of course change during the synthesis and their decomposition products will affect the structure of the product. The third and fourth conditions are energetic considerations that indicate that during the formation of the clathrasil, the optimum of the van der Waals interactions between the organic molecule and the cage or zeolite pore depends on the organic guest, and that the energy employed in changing the conformation of the organic guest to fit the geometry of the pore or the cage destabilize the organic-inorganic composite. Finally, the basicity of the molecule is related to a) the effect that a higher pH has on the kinetics of silicate hydrolysis, and b) the stabilizing effect that a higher polarizability of a molecule within the electric field created by the partial ionic character of the Si—O bond has over the total energy of formation of the composite.

What is observed if we continue to increase the size of the structure-directing agent? This question was recently addressed by Nakagawa and Zones[37]. The following series of organic molecules were synthesized and used as structure-directing agents:
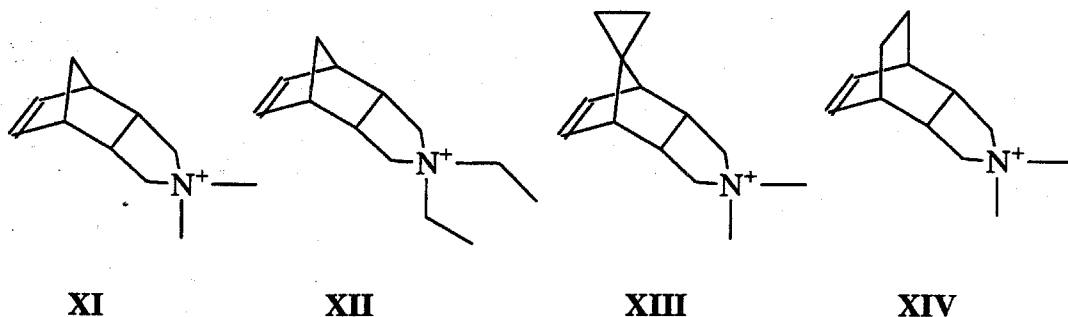
| XI | XII | XIII | XIV |

In the absence of any structure-directing agent, the product of the synthesis mixture was quartz. Using molecules **XI**, **XII**, **XIII** and **XIV**, the clathrasil nonasil and the one dimensional large–pore zeolites MTW, SSZ-31 and SSZ-31 were formed, respectively. Thus, Nakagawa and Zones found that when the size of the structure-directing agent is increased to a certain dimension, the product formed changes from a clathrasil to a microporous large-pore molecular sieve.

If instead of the size, the geometry is changed from cyclic molecules to linear molecules, there is also a transition from clathrasils to microporous molecular sieves but now to microporous silicates with 10-ring pores [15]. For example, piperidine forms the NON clathrate, but 1–aminobutane forms TON and ZSM-48 at 160 ˚C and 180 ˚C, respectively. The size of the linear organic molecule has relatively little importance compared to the effect of temperature on the structure of the zeolite formed and small molecules such as ethylenediamine (Table 2) and 1,5,9,13-tetraazatridecane [15] form ZSM-48 under approximately the same conditions.

There is another transition from unidimensional 10-ring materials to tridimensional 10-ring materials as the organic molecule geometry is changed from linear to branched.

Diethylamine and dipropylamine form ZSM-48 (a linear 10-ring) but triethylamine and tripropylamine form the MFI structure. Note that in these organic-inorganic composites the good geometrical fit reflects an optimization of the van der Waals contacts between guest and host [15].

1.3   Thermochemical Stability Of High-Silica Zeolites

Zeolites are thermodynamic metastable phases accessible by kinetically favored pathways under hydrothermal synthesis conditions [39]. Recently, Petrovic and coworkers [40] shed some new light on the thermodynamics of high-silica zeolites. The enthalpy of formation of a series of high-silica zeolites (MFI, MEL, MTW, AFI, FAU and EMT) was determined using a high-temperature solution calorimetry method. The results were compared to the enthalpy of formation of dense polymorphs of silica. All the microporous frameworks are only 7-14 kJ mol^{-1} less stable than quartz. Additionally, no clear correlation between the enthalpy of formation of the zeolites and the framework density —or degree of *openness*— secondary building units such as large or small rings in the structure, or the mean Si—O—Si angle, was found (however, see [41] for a different interpretation of the data).

In pure–silica zeolite structures, every silicon atom is bonded to four oxygen atoms in a relatively undistorted tetrahedral coordination and the oxygen atoms are connected to two silicon atoms with an average Si–O–Si angle close to 145˚. Ab initio molecular orbital calculations have shown that there is a small barrier to variations in the Si–O–Si angle between 140 and 180˚, but that there is a sharp increase in the energy for angles less than about 135˚. Therefore, based on the above evidence and to a first degree of approximation,

it seems now understandable that the energy of all these pure-silica frameworks should be very similar.

Petrovic et al. showed that there is a correlation between the fraction of Si–O–Si angles $\leq 140°$ and the enthalpy of formation of these pure-silica molecular sieves. This correlation is consistent with the shape of the potential energy curve of the Si–O–Si angle that suggests that small angles are much more destabilizing than large ones. The authors, however, note that these angles have been obtained mostly from analyses of X-ray powder diffraction data. These XRD data contain very short Si–O bond lengths (1.49 and 1.53 Å), very long Si–O bond lengths (1.67 to 1.70 Å) and a large range of O–Si–O angles (92° to 133°). By comparison, the bond lengths and O–Si–O angles of the single crystal structure determination of MFI are in very good agreement with the single crystal data from quartz. Therefore, these unexpected bond lengths and angles may be the result of the difficulty in obtaining a stable and acceptable solution with the Rietveld refinement methodology. Also, based on their work with the relatively simple structure of sodalite, Hu and Depmeir [42] have suggested that the symmetries of zeolites may have been overstated and that some zeolite structure solutions may need to be revised. In summary, to draw further conclusions it may be necessary to wait until new single crystal X-ray data or other technique improvements confirm the anomalous bond lengths and angles.

The numerical similarity of the enthalpies of formation of the different pure-silica zeolites imply that the role of the organic molecule may be to select a particular structure among many possible of similar energy —i.e., a more kinetic rather than thermodynamic role. However, the incorporation of the structure-directing agent inside the zeolite pores reduces the total free energy of formation of the composite in the same way that a solution of ethanol and water has lower total free energy of formation than pure ethanol and water. Interactions that stabilize the organic-inorganic composite are the optimization of van der Waals contacts between the organic molecule and the surface of the pores or cages.

Is it energetically favorable for the structure-directing agent to be occluded inside the zeolite pores? Although most structure-directing agents are soluble in water, studies on the interactions between tetramethylammonium (TMA), tetraethylammonium (TEA) and tetrapropylammonium (TPA) [43,44] and water indicate that the interactions between TMA and water are mainly hydrophilic in character, but TPA, in spite of its positive charge, shows mostly a hydrophobic character due to its longer hydrocarbon chains. TPA orders water around itself with a concomitant entropic cost that balances the energetic gains obtained from the solvation of the positive charge. In an attempt to investigate these interactions with a greater variety of structure-directing agents, Zones has studied the transfer of different charged organic-structure directing agents from an aqueous solution to a chloroform phase as a function of the C/N^+ ratio. He found that the percentage of transfer is low (less than 10%) for molecules with a $C/N^+<11$ and that it is very large (more than 70%) for $C/N^+>15$ (see Figure 1.2). Interestingly, it is observed that organic molecules with C/N^+ between 11 and 15 work well as structure-directing agents yielding a great variety of new high-silica molecular sieves. This trend suggests that molecules that are moderately hydrophobic are the best candidates for structure-direction. This result is also in agreement with the ideas of Gerke, Gies and Liebau [36] who indicated that the guest molecule should only have weak tendency to form complexes with the solvent. The percentage of transfer, however, does not correlate with the kinetics of zeolite crystallization, suggesting that geometrical properties also play an important role in the formation of crystal nuclei.

The size of the molecule (carbon+nitrogen atoms) correlates strongly with the selectivity of different structure-directing agents. As indicated previously, often one organic guest molecule can direct the crystallization of more than one zeolite structure. Zones has observed that as the number of carbon plus nitrogen atoms in the structure-directing molecule is increased, this tendency is reduced until finally for large molecules,

only one structure is observed. Figure 1.3 illustrates this trend for a variety of molecules. The conclusion obtained from this figure is that in order to form new structures, larger molecules should be explored more carefully as structure-directing agents. This trend has to be balanced against the effect of the C/N^+ ratio as indicated above. If only one quaternary nitrogen is included in the molecule, eventually the hydrophobicity of the molecule will overcome the solvation possibilities of water and the organic molecules may aggregate to form a separate phase.

1.4   Kinetics Of Zeolite Crystallization

The kinetic nature of the crystallization of silicate frameworks is clearly observed if a structure, less stable than quartz, is formed without the occlusion of organic molecules. This is a common experimental observation when the product of a zeolite synthesis is tridymite or cristobalite, as often occurs during the preparation of high-silica zeolites. Thermodynamic data show that these dense phase are less stable than quartz at synthesis temperature and pressure [45]. However, tridymite and cristobalite are often the product of a zeolite synthesis, indicating that the kinetics of crystal nucleation and growth are the controlling factors determining the structure of the crystallization product.

In the following section we discuss issues involving the effects of alkali-metal cations on the rate of nucleation and crystal growth of high-silica zeolites. We also briefly illustrate how one structure-directing agent can direct the crystallization of different zeolites through seeding of the synthesis gel.

1.4.1 Effect Of Alkali-Metal Cations

The synthesis of most zeolites is carried out under basic conditions using sodium or potassium cations as one of the main components of the reaction mixture. Other mineralizing agents, fluoride in particular, are also often used (this method is not covered in this review) [see 12]. The effect of alkali-metal ions on the synthesis of pure-silica zeolites was not systematically studied until it was found that the incorporation of titanium into zeolite frameworks was negatively affected by the presence of alkali-metal cations. Titanium-containing zeolites (TS-1 and TS-2) are very active catalysts for the selective oxidation of alkanes and alkenes using hydrogen peroxide as the oxidant [46]. The search for titanium-containing zeolites with new structures prompted the study of zeolite syntheses in the absence of alkali-metal cations.

It was found that most zeolite syntheses are sensitive to the presence of alkali-metal cations in the synthesis gel. Except for the MFI and the MEL structures using TPA or tetrabutylammonium (TBA) as structure-directing agents, other zeolites are very difficult to synthesize in the absence of alkali-metal cations. For example, Goepper et al. [47] studied the synthesis of pure-silica MTW in the presence and absence of alkali-metal cations at constant hydroxide concentration. They found that the addition of sodium and potassium increased the crystallization rate from 84 days to 7 days and suggested that alkali-metal ions participate in both the nucleation and crystal growth processes.

The study of the dissolution of quartz into aqueous solutions of alkali-metal cations aids the understanding of the role of sodium and potassium in the synthesis of zeolites. Brady and Walters [48] and Dove and Crerar [49] investigated the rate of dissolution of quartz in aqueous solutions of NaCl, KCl, LiCl and $MgCl_2$. They found that small concentrations of electrolytes increase the rate of dissolution by as much as 15 times, compared to the rates measured for deionized water. The effect is greatest for NaCl and KCl and increases for concentrations up to 0.05 M. The faster dissolution rates observed

for sodium and potassium relative to magnesium and lithium are probably related to their potential for adsorption onto the quartz surface. Mg^{+2} and Li^+ have a low potential for adsorption because they are strongly coordinated to water molecules in the solution as the result of their large charge to size ratio. Extrapolation of these results to zeolite synthesis suggests that sodium and potassium are involved in the polymerization and depolymerization of the silicate species in the gel and that this is at least one of the processes through which they increase the nucleation and crystal growth rates of high-silica zeolites.

The effect of high concentrations of sodium on the crystallization of zeolites has recently been reported by Zones [50,51]. Zones studied the effects of the concentration of the inorganic species in the synthesis of large-pore borosilicates using the tricyclo[5.2.1.0]decanes as structure-directing agents:

$N^+(CH_3)_3$

endo

XV

$(CH_3)_3N^+$
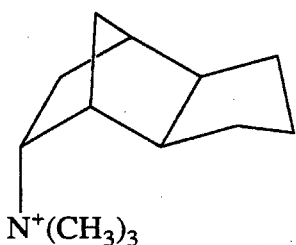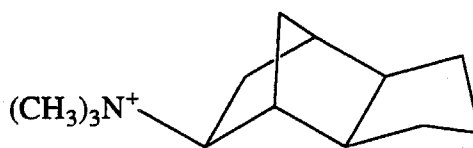
exo

XVI

The endo derivative produced zeolites SSZ-33 and SSZ-31 at high and low boron substitution, respectively. Similarly, the exo isomer yields boron zeolite beta or MTW in going from high to low boron substitution. Zones investigated the effect of increasing the sodium concentration in the synthesis gel and found that at Na/Si ratios of 0.1, microporous molecular sieves were formed. However, as the sodium concentration was

increased to Na/Si ratios of 0.18-0.26, Kenyaite (a layered silicate) is obtained as the final product. It seems that at high concentrations, alkali-metal cations begin to compete with the organic molecules in a structure-directing role.

These examples show the compromise that is needed in zeolite synthesis to obtain an optimum balance among the different effects that the components of the synthesis gel may have on the final product. Alkali-metal cations are needed to increase the rate of crystallization of high-silica zeolites, but excessive amounts of these components in the synthesis mixture will override the structure-directing effects of the organic molecules and favor the formation of layered compounds.

1.4.2 Selectivity Of A Structure-Directing Agent Towards Zeolite Formation

As was illustrated in the section on clathrasils, one structure-directing agent can be used to synthesize several clathrate structures depending on the synthesis conditions. Zones et al. [52] studied how perturbations on the synthesis procedure of SSZ-33 (using molecule **XV**) dramatically affect the product formed. Table 1.3 shows the effect of mixing molecules **XV** and **XVI** in the synthesis gel. The synthesis of SSZ-33 is sensitive to the presence of molecule **XVI**. When the ratio of **XV/XVI~5**, zeolite beta starts to be detected in the product. The yield of crystalline product and ^{13}C MAS NMR of these samples indicate that both molecules are occluded inside the pores of zeolite beta for **XV/XVI<3**. These data indicate that molecule **XV** can stabilize SSZ-33 and zeolite beta. The data also indicate that the nucleation of crystals of SSZ-33 is very sensitive to the geometry of the structure-directing agent, but that the crystal growth process is more flexible and can be accomplished simultaneously by several structure-directing agents. If seeds of SSZ-33 are added to the same set of experiments, zeolite beta is not observed any more in the final product. The effect of seeding is to bypass the need for the spontaneous formation of SSZ-

33 nuclei and effectively stop the formation of zeolite beta [52]. Harris and Zones [53] who investigated the synthesis of pure-silica nonasil, have reported a correlation between the tightness of the fit of the organic molecule in the cage and the rates of nucleation. The faster nucleation rates were observed for syntheses in which the agreement between the size of the molecule and the size of the cage was specially good, indicating that a better tightness of the fit of the organic molecule in the clathrasil cage promotes faster nucleation rates.

1.5   Pure-Silica Large–Pore Materials

There are three known pure-silica, large-pore zeolites: ZSM-12 (MTW), SSZ-24 (AFI) and SSZ-31. All these zeolites can be synthesized under the same synthesis conditions except for the use of different structure-directing agents. MTW has relatively small elongated pores (5.5 x 5.9 Å) [3] and can be synthesized using several structure-directing agents (Table 4). The MTW structure is typical of high-silica zeolites and contains 4-, 5- and 6-rings. In contrast, the pure-silica polymorph of AlPO4-5, SSZ-24, contains only 4- and 6-rings and a large 12-ring pore of 7.3 Å in diameter. In spite of these differences in shape and size, the structures of MTW and AFI appear very similar when they are viewed as an assemblage of tubular building units. From this perspective, the differences in the structures of MTW and AFI arise from assembling tubes, in two different forms, with walls formed only of 6-rings. According to the description of Kirchner and McGuire [54], both zeolites have the type 1 pores in which the pore axis is parallel to the edge of a 6-ring.

Comparison of the structure-directing agents for MTW and the structure-directing agents for AFI indicates two main differences: first, in general the structure-directing agents for MTW are formed from smaller organic molecules than the structure-directing agents for AFI (cyclohexane and benzene rings against the adamantane) and second, the

structure-directing agents for MTW are very flexible compared to the ones for AFI. The combination of these two factors suggests that the structure-directing agents used for the synthesis of AFI are large enough to not allow (by steric forces) the small elongated 12-ring pores of MTW to be formed and seem to shift the kinetics of crystal nucleation from MTW to AFI.

SSZ-31 is a pure-silica zeolite synthesized using the structure-directing agents shown in Table 1.4. Sorption experiments suggest that SSZ-31 is a one-dimensional 12-ring pore system [55]. NCL-1 is also a pure-silica large–pore zeolite [56] synthesized with bis (triethylammonium)butane. The X-ray diffraction patterns of NCL-1 are very similar to the pattern of SSZ-31. The structure-directing agents for SSZ-31 are also rigid and can be loosely described as containing a large polycyclic body with a protuberance formed by the N-methyl groups. These 'bumps' suggest that the structure-directing agents destabilize the formation of both MTW and AFI. In short, based on the size and shape of the structure-directing agent, the pores of SSZ-31 should have 'grooves' or 'pockets' to accommodate the shape of the organic guest molecules along the one-dimensional pores.

It is noteworthy that, except for only one report (*vide infra*), large structure-directing agents have not given pure-silica materials with new large-multidimensional pore systems. The reasons behind this observation are not understood, especially if contrasted with the easily synthesized multidimensional medium-pore silicalite-1 and silicalite-2. It can be speculated that T—O—T angles needed for the formation of a multidimensional pore system are not favored in pure-silica materials. Histograms of experimentally measured T—O—T angles (adapted from ref. 8) in Si—O—Si, Si—O—Al and the Si—O—B are shown in Figure 1.4. It can be observed that the variation in the Si—O—Si angle is larger than the variation in the Si—O—Al and Si—O—B. These histograms indicate that the substitution of Al or B for Si in the framework stiffens the T—O—T angle and shifts the optimum T—O—T angle to a value lower than expected in silicates.

A second reason for the absence of pure-silica materials with intersecting large pores may be the effect of defects on the stability of the silicate framework. As suggested before, in pure–silica materials, the charge of the structure-directing agent is balanced by a deprotonated silanol group in the zeolite framework. For TPA in the MFI structure, this is equivalent to a defect for each 24 Si atoms. As the void volume of the zeolite framework is increased, the ratio Si/N^+ is drastically reduced. For example, for SSZ-33 synthesized using **XV**, $Si/N^+{\sim}15$ and for zeolite beta synthesized using TEA the $Si/N^+{\sim}7$. The charge of the structure-directing agent is largely balanced by B or Al in these two examples, but these numbers suggest that for certain Si/N^+, the density of defects necessary to balance the organic charge in the pure-silica material create a large destabilization of the structure, thus inhibiting its formation. The exception to this rule was recently reported by van der Waal et al. [72], who synthesized the pure-silica polymorph of zeolite beta using dibenzyldimethylammonium hydroxide as structure-directing agent. The organic molecule contains a C/N=16, instead of C/N=8 in TEA, which therefore gives a $Si/N^+{\sim}14$. The number of defects in this preparation of zeolite beta would be about one half of the number of defects expected in a pure-silica sample of TEA. The smaller number of defects increases the stability of the final product and in this way allows the formation of the pure-silica polymorph of zeolite beta.

1.6 Heteroatoms And The Structure-Directing Effect Of Organic Molecules

The addition of small amounts of tetrahedral atoms other than silicon (B, Al, Zn, etc.) have striking effects on the structures of the zeolites formed using the *same* structure-directing agents. In this section we will look at the changes observed in the structures of zeolites

when Al, B or Zn are added to an otherwise pure-silica synthesis gel. In addition to Al, B or Zn, many other heteroatoms [2,13] have been incorporated in high-silica zeolite frameworks. In general, the effect of Ga and Fe is similar to the effect of Al, Ti has been found to have small structural effects, and Ge can substitute for Si. The reader can search in the references for more details [2,13].

An example of the effect of added Al on the structure of the zeolites formed when other variables are kept constant is illustrated with the syntheses of MTW and BEA using tetraethylammonium ions as structure-directing agent (Table 5). When the $SiO_2/Al_2O_3>50$ MTW is formed. As the amount of Al is increased beyond $SiO_2/Al_2O_3=50$, the product observed is BEA, and if the fraction of Al is increased even further ($SiO_2/Al_2O_3\sim15$) ZSM-20, an intergrowth of EMT and FAU is obtained. Analogous results are observed when boron is used instead of aluminum. For low boron concentrations MTW is the final product, and as the amount of boron is increased zeolite beta is then crystallized. Also, this effect is not restricted to TEA but is also observed for other structure-directing agents (see Table 1.5).

The structure-directing effect of other organic guest molecules that form large-pore pure-silica molecular sieves is also strongly coupled to the presence of heteroatoms in the synthesis gel. Trimethyl-2-adamantylammonium forms the one-dimensional AFI structure with pure-silica synthesis gels but forms SSZ-33 [57] when boron is added. SSZ-33 is a new zeolite with intersecting 10- and 12-ring pores that can be synthesized using several structure-directing agents [58] when boron is in the synthesis gel. Other organic molecules that form SSZ-31 with a pure-silica gel also form SSZ-33 when boron is added to the reaction mixture (Table 5). For these cases, molecules that form different structures with pure-silica form a material with the same framework structure when boron is included in the synthesis gel. On the other hand, the molecules that form MTW only crystallize BEA when boron is added to the synthesis gel.

A different result is observed when aluminum is added to the synthesis gel if molecule **XIV** is used as structure-directing agent. Neither BEA or SSZ-33 are observed as the final product, but rather a new material SSZ-37 is the crystalline solid formed [59]. The structure of SSZ-37 seems to be similar to the structure of NU-87 [60]. Slighly bigger or slighly smaller organic molecules do not yield the SSZ-37 zeolite. Note that the effect of Al and B are not the same. Although the addition of Al or B when using TEA as the structure-directing agent gives BEA in both cases, the structures of the products formed when using the heterocyclic molecule **XIV** are very different. Also, note that the molecules that form SSZ-31 and SSZ-33 have not been reported to form any crystalline material when Al is substituted for B.

As is observed with aluminum and boron, the addition of zinc to a synthesis gel also radically changes the structure of the zeolite product. In all cases, however, the molecular sieve VPI-8 is observed, regardless of the organic structure-directing agent used for its synthesis. VPI-8 was first synthesized by Annen [61,62] using zinc acetate as the source of framework zinc and TEA as the structure-directing agent. Sorption data indicate that VPI-8 is a 12-ring, large-pore one-dimensional molecular sieve. The formation of VPI-8 in the presence of a variety of organic guest molecules suggests that in these syntheses, the structure of the final product is controlled by the divalent zinc cation and that the principal role of the organic molecule is the stabilization of the voids forming the pores [63]. The Zn atoms appear to inhibit the nucleation of other zeolite structures besides VPI–8.

Trivalent and divalent T atoms in the synthesis gel are bound to have strong influence on the synthesis of high-silica zeolites for several reasons. First, the substitution of Al, B or Zn for Si in the zeolite form a negatively charged framework that will tend to coordinate much more strongly the inorganic cations (Na, K and so on) found in the synthesis gel. Second, the T—O bond lengths and in particular the T—O—T angles are

expected to influence the formation of certain secondary building units such as 4-rings. Finally, instead of the formation of a charged deprotonated silanol group in the zeolite structure to balance the charge of the organic structure-directing agent, the charge can be balanced by the anionic framework of the zeolite.

It is enlightening to compare the structures of MTW and BEA. The projection along the 12-ring pores of MTW is the same as the projection along the a and b axes of zeolite beta. Both structures are the result of the disorder stacking of silicate layers [35,64] and there are more 4-rings in the structure of BEA than in the structure of MTW. The presence of additional 4-rings in the structure of BEA may be regarded as the consequence of smaller T—O—Si angles promoted by the presence of Al or B. As was found in MTW and BEA, the projection along the 12-ring pores of AFI is the same as the projection along the 12-ring pores of SSZ-33. Also, the structures of SSZ-33 and BEA are related by the presence of similar secondary building units and both are highly faulted structures with open three-dimensional pore systems.

The trends that have been outlined here have to be regarded as tentative. They are the result of a limited number of experiments using a small number of organic molecules and relatively narrow ranges of all the synthesis parameters. Further work, in particular, the structure solution of SSZ-31 and VPI-8, is needed to be able to understand further the observed experimental results.

1.7 Examples Of Structure-Direction

The concepts of structure-direction enumerated above are now discussed in terms of recent examples. These examples show a complementary relationship between the geometry of the structure-directing agent and the geometry of the void space in the zeolite.

Zeolite SSZ-26 is an aluminosilicate molecular sieve with intersecting 10- and 12-ring pores [65]. It is synthesized using the propellane molecule **XVII** [66].
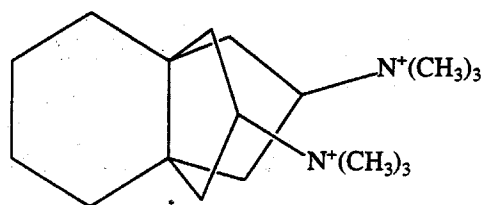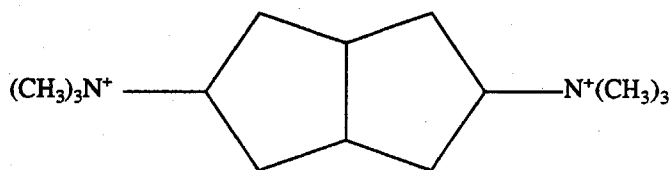
| **XVII** | **XVIII** |

Zones and Santilli [66] found that molecule **XVIII** formed MTW and argued that the inclusion of an additional ring as in **XVII** would force the formation of an intersecting pore system as illustrated in Figure 1.5. Thermogravimetric and chemical analyses indicate (based on the solution of the structure [59]) that there is one guest molecule per channel intersection. Lobo et at. [67] carried out molecular force-field calculations on the propellane molecule **XVII** inside the pores of SSZ-26 and found a very good agreement between the geometry of the pore intersection and the geometry of the organic molecule. The minimum-energy conformation of the molecule inside the pore intersections (Fig. 1.6) closely resembles the conformation suggested by Zones and Santilli [66] (Fig. 1.5). Therefore, the synthesis of SSZ-26 appears to be the first case known to the authors of where the geometry of a pore-architecture has been designed *a priori* and exemplifies the usefulness of the concepts of structure-direction as an aid in the synthesis of new molecular sieves. This example, however, is not the only one where there is a very good fit between geometry of the guest molecule and the geometry of the pore.

The structure of ZSM-18 (MEI) [68] is unique since it is the only aluminosilicate to contain 3-rings in the framework. With ZSM-18, a very good fit between the organic guest

molecule and the zeolite cage is observed. Figure 1.7 shows an ORTEP drawing of the triquaternary ammonium molecule used as a structure-directing agent inside the large cage of MEI. The rigidity, the size and, in particular, the threefold axis of rotation of the organic molecule are the characteristics that favor the formation of the cage of ZSM-18. Hong et al. [19] have carried out CP/MAS ^{13}C and static NMR on this material and found that the triquaternary ammonium ion is tightly held inside the MEI cage. Recently, Schmith and Kennedy [73] reported the synthesis of ZSM-18 using molecules **XIX** and **XX**.

XIX	**XX**
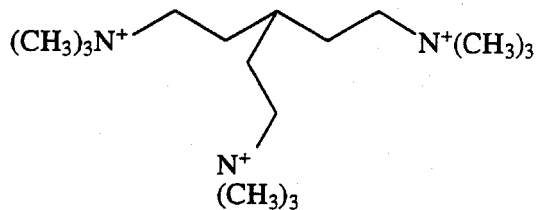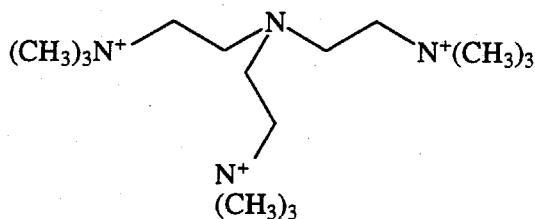
Their rationale was based on keeping the same total charge and symmetry, ease of synthesis and retaining only acyclics. The various possibilities were screened using molecular dynamics, which reduced the list to cations **XIX** and **XX**. This paper is the first example of the use of molecular dynamics to 'design' a structure-directing molecule.

Another good example of the relationship between the geometry of the structure-directing agent and the geometry of the cage is 18-crown-6 in the cages of EMT, the hexagonal polymorph of FAU. As with the triquaternary ammonium molecule in MEI, only the 18-crown-6 has been found to direct the formation of EMT. Recent crystallographic work [71] indicates that 18-crown-6 is found in the small cages of EMT and approximately conforms to the geometry of the cage.

The first example of the purposeful control of long-range order in the synthesis of zeolites through the use of structure-directing agents was shown by Arhancet and Davis [70]. By specifying the concentrations of 18-crown-6 and 15-crown-5 in the synthesis gel, Arhancet and Davis have been able to control the relative fractions of the hexagonal (EMT) and cubic (FAU) polymorphs of faujasite that are present in the zeolite product.

A second example of the control of long-range order using organic structure-directing agents has been recently reported [58]. In this case, Lobo et al. report the synthesis of two related materials CIT-1 and SSZ-33. These two zeolites are members of a family of intergrowths of two closely related structures, polymorph A and polymorph B [57]. CIT-1 is the pure polymorph B of this family of materials and SSZ-33 is an intergrowth of polymorph B and polymorph A with a 70% fraction of polymorph B. By synthesizing the materials in the presence of the structure-directing agent for CIT-1 (**XXI**) and the structure-directing agent for SSZ-33 (**XV**), the fraction of polymorph B in the final material can be carefully controlled from materials which are 70% of polymorph B and 30% polymorph A (SSZ-33) to materials which are 100% polymorph B (CIT-1)[57]. Figure 1.8 shows the experimental XRD patterns of materials with different fractions of polymorph B. These two examples also illustrate how the long-range order in zeolites can be controlled using organic guest molecules.
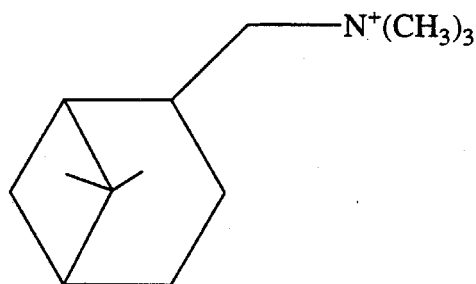
XXI

1.8 Summary

We have discussed the myriad of factors that influence in one way or another the synthesis of zeolites. In Figure 1.9 we attempt to illustrate the effects that these factors have on the structures formed.

In the absence of structure–directing agents, silicate syntheses form dense (quartz, tridymite, cristobalite) or layered materials. Using only silica as the source of tetrahedral atoms, small molecules—amines in particular—direct the formation of clathrasils. The structure of the clathrasil obtained depends on the size of the molecule, on the synthesis temperature and to a minor extent on the specific geometry of the molecule. Linear molecules form in general 1–D, 10-ring pore molecular sieves. The most important factor that defines one structure from the several that can be synthesized with pure-silica appears to be the temperature.

Branched molecules (TPA and TBA) form multidimensional medium pore zeolites while large polycyclic molecules produce MTW, AFI or SSZ-31 depending on their size and shape. No multidimensional, pure–silica, large–pore zeolites have been synthesized. Nakagawa, however, has indicated that based on adsorption experiments[71], the pure-silica zeolite SSZ-35 is a multidimensional large-pore material. The structure of SSZ-35 must be solved to answer this question.

The selectivity of the structure–directing agents towards a specific zeolite structure is increased as the size of the molecule is increased. The most selective molecules are large, i.e., formed of more than 16 carbon and nitrogen atoms, and contain two or three charges per molecule.

Small amounts of trivalent (Al, B, Ga, Fe) or divalent (Zn, Be) tetrahedral atoms have striking effects on the structures of zeolites. In general, the structures formed have

multidimensional pore systems, except for Zn that (thus far) direct the crystallization of VPI-8, regardless of the structure–directing agent. Often, the projection along the 12-ring pore of 1-D pure–silica zeolites is the same as the projection along the 12-ring pores of multidimensional materials obtained after the addition of Al or B.

The thermodynamic stability of all pure–silica molecular sieves is relatively constant. This is an encouraging fact that suggests that the synthesis of many other zeolites with novel pore architectures is feasible.

The concepts of structure–direction have shown to be of tremendous power as guiding principles for the synthesis of new molecular sieves. The results presented in this review indicate that no limits are apparent to the number of structures that can be synthesized. The results also suggest that new zeolite structures will require the synthesis of larger structure–directing agents than the ones that have been prepared so far.

1.9 References

1. M.E. Davis, *Ind. Eng. Chem. Res.* **30**, 1675 (1991).

2. J.M. Newsam, in *Solid State Chemistry: Comounds*, A.K. Cheetham and P. Day Eds, Oxford University Press, New York, (1992).

3. W.M. Meier and D.H. Olson, *Atlas of Zeolite Structure Types*, Butterworths-Heineman, Stoneham, MA, (1992).

4. J.V. Smith, *Chem. Rev.* **88** 149 (1988).

5. J. Higgins, *Catal. Today*, in press.

6. L.B. McCusker, C. Baerlocher, E. Jahn, M. Bulow, *Zeolites*, 11 308 (1991).

7. M.E. Davis, C. Montes, P.E. Hathaway, J.P. Arhancet, *J. Am. Chem. Soc.* **111** 3919 (1989).

8. G.V. Gibbs, E.P. Meagher, in *Structure and Bonding in Crystals*, H. O'Keeffe and A. Navrotsky Eds., Academic Press, New York, Vol. 1, pp 195-223 (1980).

9. M.D. Newton and G.V. Gibbs, *Phys. Chem. Miner.* **6** 221 (1980).

10. M.E. Davis and R.F. Lobo, *Chem. Mater.* **4** 756 (1992).

11. B.M. Lok, T.R. Cannon, C.A. Messina, *Zeolites*, **3** 282 (1983).

12. J.C. Jansen, in *Introduction to Zeolite Science and Practice*, H. van Bekkum, E.M. Flanigen and J.C. Jansen Eds., Elsevier, Amsterdam, pp 77-135 (1991).

13. R. Szostak, *Handbook of Molecular Sieves*, Van Nostrand-Reinhold, New York, (1992).

14. H. Gies, in *Inclusion Compounds* Academic Press, London, Vol. 5, pp 1-35 (1991).

15. H. Gies and B. Marler, *Zeolites*, **12** 42 (1992).

16. F. Liebau, in *Silicon Chemistry*, E.R. Corey, J.Y. Corey and P.P. Gaspar Eds. Ellis Horwood Limited, England, pp 308-323 (1988).

17. D.M. Bibby and M. P. Dale, *Nature*, **317** 157 (1985).

18. J. Keisper, C.J.J. den Ouden, M.F.M. Post in *Zeolites: Facts, Firues and Future, Studies in Surface Science and Catalysis*, Elsevier, Amsterdam Vol. 49, pp 237-248, (1989)

19. C.Y. Chen, personal communication (1994).

20. J.J. Pluth and J.V.Smith, in *Zeolites: Facts, Firues and Future, Studies in Surface Science and Catalysis*, Elsevier, Amsterdam Vol. 49, pp 835-844, (1989).

21. F. Liebau, *Structural Chemistry of Silicates*, Springer-Verlag, Berlin (1985).

22. S.B. Hong, H.M. Cho, M.E. Davis, *J. Phys. Chem.*, **97** 1622 (1993).

23. S.B. Hong, H.M. Cho, M.E. Davis, *J. Phys. Chem.*, **97** 1629 (1993).

24. S. Burkett and M.E. Davis, *Microporous Mater.*, **1** 265 (1993).

25. H. Gies, *Z. Kristal.* **164** 247 (1983).

26.   H. Gerke and H. Gies, *Z. Kristal.* **166** 11 (1984).

27.   G. Miehe, T. Vogt, H. Fuess, U. Muller, *Acta Cryst.* **B49** 745 (1993).

28.   H. Gies, *Z. Kristal.* **167** 73 (1984).

29.   H. Gies, *Z. Kristal.* **175** 93 (1986).

30.   L.B. McCusker, *Act. Crystal. A.* **47**, 297 (1991).

31.   L.B. McCusker, *J. Appl. Crystallography,* **21** 305 (1988).

32.   R.F. Lobo and M.E. Davis, *Microporous Mater.* in press.

33.   R.M. Dessau, K.D. Smith, G.T. Kerr, G.L. Woolery, L.B. Alemany, *J. Catal.* **104** 484 (1987).

34.   C.A. Fyfe, H. Gies, G.T. Kokotailo, B. Marler, D.E. Cox, *J. Phys. Chem.,* **94**, 3718 (1990).

35.   C.A. Fyfe, H. Gies, G.T. Kokotailo, C. Pasztor, H. Strobl, and D.E. Cox, *J. Am. Chem. Soc.,* **111**, 2470 (1990).

36.   F. Liebau, *Structural Chemistry of Silicates,* Springer-Verlag, Berlin, p 242 (1985).

37.   Y. Nakagawa and S.I. Zones, in *Synthesis of Microporous Materials,* M.L. Occelli and H. Robson Eds., Vol 1, Van Nostrand Reinhold, New York, pp 222-239 (1992).

38.   C.D. Chang and A.T. Bell, *Catal. Lett.* **8** 305, (1991).

39.   R.M. Barrer, *Hydrothermal Synthesis of Zeolites,* Academic Press, London, p 359 (1982).

40.   I. Petrovic, A. Navrotsky, S.I. Zones, M.E. Davis, *Chem. Mater.,* **5**, 1805 (1993).

41.   N.J. Henson, A.K. Cheetham and J.D. Gale, *Chem. Mater.,* submitted (1994).

42.   X. Hu and W. Depmeier, *Z. Kristal.* **201**, 99 (1992).

43.   A. Shimizu and Y. Taniguchi, *Bull. Chem. Soc. Jpn.,* **63**, 1572 (1990).

44.   A. Shimizu and Y. Taniguchi, *Bull. Chem. Soc. Jpn.*, **63**, 3295 (1990).

45.   D.T. Griffen, *Silicate Crystal Chemistry*, Oxford University Press, Oxford, pp 15 (1992).

46.   C.B. Khouw, H.X. Li, C.B. Dartt, M.E. Davis, *ACS Symp. Ser.*, **523** 293 (1993).

47.   M. Goepper, H.X. Li, M.E. Davis, *J. C. S., Chem. Commun.*, 1665 (1992).

48.   P. Brady and J.V. Walther, *Chem. Geol.* **82** 253(1990)

49.   P.M. Dove and D.A. Crerar, *Geochim. Cosmochim. Acta*, **54** 955 (1990).

50.   S.I. Zones, *Microporous Mater.* in press.

51.   S.I. Zones and Y. Nakagawa, *Microporous Mater.* in press (1994).

52.   S.I. Zones Y. Nakagawa, G. Yuen, T. Harris, *J. Am. Chem. Soc.* submitted.

53.   T.V. Harris and S.I. Zones *Proceedings of the 10th International Zeolites Conference., Garmisch-Partenkirchen, Germany*, Elsevier: Amsterdam, Vol. A, pp 29-36 (1994).

54.   R.M. Kerchner and N.K. McGuire, in *Extended Abstracts and Program, 9th International Zeolite Conference*, J.B. Higgins, R. von Ballmoos and M.M.J. Treacy Eds., Butterworth-Heinemann (1992).

55.   S.I. Zones, L. T. Yuen, Y. Nakagawa, R. A. Van Nordstrnad and S.D. Toto, *in Proceedings of the 9th International Zeolites Conference*, R. von Ballmoos, J.B. Higgins and M.M. Treacy Eds. Butterworth-Heinemann, Tonehalm MA, Vol.1, pp 163-170 (1993).

56.   R. Kumar, K. Ramesh Reddy, Ahuj Raj and P. Ratnasamy, *in Proceedings of the 9th International Zeolites Conference*, R. von Ballmoos, J.B. Higgins and M.M. Treacy Eds. Butterworth-Heinemann, Tonehalm, MA, Vol.1, pp 189-196 (1993).

57.   R.F. Lobo, M. Pan, I. Chan, H.X. Li, R.C. Medrud, S.I. Zones, P.A. Crozier and M.E. Davis, *Science*, **262** 1543 (1993).

58.   R.F. Lobo, S.I. Zones, M.E. Davis, *Proceedings of the 10th International Zeolites Conference., Garmisch-Partenkirchen, Germany*, Elsevier: Amsterdam, Vol. A, p 461-468 (1994).

59.   Y. Nakagawa, U.S. Patent 5,254,514 (1993).

60.   Y. Nakagawa, *Proceedings of the 10th International Zeolites Conference, Garmisch-Partenkirchen, Germany*, Elsevier: Amsterdam, Vol. A, p 323-330 (1994).

61.   M.J. Annen, Ph.D. Thesis, Virgina Polytechnic Institute, Blacksburg, VA (1992).

62.   M.J. Annen, M.E. Davis, *Microporous Mater.* **1** 57 (1993)

63.   M.A. Camblor, S.I. Zones and M.E. Davis, in preparation.

64.   J.M. Newsam, M.M.J. Treacy, W.T. Koetsier and C.B. de Gruyter, *Proc. R. Soc. Lond. A* **420** 375 (1988).

65.   S.I. Zones, M.M. Olmstead, and D.S. Santilli, *J. Am. Chem. Soc.* **114** 4195 (1992).

66.   S.I. Zones and D.S. Santilli, *in Proceedings of the 9th International Zeolites Conference*, R. von Ballmoos, J.B. Higgins and M.M. Treacy Eds. Butterworth-Heinemann, Tonehalm, MA, Vol.1, pp 171-179 (1993).

67.   R.F. Lobo, M. Pan, I. Chan, S.I. Zones, P.A. Crozier, M.E. Davis, *J. Phys. Chem.*, in press.

68.   S.L. Lawton and W.J. Rohrbaugh *Science* **247** 1319 (1990).

69.   L.C. McCusker, *Microporous Mater.* in press.

70.   J.P. Arhancet and M.E. Davis, *Chem. Mater.* **3** 567 (1991).

71.   Y. Nakagawa, U.S. Patent 5,271,921 (1993).

72.   J.C. van der Waal, M.S. Rigutto, H. van Bekkum, *J. Chem. Soc., Chem. Commun.*, 1241 (1994).

73.   K.D. Schmith and G.J. Kennedy, *Zeolites*, in press.
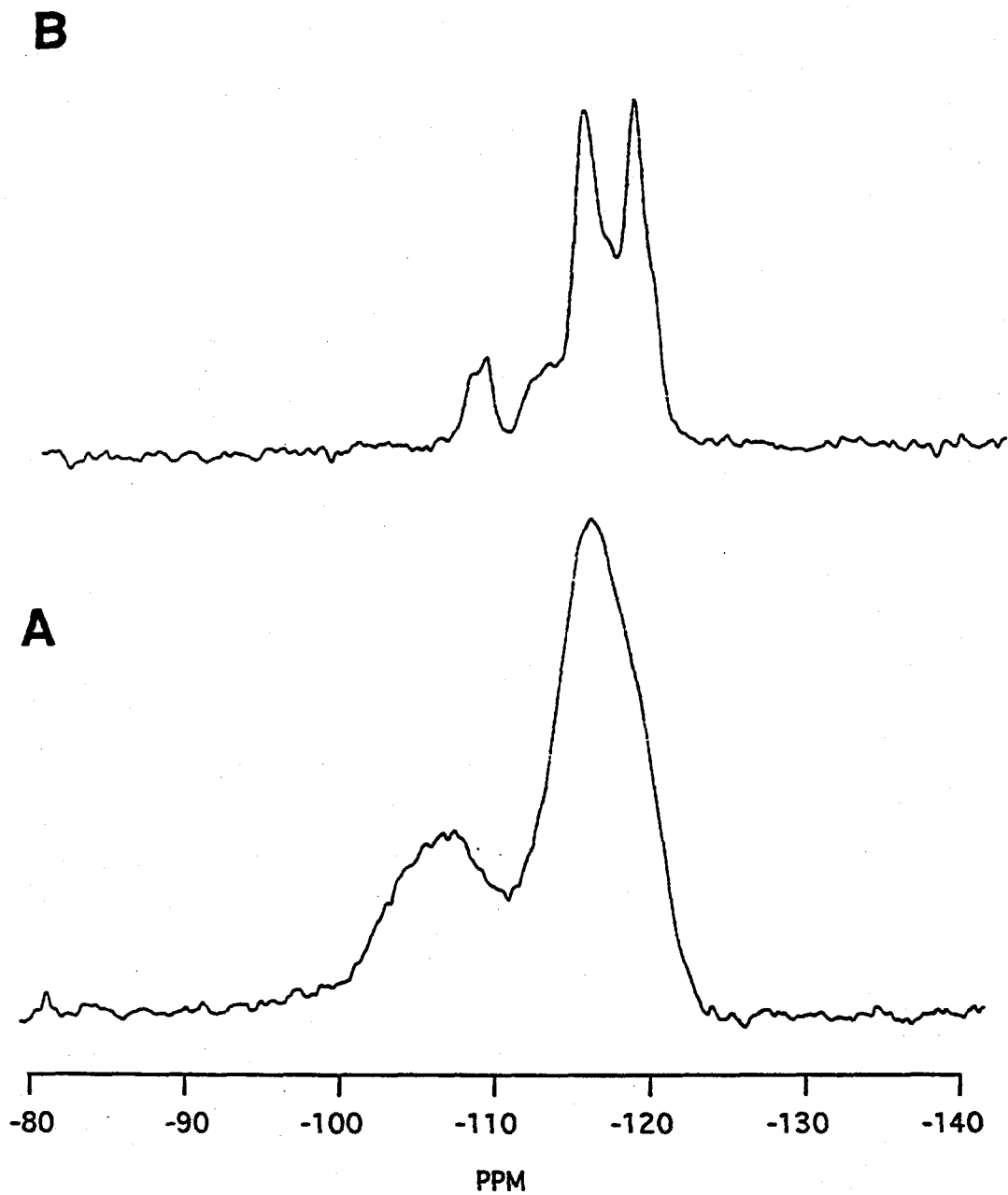
Figure 1.1 ^{29}Si CP/MAS NMR spectra of samples of pure-silica nonasil (NON) synthesized using a quaternary ammonium cation (A) and an organic amine (B) as structure-directing agent.
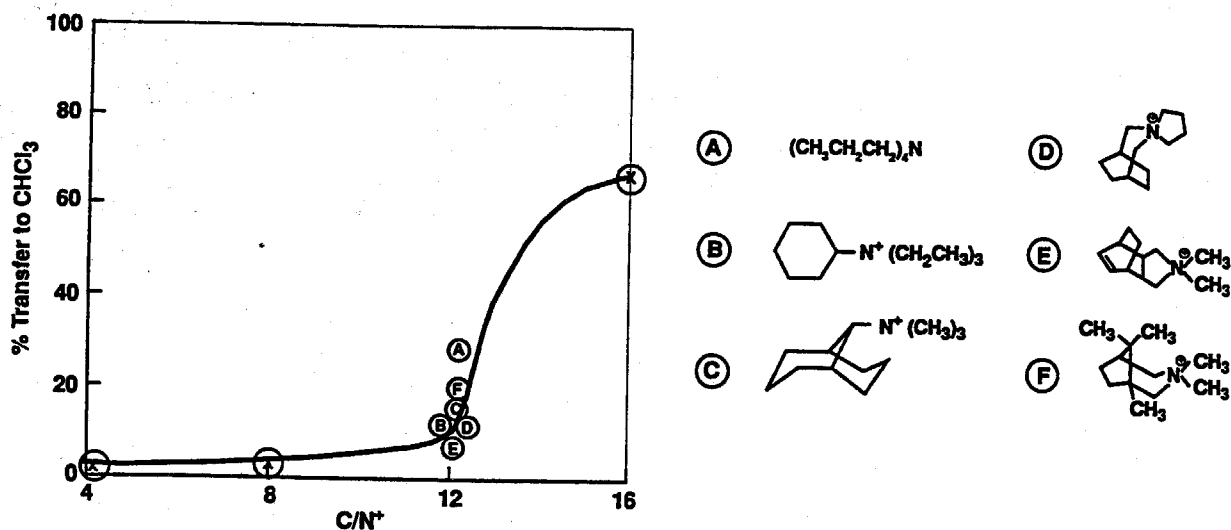
Figure 1.2 Partition of quaternary ammonium compounds between water and CHCl₃.
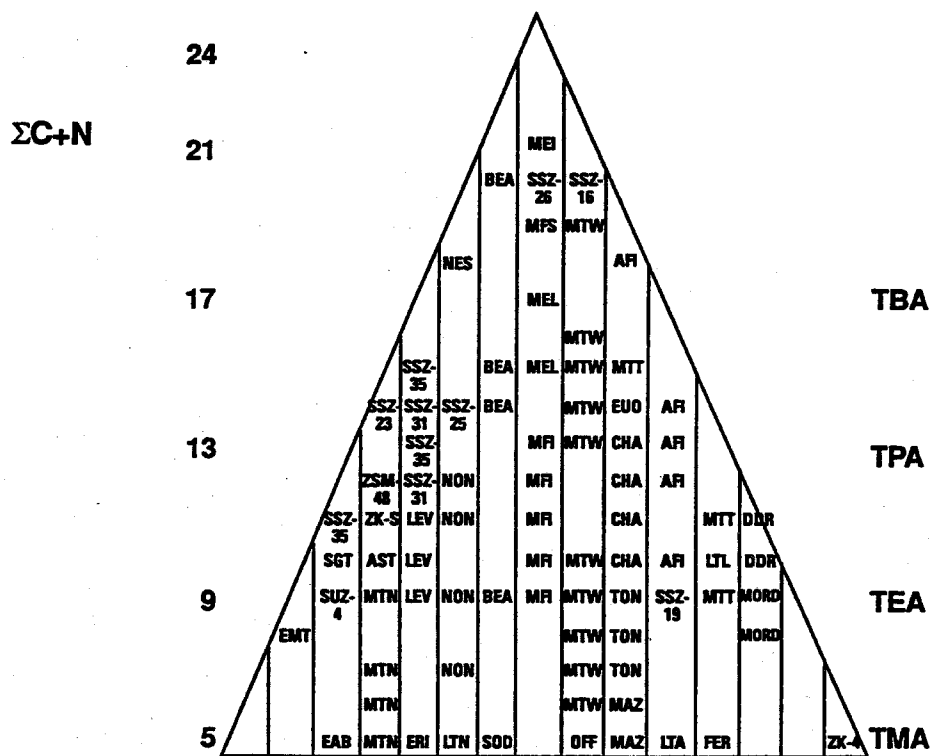
Figure 1.3 Illustration of the increased selectivity of different structure–directing agents as the size of the molecule (C+N) is increased.
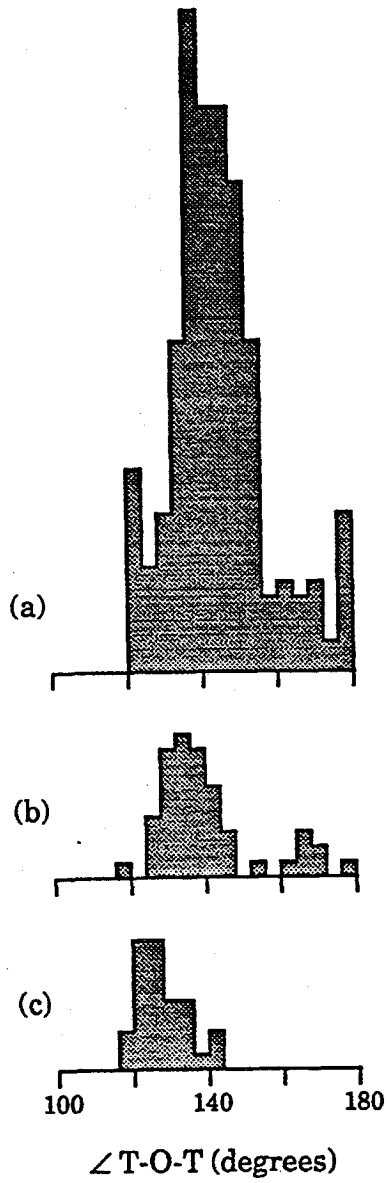
Figure 1.4 Histogram of experimentally observed T—O—T angles in a) Si—O—Si,

b) Si—O—Al, c) Si—O—B (adapted from ref. 9).
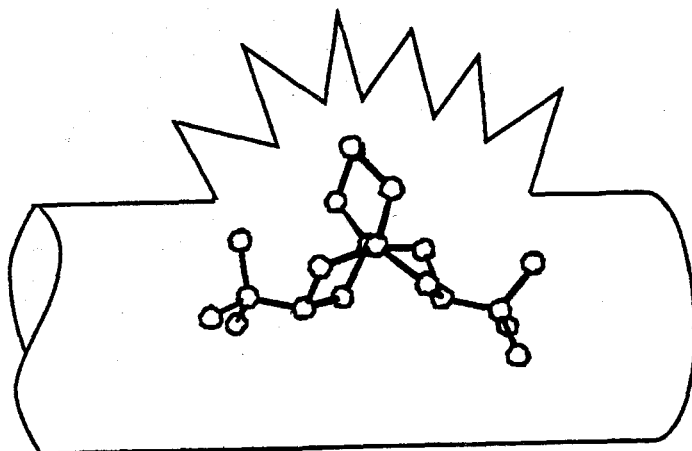
Figure 1.5 Proposed model for the formation of pore intersections using the propellane molecule **XXI**.
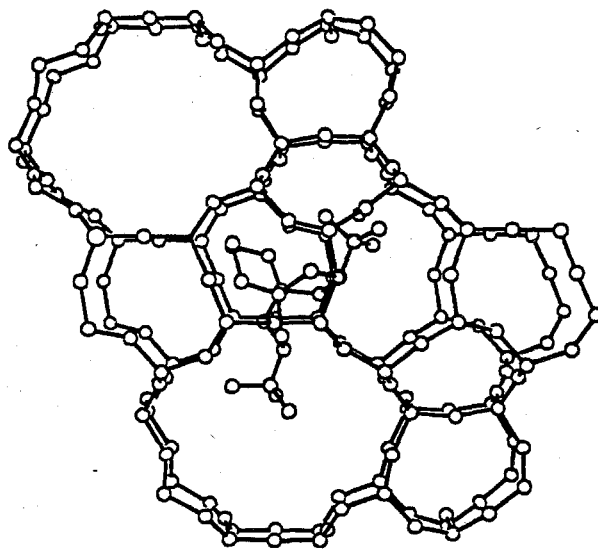
Figure 1.6 Minimum-energy conformation for the propellane molecule (**XXI**) in the pores of SSZ-26 as obtained from force-field calculations.
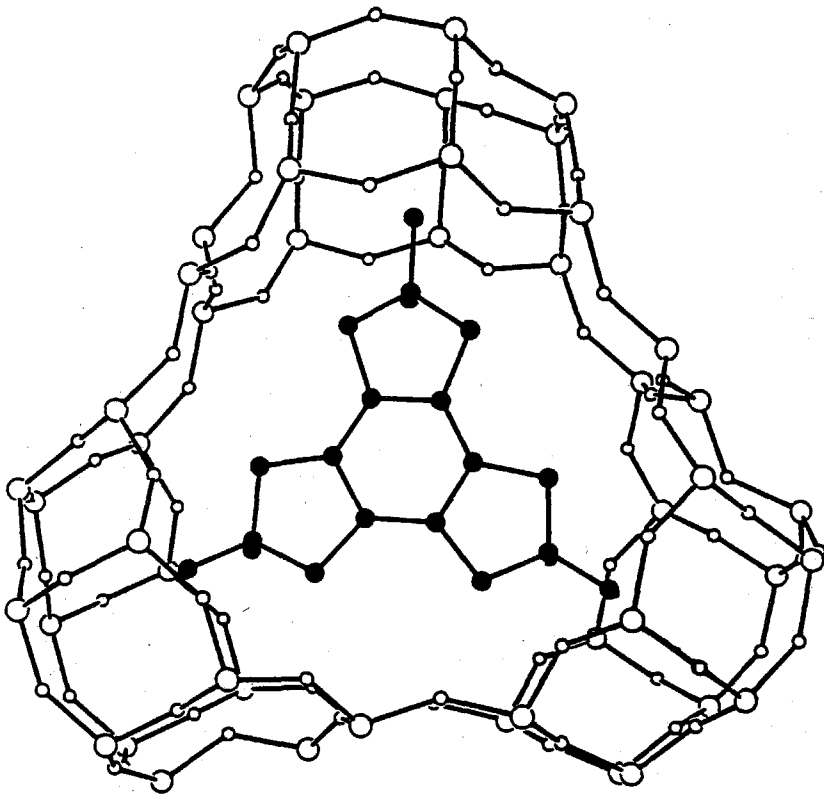
Figure 1.7 Position of the triquaternary ammonium molecule used as structure-directing agent in ZSM-18.
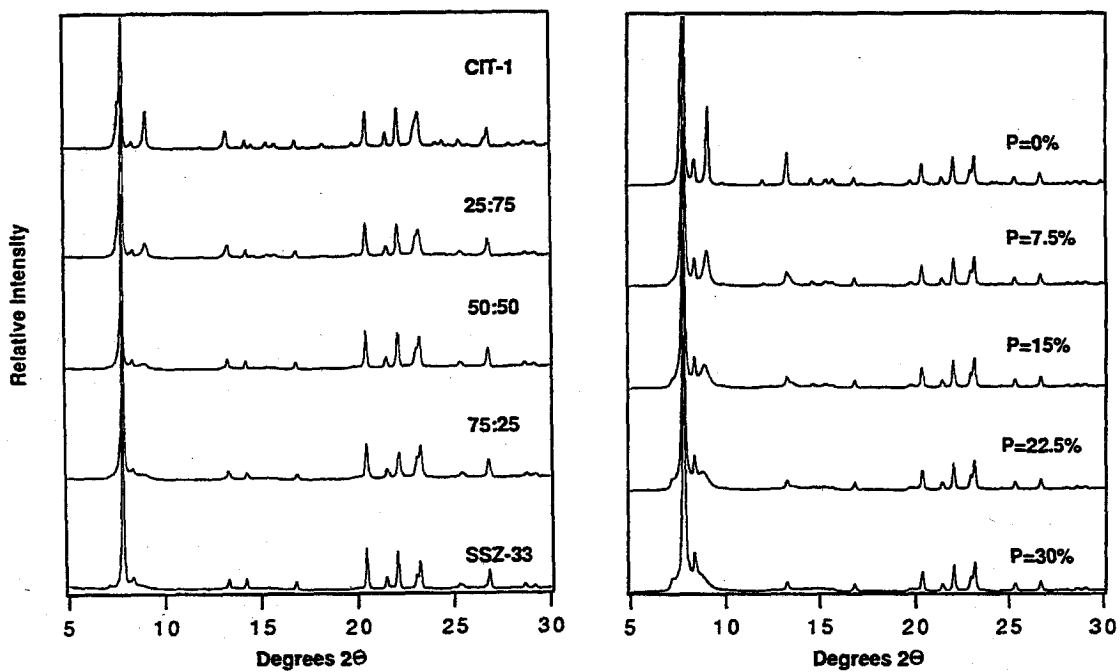
Figure 1.8 Experimental (A) and calculated XRD (B) patterns for intergrowths of polymorph A and polymorph B of SSZ-33.
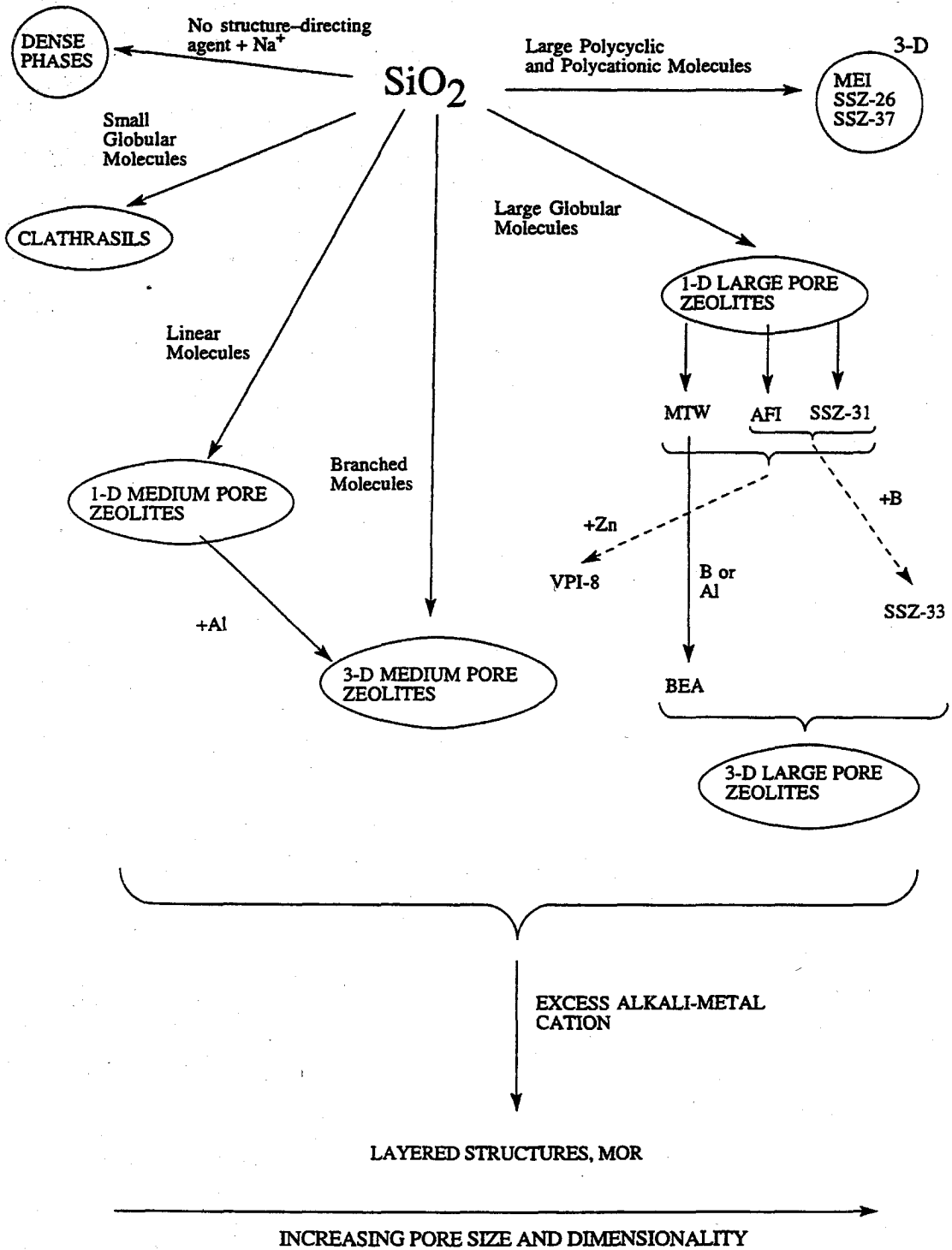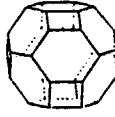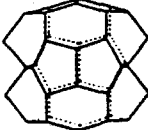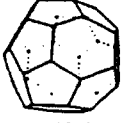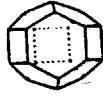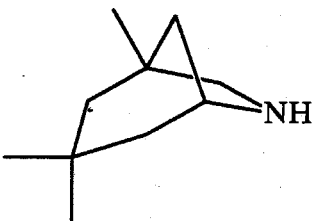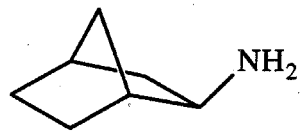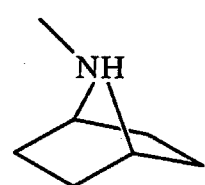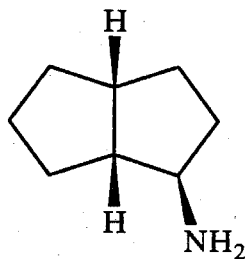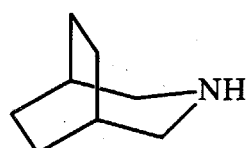
Figure 1.9 Summary of the trends between structure–directing agents and zeolite structures.

Table 1.1   Summary of the different cages found in the structures of clathrasils [15].

Clathrasil	Code	FD (T nm^{-1})	V of Largest Cage (nm^3)	Clathrasil Cages		
Melanophlogites	MEP	18.9	0.160	$[5^{12}]$	$[5^{12}6^2]$	—
Dodecasils 3C	MTN	18.7	0.250	$[5^{12}]$	$[5^{12}6^4]$	—
Octa-decasil	AST	16.7	0.280	$[4^6]$	—	$[4^6 6^{12}]$
Nonasil	NON	19.3	0.290	$[4^1 5^8]$	$[5^8 6^{12}]$	$[5^5 6^4]$
Deca–dodecasil 3R	DDR	17.6	0.350	$[5^{12}]$	—	$[4^3 5^{12} 6^1 8^3]$
Sigma-2	SGT	17.8	0.390	$[4^3 5^6 6^1]$	$[5^{12} 6^8]$	—
Dodecasil 1H	DOH	18.5	0.430	$[5^{12}]$	$[4^3 5^6 6^3]$	$[5^{12} 6^8]$
Deca–dodecasil 3H	—	—	0.540	$[5^{12}]$	—	$[5^{18} 6^2 8^3]$
Sodalite	SOD	17.2	0.230	—	$[4^6 6^8]$	—

Table 1.2 Results from the synthesis of pure-silica clathrasils using different organic molecules as structure-directing agents.

Structure Directing Agent	Clathrasil
(structure) =NH	DOH
(structure) NH$_2$	DOH
(structure) NH	STG, DOH
(structure) H, H, NH$_2$	NON
(structure) —NH	NON

Table 1.3 Products from syntheses using mixtures of structure-directing agents XV and XVI.

Ratio XV to XVI	SSZ-33	B-Zeolite Beta
19 to 1	100%	0%
9 to 1	100%	0%
5.7 to 1	Major	Minor
4 to 1	Minor	Major
3 to 1	0%	100%

Table 1.4 Structure-Directing agents for the synthesis of MTW, AFI and SSZ-31.
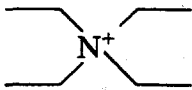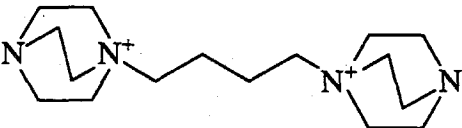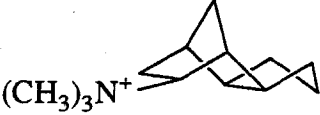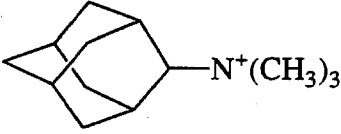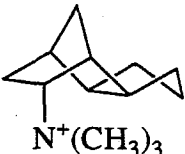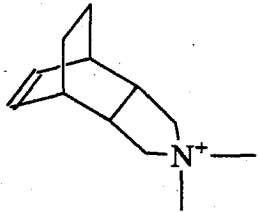
MTW[a]	AFI[b]	SSZ-31[c]

a   See ref. 13, 47.

b   See ref. 32, 56, ref. therein and Y. Nakagawa U.S. Patent 5,271,921 (1993).

c   See ref. 37 and 57.

Table 1.5 Effect of aluminum, boron and zinc on the structure of zeolites obtained using organic structure-directing agents.[a]

	SiO_2	SiO_2/Al_2O_3 <50	SiO_2/B_2O_3 <30	SiO_2/ZnO 20
	MTW	BEA	BEA	VPI-8
	MTW	BEA	BEA	VPI-8
$(CH_3)_3N^+$	MTW	MOR	BEA	Layered
$-N^+(CH_3)_3$	AFI	SSZ-25	SSZ-33	VPI-8
$N^+(CH_3)_3$	SSZ-31	MOR	SSZ-33	__b
$-N^+-$	SSZ-31	SSZ-37	SSZ-33	__b

a   From references 37, 51, 56, 61, 62, 63. Some of these results are from experiments carried out in our laboratories and not yet published.
b.   No product formed after several weeks.

Chapter Two

Synthesis and Characterization of Pure-Silica and Boron-substituted SSZ-24 Using N(16)-Methylsparteinium Bromide as Structure–Directing Agent

Synthesis and Characterization of Pure-Silica and Boron-substituted SSZ-24 Using N(16) Methylsparteinium Bromide as Structure–Directing Agent

Raul F. Lobo and Mark E. Davis

Chemical Engineering, California Institute of Technology

Pasadena, CA 91125

Abstract

SSZ-24, the high-silica molecular sieve isostructural with AlPO4–5 (AFI), is synthesized using N(16) methylsparteinium bromide as structure-directing agent and is characterized using X-ray powder diffraction, magic-angle spinning NMR spectroscopy, Fourier transform infrared spectroscopy and the physical adsorption of N_2. Unlike other structure-directing agents used for the synthesis of SSZ-24, N(16) methylsparteinium allows for the direct incorporation of boron into the zeolite framework using sodium borate as the source of boron in the synthesis medium. Boron can be removed from the structure and replaced by aluminum by refluxing the calcined sample in an aluminum nitrate solution. It is speculated that the incorporation of boron in the framework is related to the hydrophobicity of the sparteinium cation.

2.1 Introduction

SSZ-24 is a high-silica molecular sieve isostructural with AlPO4–5 (AFI) [1,2] and was first synthesized by Zones and coworkers [3,4] in its pure–silica form using N,N,N–trimethyl–1–adamantyl ammonium (I) hydroxide as the structure-directing agent. The isomorphous substitution of other atoms for framework Si proved difficult until the substitution of B for Si was achieved using a calcined form of boron–substituted zeolite beta (BEA) as the source of boron atoms [5,6]. Here we report a new method for the synthesis of SSZ-24 and boron-substituted SSZ-24 using N(16) methylsparteinium (II) as structure-directing agent and using sodium borate as the source of boron. This paper describes the synthesis and characterization of these materials and compares our results to those reported previously. Additionally, we speculate why the incorporation of B in the framework is easily accomplished.
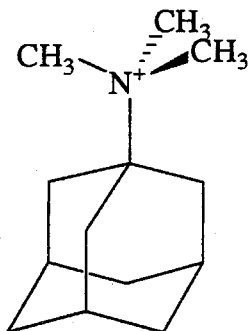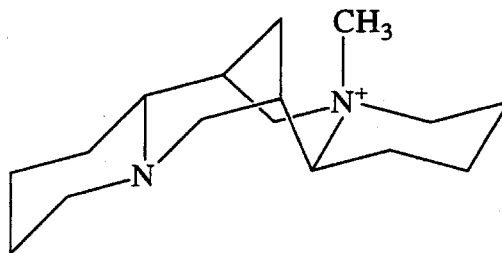
I   II

2.2 Experimental

2.2.1 Synthesis of the Organic Structure-directing Agent

N(16) methylsparteinium iodide was synthesized from (–)sparteine using the following procedure: 21.1 g (50 mmol) of (–)sparteine sulphate pentahydrate (Aldrich) were added to 50 ml of a 3M NaOH solution. The suspension was stirred until the crystals were completely dissolved and two phases were formed. The organic phase was extracted three times with 25 ml portions of ethyl ether and the combined extracts were dried over solid KOH (85%) and filtered. The solvent was then evaporated at room temperature under vacuum. The recovered (–)sparteine was dissolved in 100 ml of acetone containing 28.3 g (1.5 equivalents) of methyl iodide. The reaction mixture was stirred in the dark for 24 h and the yellow solid product formed was filtered after the addition of 50 ml of ethyl ether. The recovered solid (15.2 g, 81% yield) was recrystallized twice in 2-propanol by adding ethyl acetate until turbidity to give 13.7 g (73% yield) of slightly yellow crystals. Analyses: Calculated for $C_{16}H_{29}N_2I$: C, 51.1%; H, 7.7%; N, 7.4%; I, 33.8%. Found: C, 51.0%; H, 7.9%; N, 7.4%; I, 33.7%. The IR spectrum of this material agreed with a previously reported spectrum for N(16) methylsparteinium iodide [7]. The preferred conformation of methylsparteinium, as found by X-ray crystallography is shown in II [7].

Amberlite IRA-400(Cl) (Aldrich) anion exchange resin, exchanged to the bromide form, was used to convert the iodide salt prepared as above to the corresponding bromide. Typically, 7.52 g of N(16) methylsparteinium iodide (20 mmol) were dissolved in 50 ml of water and exchanged in an ion exchange column containing 100 ml of anion exchange resin (with 140 mmol of exchange capacity). After washing the column with an additional 200 ml of distilled water, the aqueous solution obtained was evaporated in a rotavapor until dryness and recrystallized as described before from 2-propanol–ethyl acetate. The elemental analyses indicated a yield of 95% for the bromide form. Similarly, the hydroxide

form of II was obtained using Amberlite IRA-400(OH) anion exchange resin. After exchange, the aqueous solution was concentrated to 50 ml. The yield was 92.8% based on titration of the resultant solution and gives a concentration of 0.371 M of N(16)-methylsparteinium hydroxide.

2.2.1 Zeolite Synthesis

SSZ-24 was synthesized from gels of composition:

$$50 \, SiO_2 : x \, B_2O_3 : 10 \, R: y \, NaOH : z \, H_2O$$
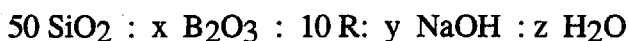
where R is molecule II in the bromide or hydroxide form, with $0<x<2$, $5<y<10$, and $2500<z<5000$. The synthesis temperatures were 150 °C and 175 °C. A typical synthesis with a gel composition where x=2, y=5 and z=2500 was carried out as follows: 0.27 g of sodium borate decahydrate ($Na_2B_4O_7 \cdot 10 \, H_2O$, Fisher) were dissolved in 15 g of distilled water. After dissolution of the borate, 1.1 g of N(16)methylsparteinium bromide, 0.13 g of NaOH (50% wt/wt aqueous solution) and 1 g of fumed silica (Cab-O-Sil, M-5) were then added and stirred until a homogeneous gel was obtained. The mixture was subsequently sealed in pure-silica glass tubes (12 mm I.D., ~75 mm long). About 10% of the tube volume was left empty. For certain synthesis, 2.5 mg of as-synthesized boron-substituted zeolite beta [5,8] (amount equal to 1~2% of recovered solids) were added to the tube prior to the addition of the synthesis mixture, and the gel was agitated after sealing to disperse the crystals evenly in the solution. The synthesis was carried out statically in a convection oven at 175 °C for 10 days. The white crystals were recovered by filtration and dried in air at room temperature. Seeding the gel with as-synthesized SSZ-24 or addition of as-synthesized, boron–substituted zeolite beta [8] was found to reduce the formation of Kenyaite, a layered sodium silicate that was often found as impurity in the final product. Careful recrystallization of the structure-directing agent was necessary to obtain pure SSZ–24 materials.

To remove the occluded organic molecule, the sample was heated at a rate of 5 °C min^{-1} to 650 °C in air and kept at this temperature for at least one hour. The removal of tetrahedral framework boron and insertion of aluminum was accomplished as follows: the calcined sample (~0.25 g) was stirred for 24 h in 12.5 ml of an aqueous solution of $Al(NO_3)_3$ (2% w/w) at 100 °C, filtered, washed with distilled water and dried in air at room temperature.

2.2.3 Analytical Methods

X-ray powder diffraction (XRD) patterns were collected on a Scintag XDS 2000 diffractometer using Cu-Kα radiation and a solid-state Ge detector. The diffraction profiles were scanned over the range of $2° < 2\Theta < 50°$ in steps of 0.02° with a count time of 15 s at each point. Fluorophologopite mica (Standard Reference Material 675, National Bureau of Standards) was used as an external standard. Fourier-Transform infrared (FTIR) spectroscopy was carried out on a Nicolet System 800. The samples were prepared using the KBr pellet technique. Thermogravimetric analyses (TGA) were performed on a DuPont 951 thermogravimetric analyzer with a heating rate of 5 °C min-1. Nitrogen adsorption isotherms were collected at 77 K on an Omnisorp 100 analyzer. The scanning electron micrographs (SEM) were recorded on a Camscan series 2-LV scanning electron microscope. Elemental analyses were performed at Galbraith Laboratories Inc., Knoxville, Tennessee.

Liquid ^{13}C NMR spectra were collected on a GE 300 NMR QE Plus spectrometer. Solid-state NMR spectra were collected on a Bruker AM 300 spectrometer equipped with a Bruker solid-state cross-polarization, magic angle spinning (CP/MAS) accessory. The ^{13}C spectra (75.5 MHz, 500 scans) were recorded with a pulse length of 4 μs and a spinning rate of 3 kHz and were referenced to an adamantane standard (downfield resonance at 38.4 ppm). ^{29}Si spectra (59.63 MHz) were collected using MAS (1600 scans) and CP/MAS

(800 scans) and were referenced to a tetrakis(trimethylsilyl)silane standard (downfield resonance at -10.053 ppm). The ^{27}Al spectra (78.2 MHz) were recorded using MAS at a spinning rate of 5 kHz and were referenced to a 1M aqueous aluminum nitrate solution (resonance at 0 ppm), and the ^{11}B spectra (96.3 MHz, 200 scans) were recorded using MAS at a spinning rate of 4 kHz and were referenced to an aqueous solution of 1M boric acid (resonance at 0 ppm). Samples were packed into ZrO_2 rotors.

2.3 Results And Discussion

Figure 2.1 shows the XRD pattern obtained from the calcined boron-substituted SSZ-24 sample synthesized here. No crystalline impurities are observed in this sample. The lattice parameters of the as-synthesized and calcined materials are in agreement with previously reported data (Table 2.1). The boron containing sample shows smaller unit cell lattice parameters than the pure-silica sample as expected. The presence of the methylsparteinium molecule was confirmed from the ^{13}C MAS NMR spectrum shown in Figure 2.2. Although not all the peaks are resolved in the MAS spectrum, comparison of the MAS spectrum to the liquid ^{13}C NMR spectrum (Figure 2.3) shows that molecule II did not decompose under synthesis conditions. The static 13C NMR spectrum of the as-synthesized material contains only two broad peaks at 28 ppm and 70 ppm, indicating that at room temperature, the structure–directing agent is rigidly held inside the zeolite pores.

The crystallization of SSZ-24 using II was faster (10 days) than the crystallization of SSZ-24 using I [2] (21 days), but longer than the rate of crystallization of SSZ-24 using I if calcined B-subsituted zeolite beta is used as the source of silica (3 days) [5]. The differences in the rate of crystallization may be due to differences in the synthesis conditions and source of silica. We were unable to synthesize SSZ-24 with II using the calcined form of zeolite beta as the source of silica as reported by Van Nordstrand [5]. It

seems that early in the zeolite synthesis the organic molecule (II) is adsorbed inside the pores of zeolite beta where it stabilizes the organic-inorganic composite. This stabilization stops any further transformation of the zeolite beta framework.

The ^{11}B MAS NMR spectrum of the as-synthesized sample shows only one strong peak at -3 ppm, indicating that boron is located only in tetrahedrally coordinated environments. From elemental analysis, it is found that the fraction of isomorphous substitution of boron for silicon in the sample is weakly dependent on the SiO_2/B_2O_3 ratio in the synthesis mixture under the conditions used in this work (Table 2.2). The fraction of boron incorporation in the zeolite framework in the samples prepared in this work is the same as the amount reported for SSZ-24 synthesized using boron-substituted zeolite beta as the source of tetrahedral atoms [5]. This can be understood in terms of the need for a counter-balancing cation in the zeolite pores for each boron atom that is incorporated in the framework. It has been shown that the counter-balancing cation in boron substituted high-silica MFI is the tetrapropylammonium ion, and that the sodium present in the synthesis gel is not found inside the crystals [14]. Therefore, the amount of isomorphous substitution of boron for silicon in SSZ-24 seems to be limited by the number of N(16) methylsparteinium molecules occluded inside the zeolite pores per unit cell. The ^{29}Si MAS of the as-synthesized, pure-silica sample (Figure 2.4A) shows two bands that can be assigned to Q^3 and Q^4 peaks, suggesting that the charge of the organic structure-directing agent is balanced by a defect in the structure of the zeolite. The ratio of the areas of the Q^3 and Q^4 peaks in the ^{29}Si MAS of the as-synthesized, boron-substituted sample (Figure 2.4B) is smaller than the ratio of the pure-silica sample (Fig. 2.4A). This is the expected result of the partial substitution of boron for silicon in the framework of SSZ-24. The small Q^3 shoulder of the boron-substituted sample may come from silanol groups at the surface of the crystals. These results suggest that even in the presence of boron in the gel, some of the charge of the structure-directing agent may be balanced by defects in the zeolite pores.

These data are in agreement with previous studies of ZSM-5 reported by Dessau et al. [9]. They reported that for ZSM-5 samples synthesized using tetrapropylammonium and a $SiO_2/Al_2O_3 > 20$, a fraction of the charge of the organic structure-directing agent is balanced by defects in the structure of ZSM–5.

The TGA of the as-synthesized samples of SSZ-24 show a weight loss of 10% at temperatures above 200 °C that is assigned to the decomposition of the organic molecules occluded in zeolite pores [6]. This weight loss is equivalent to at most 0.67 organic molecules per unit cell (calculated as $C_{16}H_{29}N_2$), roughly in agreement with the amount of boron incorporated in the framework (Table 2.2). The TGA data of calcined, boron–substituted SSZ-24 and pure–silica SSZ-24 show a water weight loss of 3%, indicating that these materials are hydrophobic.

The morphology of the crystals is dependent on the presence or absence of boron in the synthesis mixture (Figure 2.5). The samples synthesized in the presence of boron (Figure 2.5A) show a characteristic starburst morphology, very different from the pure-silica samples (Figure 2.5B) and from pure-silica SSZ-24 synthesized using I as previously reported [2]. In addition to the morphologies indicated in Fig. 2.5, a small fraction of the boron–containing sample has the hexagonal shape shown in Fig. 2.5A and, similarly, a small fraction of the pure-silica sample crystallized with the starburst morphology.

FTIR spectra from the calcined, B–substituted SSZ-24 samples show the presence of a small band at 928 cm^{-1} that can be assigned to the symmetric stretching of the Si–O–B moiety (Figure 2.6). This band is found in other zeolites in which boron has been incorporated into the framework [11,12]. Additionally, an absorption band normally attributed to the formation of trigonal boron appears at 1400 cm^{-1} as expected from the loss of framework boron after direct calcination in air. The FTIR spectrum of pure-silica SSZ-24 is exactly like that reported previously [4].

The nitrogen isotherms of calcined, pure-silica SSZ-24, B-SSZ-24 and the sample treated with the $Al(NO_3)_3$ solution gave an adsorption capacity of 0.12 g of N_2 (g of zeolite)$^{-1}$ in agreement with the N_2 adsorption capacity of $AlPO_4$-5 [12] (Figure 2.7). Although direct air calcination of boron zeolites [12,14] leads to loss of framework boron that may be occluded in the zeolite pores, little effect on the microporosity was detected here.

After the treatment of the boron–containing zeolite with the aluminum nitrate solution, the ^{27}Al MAS NMR spectrum of the treated sample shows a strong peak at 52 ppm, which is assigned to tetrahedrally coordinated aluminum. Similar results were previously reported by Van Nordstrand et al. [5] for a SSZ-24 sample synthesized using boron-substituted zeolite beta as the source of silica. No boron is detected by ^{11}B MAS NMR in this sample after 100 scans. The unit cell of the zeolite increases upon loss of boron in agreement with the insertion of Al into the framework (Table 2.1). We were unable to directly synthesize the aluminum version of SSZ-24 by substitution of the sodium borate for an equivalent amount of sodium aluminate or aluminum nitrate (SiO_2/Al_2O_3=50) in the synthesis gel. The same limitations have been observed for the synthesis of SSZ-24 using I [5].

The method we outline here for preparing the samples of B-SSZ-24 and Al-SSZ-24 is more convenient than the procedure used by Zones and coworkers [5] because it does not involve the preparation of a highly active source of silica and boron (zeolite B-beta), which also requires the synthesis of another structure-directing agent. The reasons behind the boron incorporation in the framework using the derivative of sparteine and not the methylated form of adamantamine may have important consequences for the synthesis of new B-substituted molecular sieves. Recently, Ruiter et al. [14] indicated that the hydrophobicity of the structure-directing agent aids in the incorporation of boron in the framework of MFI. Our results are in agreement with their conclusions. The methylated

form of sparteine (II) has a positive charge surrounded by a large hydrophobic and relatively rigid organic environment, while the methylated form of adamantamine (I) contains the positive charge in a nitrogen atom that is separated from water molecules by only three methyl groups. It has been previously shown [15,16] that tetramethylammonium ions present predominantly hydrophilic character in aqueous solutions, i.e., they behave as hard ions, and that tetrapropylammonium ions have an effect that is characterized as hydrophobic according to the structure of water molecules around the cation. Therefore, it may be that the property of molecule II that allows the incorporation of boron into the framework of SSZ-24 is its hydrophobic organic surface.

Interestingly, the unit cell volume of the pure-silica and the boron-substituted samples of SSZ-24 increases after calcination of the as-synthesized samples. The volume increase of the unit cell may be due to the presence of attractive forces between the structure-directing agent and the zeolite framework which are eliminated upon calcination of the sample. However, because the largest increase in the unit cell volume was found in the pure-silica sample, it is possible that the increase in the cell volume may be also due to the annealing of the defects found in the framework of the pure-silica sample (Figure 2.4).

2.4 Conclusions

A new structure-directing agent, N(16) methylsparteinium bromide, has been used to synthesize SSZ-24. The organic molecule is located intact inside the zeolite pores. This new synthesis method allows the isomorphic substitution of boron for silicon in the framework using sodium borate as the boron reagent. The framework boron can be easily exchanged to aluminum by refluxing the calcined sample in an $Al(NO_3)_3$ solution. It is suggested that the incorporation of boron in the framework is related to the hydrophobicity of the structure-directing agent.

2.5 References

1. W.M. Meier and D.H. Olson, *Atlas of Zeolite Structure Types*, 3rd. revised Ed., Butterworths, Stoneham, MA, 1992.

2. R. Bialek, W.M. Meier, M.E. Davis, M.J. Annen, *Zeolites*, **11** (1991) 438.

3. S.I. Zones, US Pat. 4 665 110 (1987).

4. R.A. Van Nordstrand, D.S. Santilli, S.I. Zones, *ACS Symp. Ser,* **368**, 1988, pp. 236.

5. R.A. Van Nordstrand, D.S. Santilli, S.I. Zones in Occelli and H. Robson (Eds.), *Synthesis of Microporous Materials* Vol. I., Van Nordstrand Reinhold, New York, 1992, pp 373.

6. S.I. Zones, L.T. Yuen, Y. Nakagwa, R.A. Van Nordstrand and S.D. Toto in R. von Ballmos, J.B. Higgins, M.M.J. Treacy (Eds.), *Proceedings from the Ninth Zeolite Conference* Vol. I, Butterworth-Heinemann, Stoneham, MA, 1993, pp 163.

7. U. Majchrzak-Kuczynska, A.E. Koziol, K. Langowska, M. Wiewiorowski, *Bull. Polish Acad. Sc.,* **32**(1984) 233.

8. S.I. Zones, D.L. Holtermann, L.W. Jossesns, D.S. Santilli, A. Rainis, J.N. Ziemer, Pat Appl. WO 91/00777, 1991.

9. R.M. Dessau, K.D. Smith, G.T. Kerr, G.L. Woolery, L.B. Alemany, *J. Catal.,* **104** (1987) 484.

10. C. Cordurier, A. Auroux, J.C. Vedrine, R.D. Forlee, L. Abrams, R.D. Shannon, *J. Catal.,* **108** (1987) 1.

11. R. de Ruiter, A.P.M. Kentgens, J. Grootendrost, J.C. Jansen and H. van Bekkum, *Zeolites*, **13** (1993) 128.

12. M.E. Davis, C. Montes, P.E. Hathaway, J.P. Arhancet, D.L. Hasha, J.M. Garces, *J. Am. Chem. Soc.*, **111** (1989) 3919.

13. B. Unger, K.P. Wendlandt, H. Tougar, W. Schuieger, K.H. Bergk, E. Brunner, *J. Chem. Soc. Faraday Trans.*, **87** (1991) 3099.

14. R. de Ruiter, J.C. Jansen, H. van Bekkum, *Zeolites*, **12** (1992) 56.

15. F. Franks, Water, *The Royal Society of Chemistry*, London, 1983.

16. A. Shimizu and Y. Taniguchi, *Bull. Chem. Soc. Jpn.*, **63** (1990) 3295.
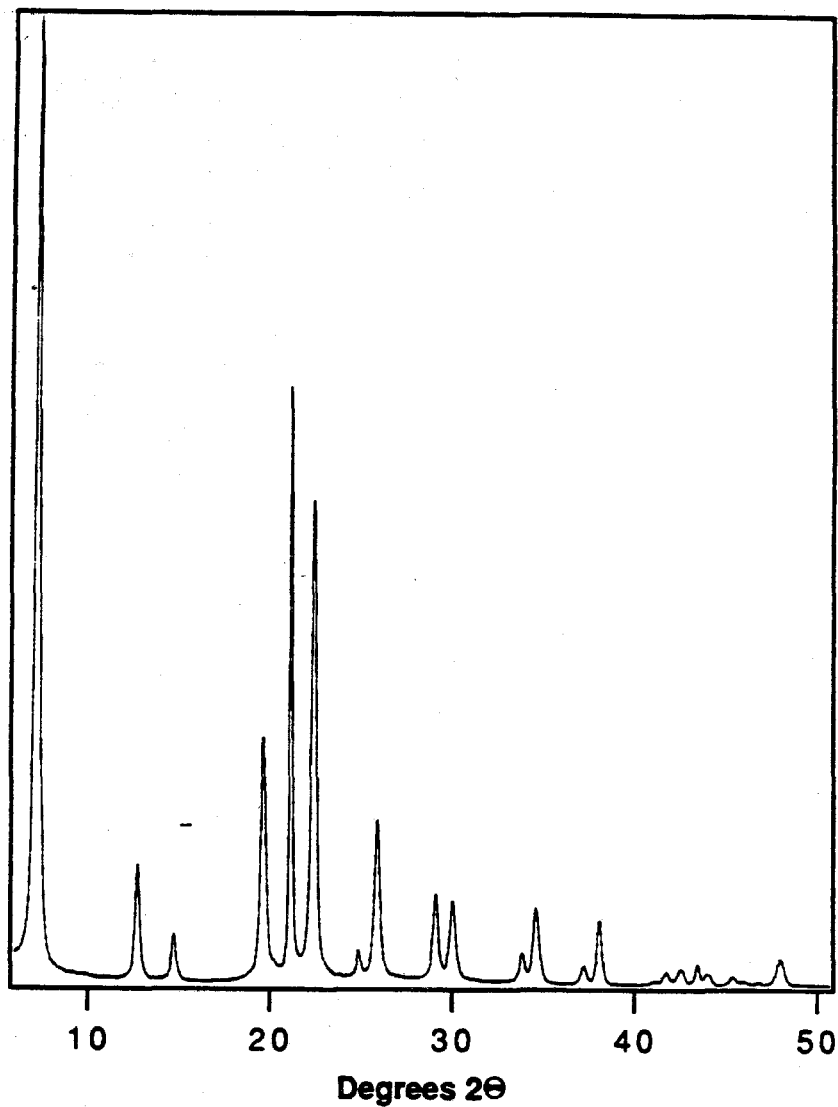
Figure 2.1   X-ray powder diffraction pattern of a calcined sample of B-SSZ-24 prepared using N(16) methylsparteinium bromide as structure directing agent (Cu Kα radiation).
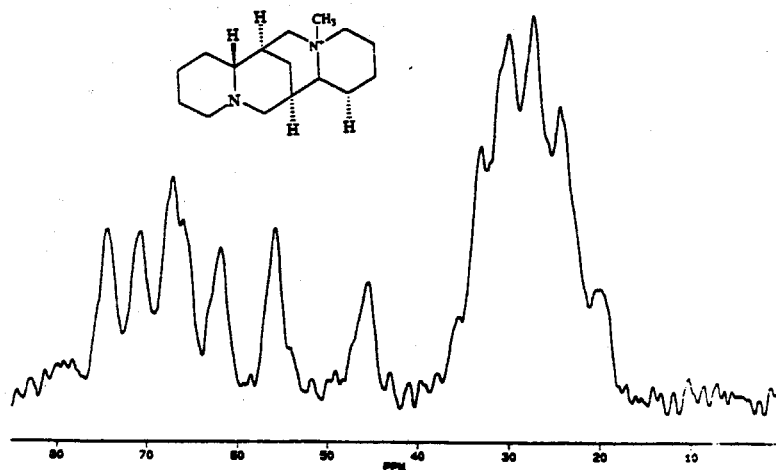
Figure 2.2 ^{13}C MAS NMR spectrum of N(16) methylsparteinium inside the pores of SSZ-24.
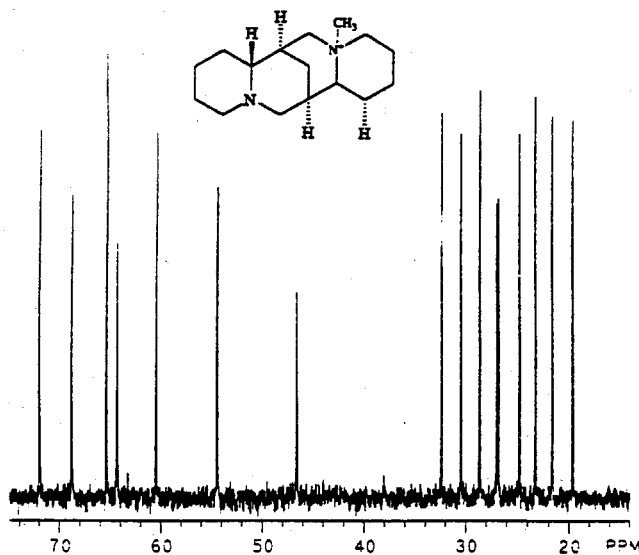
Figure 2.3 ^{13}C NMR spectrum of N(16) methylsparteinium bromide in CDCl$_3$.
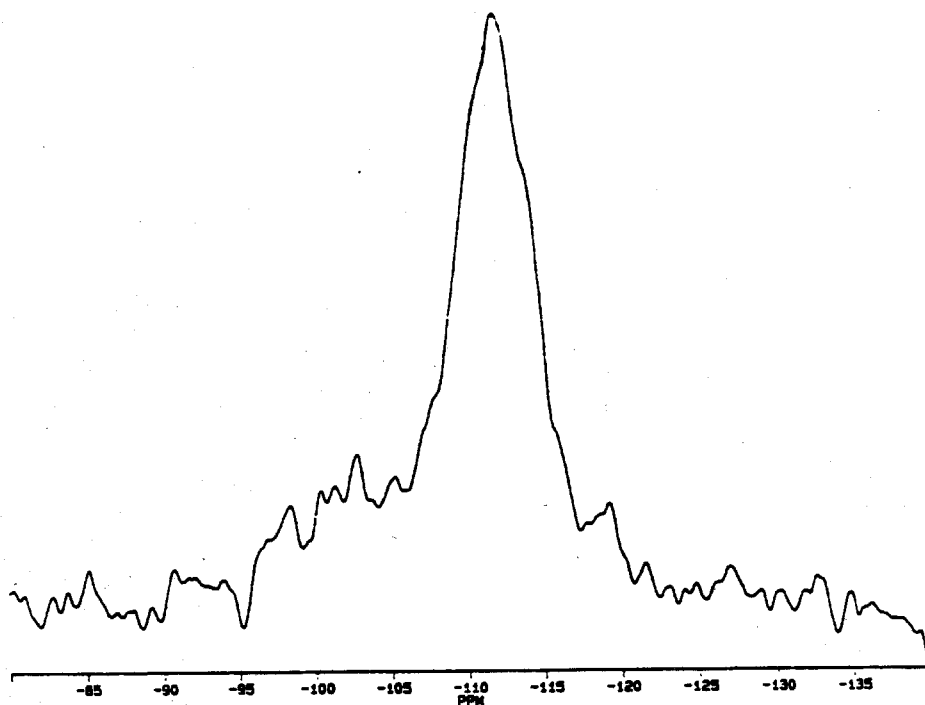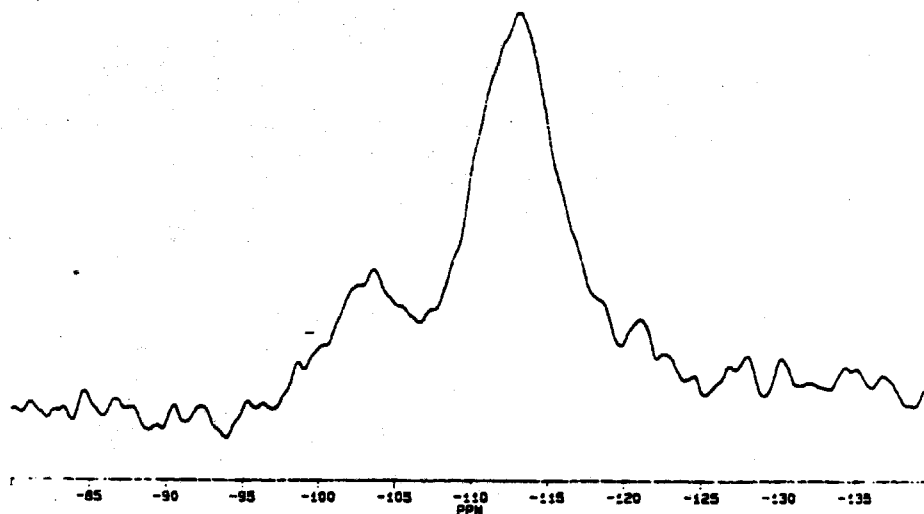
Figure 2.4 (A) ^{29}Si MAS NMR spectrum of an as-synthesized pure-silica sample of SSZ-24. (B) ^{29}Si MAS NMR spectrum of an as-synthesized boron-substituted sample of SSZ-24.
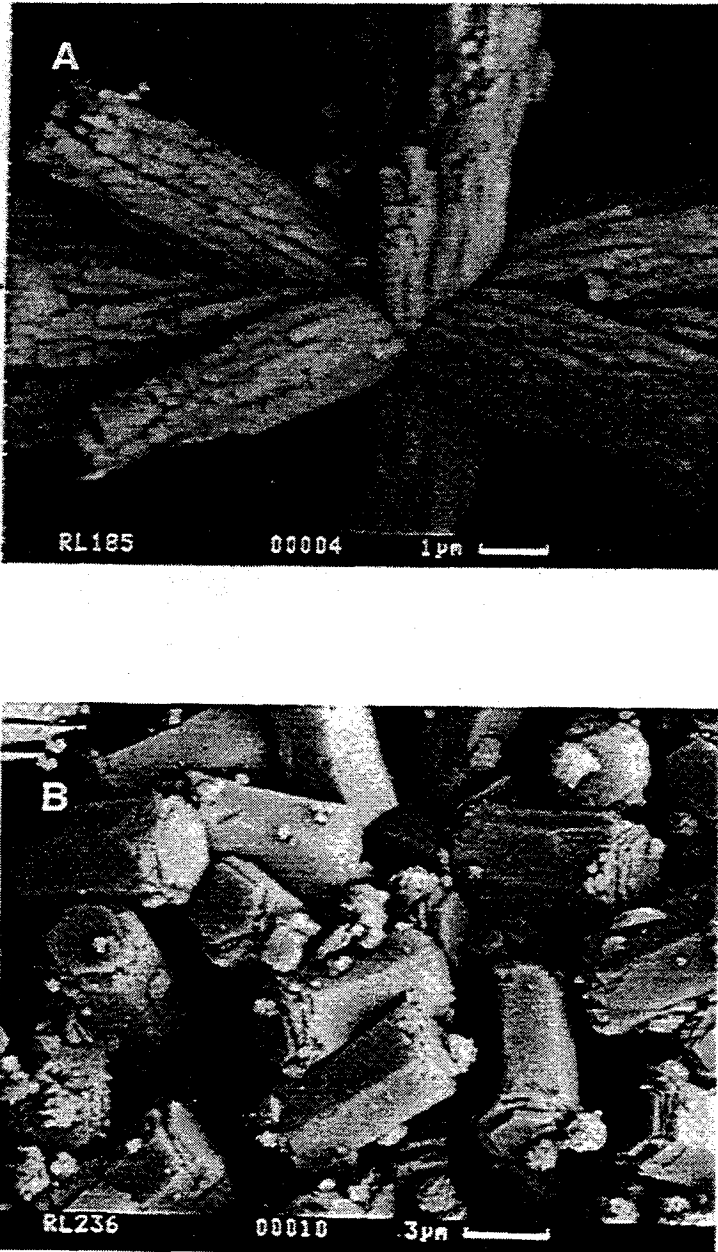
Figure 2.5   Scaning electron micrographs of SSZ-24. The starburst morphology (A) is

obtained when boron is included in the synthesis mixture.   The hexagonal crystal

morphology (B) is obtained from pure-silica synthesis gels. The second morphology in

(B) is Kenyaite.
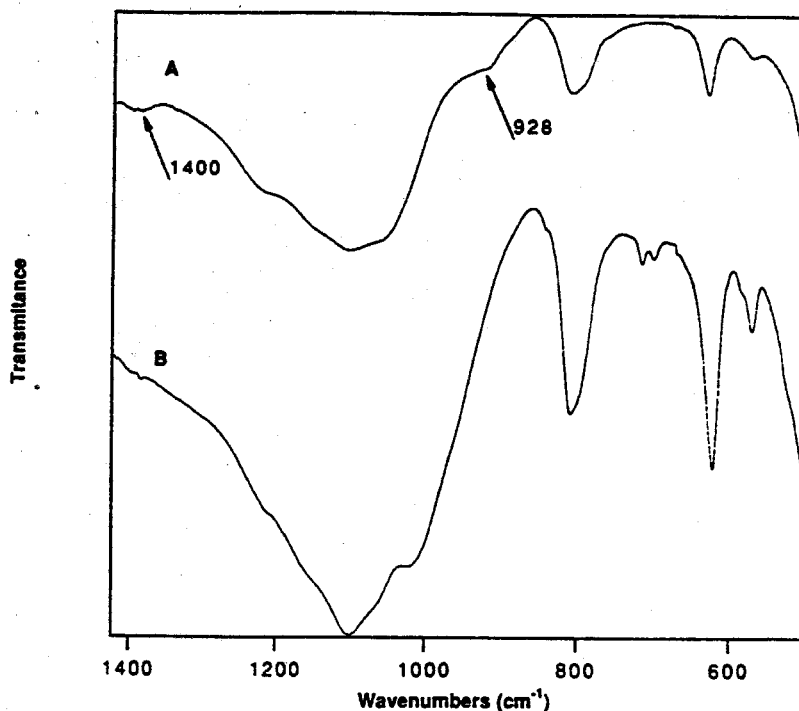
Figure 2.6   FTIR spectra of a calcined, boron–substituted SSZ-24 (A) and of pure-silica SSZ-24 (B). The presence of a band at 928 cm^{-1} is indicative of the presence of boron in tetrahedral coordination in the zeolite framework in (A). The band at 1400 cm^{-1} is assigned to trigonal boron formed after calcination of the sample.
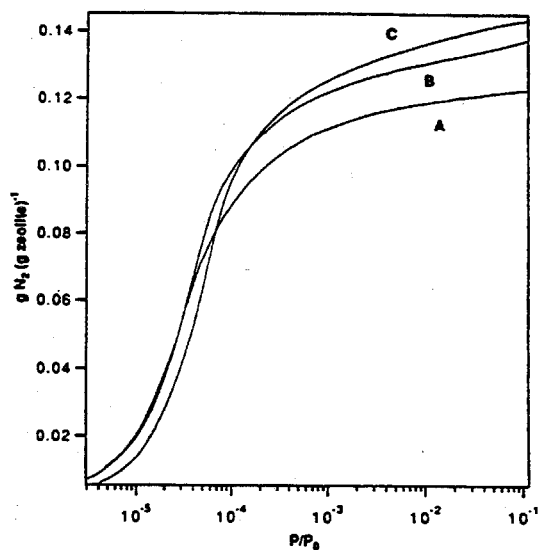
Figure 2.7   Nitrogen adsorption isotherms at 77 K of calcined samples of (A) pure-silica SSZ-24, (B) of B-SSZ-24 and (C) aluminum treated SSZ-24.

Table 2.1 Unit cell lattice parameters for SSZ-24 (hexagonal unit cell with standard deviation in parenthesis).

Material	a (Å)	c (Å)	Unit Cell Volume (Å^3)	Reference
SSZ-24[a] As synthesized	13.645(4)	8.283(3)	1337	This work
SSZ-24[a] Calcined	13.665(4)	8.322(4)	1345	This work
B-SSZ-24[a] As synthesized	13.592(2)	8.266(2)	1322	This work
B-SSZ-24[a] Calcined	13.592(3)	8.284(3)	1325	This work
Al-SSZ-24[a] Calcined	13.634(2)	8.327(2)	1341	This work
SSZ-24[a] As synthesized	13.60	8.28	1326	2
SSZ-24[a] Calcined	13.67	8.33	1348	2
B-SSZ-24[a] Calcined	13.61	8.3	1331	5
Al-SSZ-24[a] Calcined	13.68	8.34	1351	5

a.   Pure SiO_2 polymorph

Table 2.2 Boron concentration in the synthesis gel and calcined SSZ-24 samples using N(16) methylsparteinium bromide as structure–directing agent.[a]

SiO_2/B_2O_3 in synthesis gel	SiO_2/B_2O_3 from elemental analysis	Boron atoms per unit cell
50	106	0.46
50[b]	116	0.42
25	93	0.51
12.5	82	0.58

a.   The composition of the synthesis gel was 50 SiO_2 : x B_2O_3 : 10 R : 5 NaOH : 2500 H_2O, where R is the structure-directing agent. Synthesis temperature was 175 °C.
b.   In this gel the structure-direting agent was in the hydroxide form.

Chapter Three

SSZ-26 and SSZ-33: Two Molecular Sieves with Intersecting 10- and 12-Ring Pores

[Raul F. Lobo, Ming Pan, Ignatius Chan, Hong-Xin Li, Ronald C. Medrud,

Stacey I. Zones, Peter A. Crozier, Mark E. Davis, *Science*, **262** (1993) 1543-1546]

SSZ-26 and SSZ-33: Two Molecular Sieves with Intersecting 10- and 12-Ring Pores

Raul F. Lobo, Ming Pan[†], Ignatius Chan[¶], Hong-Xin Li, Ronald C. Medrud,[¶]

Stacey I. Zones,[¶] Peter A. Crozier,[†] Mark E. Davis

Chemical Engineering, California Institute of Technology,

Pasadena, CA 91125

[†]*Center for Solid State Science, Arizona State University*

Tempe, AZ 85287-1704

[¶]*Chevron Research and Technology Company, 100 Chevron Way,*

Richmond, CA 94802-0627

Abstract

The framework structures of two closely related novel molecular sieves, SSZ-26 and SSZ-33, are described. These materials possess a previously missing but highly desired structural feature in a group of industrially significant zeolites. They contain a three-dimensional pore system that provides access to the crystal interior through both 10- and 12-rings. This property is a consequence of the organic structure-directing agents used in the synthesis of these materials. These materials are the first examples of the purposeful design of a micropore architecture. Both SSZ-26 and SSZ-33 contain the 4–4=1 building unit that had been previously found only in natural zeolites.

3.1 Introduction

Inorganic molecular sieves, such as zeolites, are extensively used in catalytic and separation processes, especially in the petrochemical and refining industries (1, 2). New large-pore materials, those with pores bounded by rings comprised of 12 tetrahedral (T) atoms (Si, Al, B, and so forth) with an open pore diameter of ~7 Å (3,4), can be used for controlled shape-selective catalysis of molecules with relatively complex architectures. Large-pore materials with intersecting channels also have increased resistance to fouling and enhanced intracrystalline diffusion properties over materials with unidimensional channels; however, only a few zeolites are known with both large and intersecting pores. Zeolites Y and beta have intersecting 12-ring pores and have found extensive application in refinery processes, as also has zeolite ZSM-5, which has intersecting 10-ring (medium) pores. Additionally, as environmental factors play more significant roles in the design of new process chemistries, zeolite solid acids — due to their ease of handling and disposal— are receiving close attention as possible substitutes of the currently used liquid acids.

A molecular sieve with intersecting 10- and 12-ring pores is likely to offer a combination of reaction activity, selectivity, and stability not found in any other material (4). Only recently, a zeolite with intersecting 10- and 12-ring pores was found in the rare mineral boggsite (5). Additionally, the synthetic material NU-87 (6), has a 10- and 12-ring pore system, but access to the crystal interior can only be achieved through the 10-ring pores. Thus, this type of zeolite is of extreme interest for catalytic applications in the petrochemical industry, but until now was only available in the minute quantities of boggsite, too low for even laboratory-scale evaluation.

Several factors prompted us to study the structures of the synthetic zeolites SSZ-26 and the related SSZ-33. First, preliminary sorption experiments indicated that these

materials had a multidimensional pore system with at least one of the pores being a 12-ring. Second, the structure-directing agents used for the synthesis of both materials were carefully chosen such that they would form a multidimensional pore system (7). Additionally, the concepts of structure-direction could be tested if a close relation between the structure-directing agent and the pore geometry could be found.

3.2   Results And Discussion

SSZ-26 and SSZ-33 (7-9) are synthesized under hydrothermal conditions with the use of organic structure-directing agents **I** and **II** respectively. SSZ-26 is typically synthesized with a SiO_2/Al_2O_3 ratio of 20-50 while SSZ-33 is normally crystallized with a SiO_2/B_2O_3 ratio of ~30. Similarities in their X-ray powder diffraction (XRD) patterns, sorption data, and catalytic properties suggested that these two materials have related crystal structures.

I   **II**
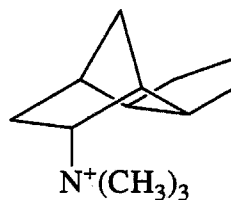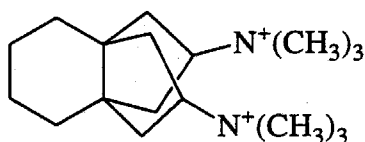
The synchrotron XRD pattern of SSZ-33 showed a combination of sharp and broad features that suggested the presence of stacking disorder in the structure. The sharp reflections were indexed on an orthorhombic unit cell with dimensions a=13.26 Å, b=12.33 Å, and c=21.08 Å. Except for the (0 1 0) reflection, the remaining reflections were of the form (h 3n l), n=0,1,2, which is indicative of shears associated with faulting of ± 1/3 b. This kind of faulting is also present in zeolite beta (10) and in NU-86 (11).

Single-crystal electron diffraction (ED) patterns along one zone axis contained sharp diffraction intensities for every third column of reflections and streakings for the remaining reflections. Such characteristic intensity distribution is a manifestation of a layered structure with heavy stacking faults as a result of the presence of both ABABAB... and ABCABC... stacking sequences. The lateral displacement for successive layers is one third of the intralayer spacing. This observation is consistent with the XRD data. The ED data obtained by systematically tilting the crystal showed that the crystallites had an orthorhombic structure with lattice parameters similar to those obtained by XRD.

A low-dose high resolution electron micrograph (HREM) recorded in the [100] projection (Fig. 3.1A) shows direct evidence for the two different stacking sequences deduced from the XRD and ED patterns (12). Careful analysis of the image intensities indicates that the main pores (large bright dots) are 10-rings and the secondary features (small bright dots) represent eight 5- and two 6-rings in the structure (13,14).

Two related structures consistent with the unit cell dimensions and physical properties of SSZ-33 were constructed. The structures can be thought of as being formed by sheets related by translation of [1/2, ±1/3, 1/2] (using the basis vectors of the orthorhombic unit cell described above). If the sheets are arranged with alternate translations (ABABAB... stacking sequence) a structure with orthorhombic symmetry is formed. By analogy to the nomenclature developed for zeolite beta by Newsam *et al.* (10), this structure is called polymorph A and belongs to the space group *Pmna* (no. 53) with unit cell dimensions $a=13.26$ Å, $b=12.33$ Å, and $c=21.08$ Å (Fig. 3.2A and 3.2B). If the sheets are arranged with translations always in the same direction (ABCABC... stacking sequence), a monoclinic polymorph B is formed with space group *B 2/m* (no. 12) and unit cell dimensions $a=13.26$ Å, $b=12.33$ Å, $c=22.62$ Å, and $\alpha=68.7^{\circ}$ (Fig. 3.2C and 2D). Both polymorphs have a three-dimensional pore system formed by intersecting 10- and 12-ring pores. The atomic coordinates of the oxygen and T atoms were optimized

with distance least-squares refinement [DLS-76, (15,16)] (see Tables 3.1 and 3.2), and HREM images of each polymorph were simulated and compared to the experimental data. Very good agreement is observed between the model for polymorph A and the experimental image (Fig. 3.1B). The synchrotron XRD, ED and the HREM (Fig. 3.1A) indicate, however, that SSZ-33 is an intergrowth of these two structures. Simulated XRD patterns incorporating the disorder [using DIFFaX (17)] are illustrated in Fig. 3.3. Comparison of the simulated to the experimental XRD patterns indicates that SSZ-33 is an intergrowth of polymorph A and polymorph B with a predominance of polymorph B and with a fault probability close to 30% (Fig. 3.4).

For the zeolite SSZ-26, the isomorphous substitution of Al for B creates an increase in the unit cell dimensions due to the longer Al–O bond (1. 72 Å) compared to the B–O bond (1.48 Å). Based on the indexing of the sharp reflections of the XRD pattern of SSZ-26, the unit cell dimensions of polymorph A are a= 13.43 Å, b= 12.40 Å, and c= 21.23 Å, and the unit cell dimensions of polymorph B are a= 13.43 Å, b= 12.40 Å, c= 22.78 Å, and α= 68.8°. Comparison of the simulated and experimental XRD patterns indicated that there is also a predominance of polymorph B in SSZ-26, but the faulting probability is close to 15% (Fig. 3.5). Complete details of the structure solution of SSZ-33 and SSZ-26 will be given elsewhere (18).

Unlike zeolite beta, which crystallizes with a stacking probability of 50% whether synthesized as borosilicate, aluminosilicate or gallosilicate (10), the existence of SSZ-26 and SSZ-33 suggests that materials with a fault probability from 0 to 100% may be prepared.

3.3 Conclusions

These materials fill a long existing gap in the type of molecular sieve materials available. SSZ-26 and SSZ-33 are the first examples of molecular sieves whose multidimensional pore systems have been formed by the purposeful design of their organic structure-directing agents (7). Experimentally, it has been observed that the structure-directing agent is intact inside the pores of SSZ-26 (7) and that the number of molecules per unit cell is the same as the number of pore intersections. Additionally, molecular simulations indicate that the structure-directing agent of SSZ-26 conforms to the geometry of the intersection of the 10- and 12-ring pores (18) as originally proposed (19). The geometry of the organic molecule is the most important factor in obtaining a pore system intermediate in size to the zeolites ZSM-5 and beta. In addition to the novel pore system, the frameworks of SSZ-26 and SSZ-33 are the first high-silica molecular sieves to contain the 4-4=1 secondary building unit (3). This unit has only been found in natural zeolites prior to the synthesis of SSZ-26. Numerous natural zeolites such as heulandite, stilbite and boggsite have the 4-4=1 building unit among their structural building blocks and have not been readily synthesized under hydrothermal conditions in the laboratory. The synthesis of SSZ-26 and SSZ-33 suggests that other large-pore materials that include this unit may be synthesized.

3.4 References And Notes

1.   J.M. Newsam, in *Solid State Chemistry: Compounds*, A. K. Cheetham and P. Day Eds. (Oxford Univ. Press, New York, 1992).

2.   M.E. Davis, *Chem. Ind. (London)*, 137 (1992).

3. W.M. Meier and D.H. Olson, *Atlas of Zeolite Structure Types* Butterworths-Heineman, Stoneham, MA, (1992).

4. M.E. Davis and R. F. Lobo, *Chem. Mater.* **4**, 756 (1992).

5. J.J. Pluth and J.V. Smith, *Am. Miner.* **75**, 501 (1990).

6. M.D. Shannon, J.L. Casci, P.A. Cox and S.J. Andrews, *Nature,* **353**, 417 (1991).

7. S.I. Zones, M.M. Olmstead, D.S. Santilli, *J. Am. Chem. Soc.*, **114**, 4195 (1992).

8. S.I. Zones *et al.*, U.S. Patent 4,910,006 (1990)

9. S.I. Zones, U.S. Patent 4,963,337 (1990)

10. J.M. Newsam, M.M.J. Treacy, W.T. Koetsier, C.B. de Gruyter, *Proc. R. Soc. London Ser. A.* **420**, 375 (1988).

11. M.D. Shannon, in *Proceedings of the 9th International Zeolites Conference*, R. von Ballmoos, J.B. Higgins, M.M. Treacy Eds. (Butterworth-Heinemann, Stoneham MA, 1993), Vol. 1, pp 389-398.

12. M. Pan and P.A. Crozier, *Ultramicroscopy,* **48** (1993) 322.

13. M. Pan and P.A. Crozier, *Ultramicroscopy*, in press.

14. M. Pan *et al.*, in preparation.

15. Ch. Baerlocher, A. Hepp, W.M. Meier. *DLS-76,* (Institut für Kristallographie, ETH, Zürich, 1976). The weighted agreement values for polymorph A were R=0.0013, σ=0.007 and for polymorph B were R=0.001, σ=0.005. The unit cell dimensions were held constant during the optimization by using the values obtained from the indexing of the synchrotron XRD pattern of SSZ-33. <T–O>=1.60 Å (assuming Si:B=15, Si–O=1.605 Å (10) and B–O=1.48 Å).

16. The distance least-square refinement and the simulation of the XRD patterns of polymorph A and polymorph B were carried out with the program CERIUS 3.1 from Molecular Simulations.

17. M.M.J. Treacy, M.W. Deem, J.M. Newsam, *Proc. R. Soc. London Ser. A* **433**, 499 (1991). The simulations were carried out using the atom positions obtained from the distance least-square optimization of polymorph A. Silicon was used in all T atom positions.

18. Raul F. Lobo *et al.*, *J. Phys. Chem.* in press.

19. S.I. Zones and D.S. Santilli, in *Proceedings of the 9th International Zeolites Conference*, R. von Ballmoos, J.B. Higgins, M.M. Treacy Eds. Butterworth-Heinemann, Stoneham, MA (1993), Vol. 1, pp 171-179.
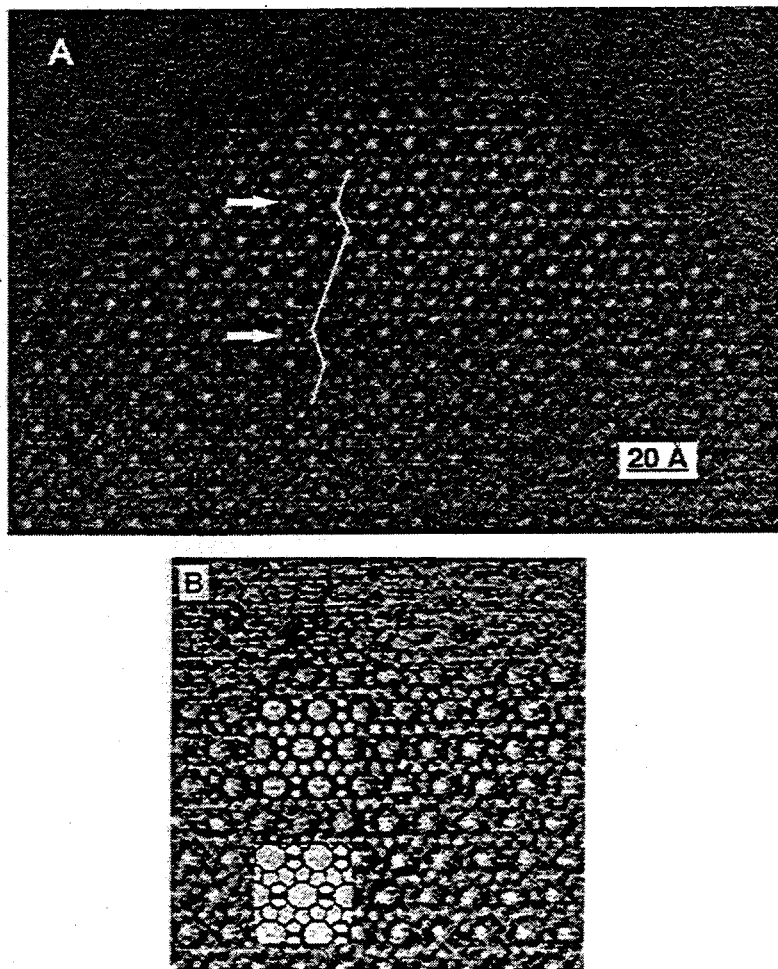
Figure 3.1 (A) Low-dose HREM image of a small crystal of SSZ-33 viewed along the [100] direction. Large bright dots in the image show the location of the 10-ring pores in this projection. Intergrowth of both polymorphs A (zig-zag line) and B (straight line) are indicated. This image was recorded digitally using a slow-scan CCD camera. (B) An enlarged HREM image showing the structure details of polymorph A. The simulated image and structure projection are top and bottom insets.
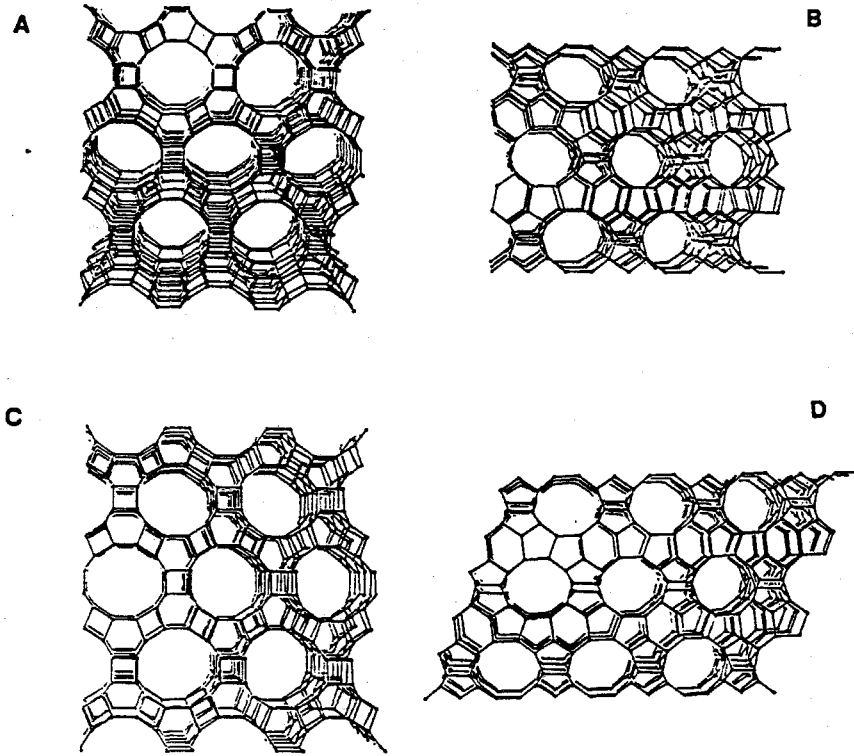
Figure 3.2 Framework structure of polymorph A viewed along the 12-ring pores (A) and along the 10-ring pores (**B**), and framework structure of polymorph B viewed along the 12-ring pores (**C**) and the 10-ring pores (**D**). The view along the 10-ring pores of polymorph A (**B**) shows the effect of the shears of ±1/3 b in alternate sequence (ABAB...stacking sequence). Similarly, the view along the 10-ring pores of polymorph B (**D**) shows the effect of consecutive shears of 1/3 b in one direction (ABCABC...stacking sequence).
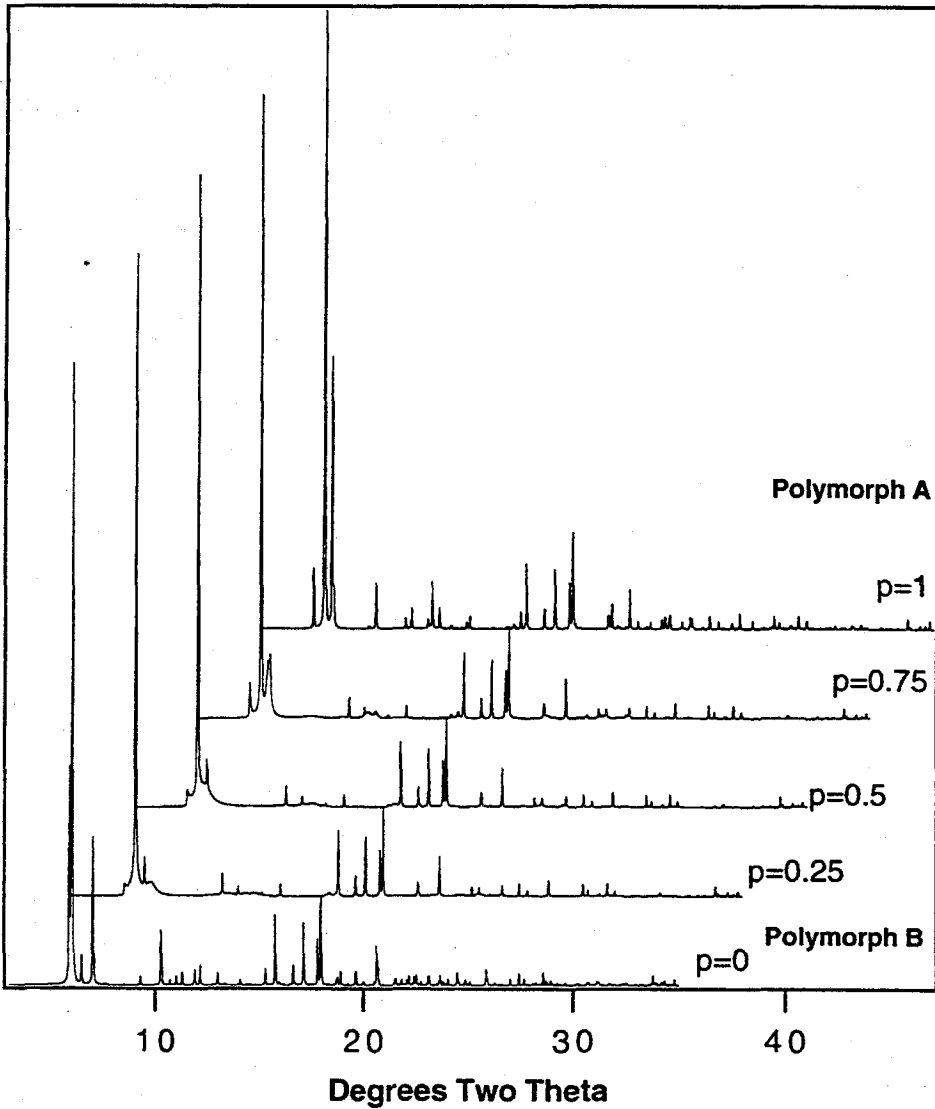
Figure 3.3   Effect of faulting on the XRD pattern. The faulting probability p is defined as the probability of reversal in the direction of stacking. A value of p=0 forms the end member polymorph B where all the layers are stacked in the same direction with respect to the previous one, and a value of p=1 gives the XRD pattern of polymorph A, where the direction of stacking is changed in each layer. The simulations were carried out with synchrotron radiation with a wavelength λ of 1.19505 Å.
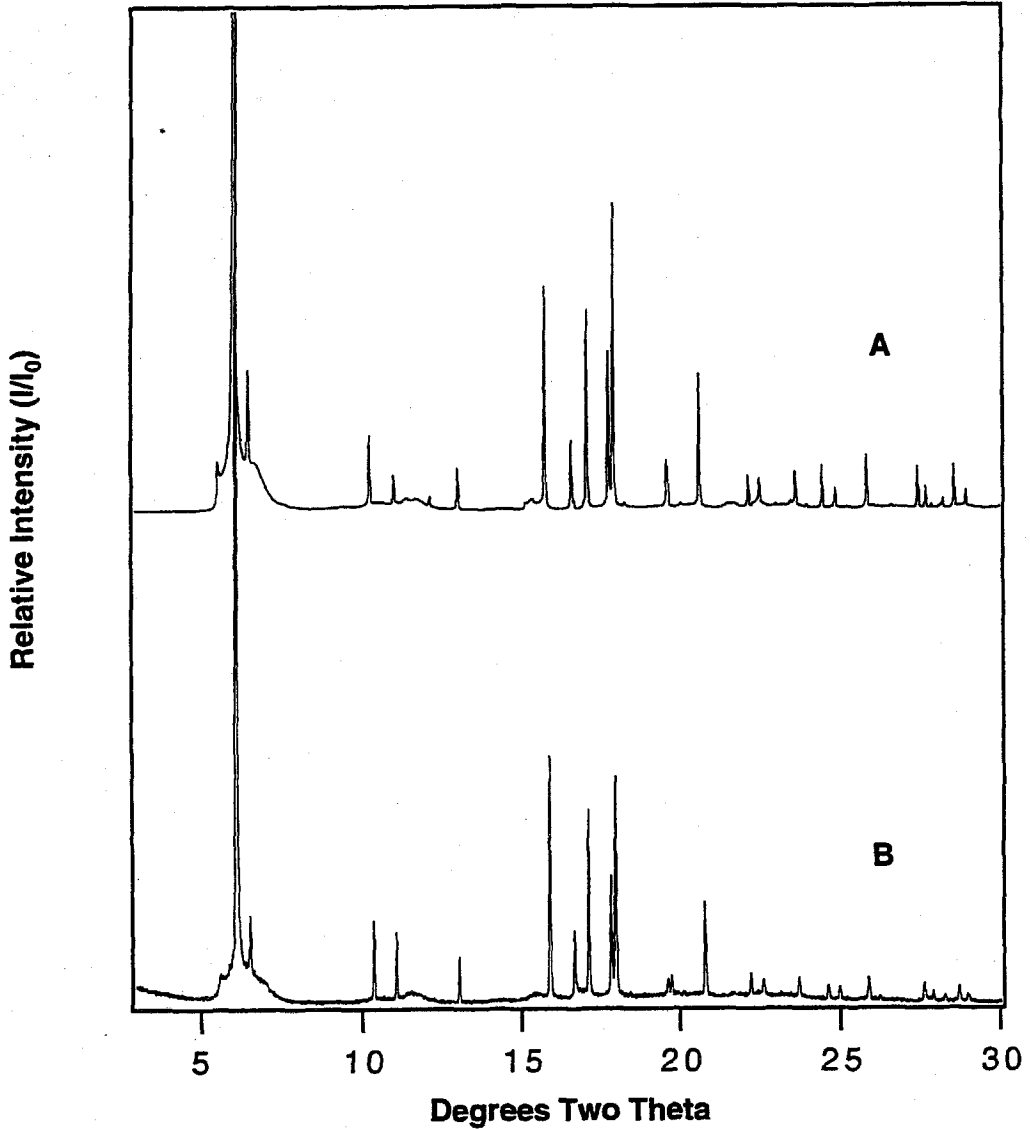
Figure 3.4   Comparison of the calculated synchrotron XRD pattern of SSZ-33 (A) and the experimental XRD pattern (B) of the intergrowth with a fault probability p=0.3 (λ=1.19505 Å).
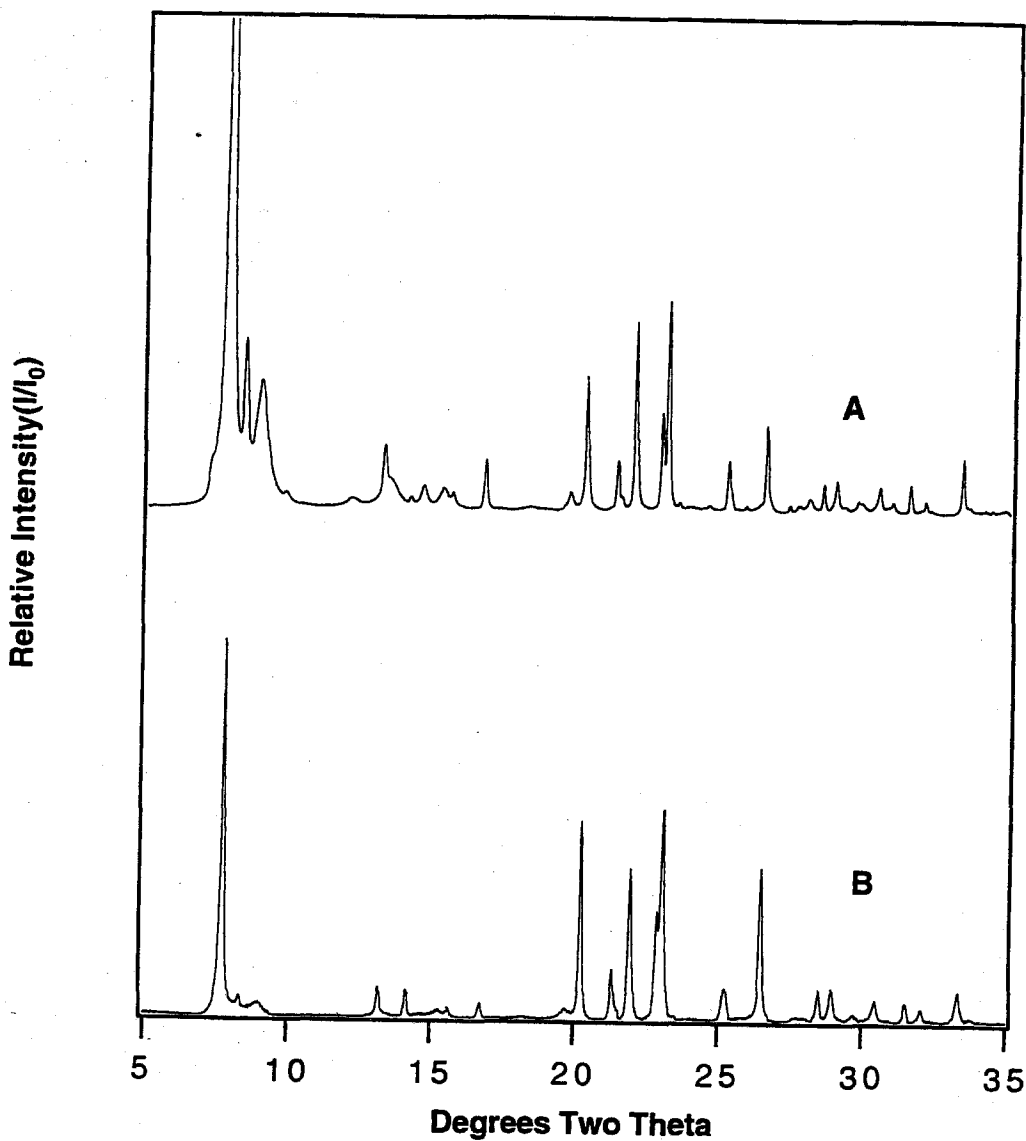
Figure 3.5   Comparison of the calculated XRD pattern of SSZ-26 (**A**) and the experimental XRD pattern (**B**) of the intergrowth with a fault probability p=0.15 (λ =1.5406 Å).

Table 3.1 Distance least-squares optimized atomic coordinates for Polymorph A [space group *Pmna* (no. 53). a=13.26 Å, b=12.33 Å, and c=21.08 Å].

Atom*	x	y	z
T1	0.111	0.208	0.074
T2	0.114	0.158	0.927
T3	0.211	0.030	0.150
T4	0.113	0.463	0.072
T5	0.198	0.359	0.849
T6	0.112	0.960	0.271
T7	0.116	0.711	0.278
O1	0.192	0.148	0.117
O2	0.123	0.168	0.002
O3	0.129	0.336	0.078
O4	0.000	0.180	0.099
O5	0.150	0.269	0.895
O6	0.184	0.061	0.903
O7	0.000	0.135	0.908
O8	0.311	0.017	0.181
O9	0.117	0.018	0.204
O10	0.000	0.494	0.091
O11	0.134	0.500	0.000
O12	0.190	0.525	0.118
O13	0.314	0.330	0.836
O14	0.137	0.361	0.783
O15	0.000	0.969	0.299
O16	0.141	0.835	0.263
O17	0.000	0.700	0.298

*   T=tetrahedral atoms

Table 3.2 Distance least-squares optimized atomic coordinates for Polymorph B [space group $B\, 2/m\, 1\, 1$ (No. 12) a= 13.26 Å, b= 12.33 Å, c= 22.62 Å, and α=68.7°].

Atom[b]	x	y	z
T1	0.118	0.500	0.068
T2	0.199	0.267	0.147
T3	0.111	0.751	0.072
T4	0.115	0.101	0.274
T5	0.115	0.849	0.279
T6	0.114	0.123	0.074
T7	0.200	0.872	0.153
O1	0.000	0.472	0.077
O2	0.139	0.626	0.071
O3	0.180	0.404	0.123
O4	0.153	0.500	0.000
O5	0.127	0.203	0.206
O6	0.174	0.221	0.091
O7	0.314	0.239	0.168
O8	0.000	0.748	0.100
O9	0.114	0.845	0.001
O10	0.191	0.786	0.115
O11	0.000	0.094	0.296
O12	0.147	0.980	0.269
O13	0.186	0.127	0.324
O14	0.127	0.827	0.214
O15	0.000	0.828	0.302
O16	0.000	0.117	0.099
O17	0.167	0:000	0.109

*   T=tetrahedral atoms

Chapter Four

Physicochemical Characterization of Zeolites SSZ-26 and SSZ-33

[Raul F. Lobo, Ming Pan, Ignatius Chan, Ronald C. Medrud,

Stacey I. Zones, Peter A. Crozier, Mark E. Davis, *J. Phys. Chem.*, in press]

Physicochemical Characterization of Zeolites SSZ-26 and SSZ-33

Raul F. Lobo,[a] Ming Pan,[b] Ignatius Chan,[c] Ronald C. Medrud,[c]
Stacey I. Zones,[c] Peter A. Crozier,[b] Mark E. Davis[a]*

[a]*Chemical Engineering, California Institute of Technology,
Pasadena, CA 91125*

[b] *Center for Solid State Science, Arizona State University,
Tempe, AZ 85287-1704*

[c] *Chevron Research and Technology Company, 100 Chevron Way,
Richmond, CA 94802-0627*

Abstract

Detailed characterization of zeolites SSZ-26 and SSZ-33 are presented and include data from adsorption experiments, X-ray powder diffraction (XRD), electron diffraction (ED) and high-resolution electron microscopy (HREM). Simulated XRD patterns and HREM images of the proposed structures agree very well with all the experimental data. These zeolites are the first synthetic high-silica molecular sieves to contain a three-dimensional pore system comprised of intersecting 10- and 12-ring pores. The structures of SSZ-26 and SSZ-33 are compared to the structures of known zeolites, and the relationships between the geometry of the structure-directing agents used in the synthesis of SSZ-26 and the geometry of the pores are analyzed using energy minimization calculations. Several hypothetical zeolite structures are derived based on the proposed models for SSZ-26 and SSZ-33. SSZ-26 and SSZ-33 are the first examples of molecular sieves whose multidimensional pore systems have been formed by the purposeful design of their organic structure-directing agents.

4.1 Introduction

The close relationship between the macroscopic properties and the microscopic structure of zeolites and molecular sieves has been a large driving force behind the efforts to characterize the structure of new zeolitic materials. This task is often hampered by the small size of synthetic zeolite crystals, disorder in the structure and the structural complexity of these materials. In this paper we present the detailed characterizations of the zeolites SSZ-26 and SSZ-33, which are examples of disordered materials that can only be prepared in small crystal sizes (1-5μ).

Zeolites SSZ-26 and SSZ-33[1] are members of a family of crystalline materials in which the two end members are formed by the stacking of layers in an ABAB... sequence or an ABCABC... sequence. The framework formed by the ABAB... stacking sequence (polymorph A) is of orthorhombic symmetry (Pmna) and the framework formed by the ABCABC... stacking sequence (polymorph B) is of monoclinic symmetry (B 2/m 1 1) (see Fig. 4.1). Between these two end member polymorphs, there is a whole family of materials that can be characterized by a fault probability p. The fault probabilities of p=0% and p=100% represent the end members polymorph B and polymorph A, respectively. The aluminosilicate SSZ-26 and the borosilicate SSZ-33 are members of this family of materials with fault probabilities of approximately 15% and 30%. These zeolites are the first synthetic high-silica molecular sieves to contain a three-dimensional pore system comprised of intersecting 10- and 12-ring pores[1] (n-rings are the number of either tetrahedral (T) or oxygen atoms forming the rings that control the access of molecules to the intracrystalline space).

Here, we characterize SSZ-26 and SSZ-33 using data from physical adsorption experiments, X-ray powder diffraction (XRD), electron diffraction (ED) and high-

resolution electron microscopy (HREM). We also indicate how the structures of SSZ-26 and SSZ-33 were solved based on the information obtained from these techniques. Next, we compare the structures of SSZ-26 and SSZ-33 to the structures of known zeolites. Finally, the relationships between the geometry of the structure-directing agents used in the synthesis of SSZ-26 and the final organic-inorganic composite structure are analyzed using energy minimization calculations.

4.2 Experimental Section

4.2.1 Zeolite Synthesis

SSZ-26 and SSZ-33 were synthesized under hydrothermal conditions as indicated previously.[2,3,4] The aluminosilicate SSZ-26 was synthesized using molecule **1** as a structure-directing agent with a SiO_2/Al_2O_3 ratio of 20 to 50, and the borosilicate SSZ-33 was a prepared using molecule **2** and a SiO_2/B_2O_3 ratio of 30.
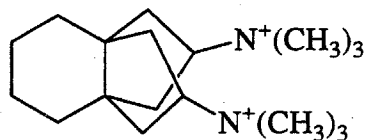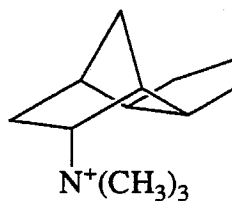
1   **2**

4.2.2 Analytical Methods

The density of SSZ-33 was measured by pycnometry using triisopropylbenzene (Aldrich, 99+%) following standard methods.[5] X-ray powder diffraction patterns were collected on a Scintag XDS 2000 diffractometer using Cu-Kα radiation and a solid-state Ge detector. The diffraction profiles were scanned over the range $2^0 < 2\Theta < 50^0$ in steps of 0.02^0 with a count time of 15 s at each point. Fluorophologopite mica (Standard reference material 675,

NBS) was used as external standard. Synchrotron diffraction data (λ=1.19505 Å) were collected at the Brookhaven National Laboratory for the calcined sample of SSZ-33.

4.2.3 Electron Diffraction and HREM

To prepare transmission electron microscopy (TEM) samples, powders of SSZ-26 and SSZ-33 were ground into fine particles, ultrasonically dispersed in 2-propanol and mounted onto a holey carbon grid by dipping the grid into the suspension. Microtomed samples were used here as well. Electron diffraction and large angle tilting experiments were carried out on a Philips 400T and a JEOL JEM2000FX electron microscopes operated at 100kV and 200kV, respectively. HREM was performed on a JEOL JEM 4000EX electron microscope operated at 400 kV (point resolution of 1.7 Å) with a Gatan 679 slow-scan CCD (charge-coupled device) camera. The CCD camera has 1024 x 1024 pixels and each pixel is 24 x 24 μm^2. The microscope magnification was set at about 500,000x for high-resolution imaging and the low-dose technique was employed.[6] A real-space averaging technique was used to suppress image noise and bring out high-resolution structure information.[6]

4.3   Results And Discussion

4.3.1 Structure Solutions for SSZ-26 and SSZ-33

Adsorption data

The adsorption capacity of several molecular sieves is shown in Table 4.1. Information relative to the pore size, pore dimensionally and void volume of the samples can be obtained from these data. The N_2 adsorption capacity of SSZ-26 and SSZ-33 is larger than the adsorption capacity of a multidimensional, 10-ring material (MFI) and a one-dimensional 12-ring material (AFI). However, it is lower than the adsorption capacity from three-dimensional, 12-ring zeolites (FAU, BEA). The fact that 2,2-dimethylbutane

adsorbs into SSZ-26 and SSZ-33 suggests that both materials have open 12-ring pores. The 2,2-dimethylbutane adsorption capacity of SSZ-26 and SSZ-33 is larger than the adsorption capacity from a one-dimensional, 12-ring structures (AFI) but lower than the adsorption capacity from three-dimensional, 12-ring materials (FAU, BEA). The quantitative agreement between the adsorption capacity measured with N_2 and 2,2-dimethylbutane suggests that there are no void spaces accessible through small pores (8-ring) that may be filled with N_2 but not with 2,2-dimethylbutane. The presence of voids accessible only through 6-rings, e.g., sodalite cages, could have been tested in principle by the adsorption of water. However, since the materials are relatively hydrophobic, complete micropore filling with water cannot be obtained.

Density

The density of calcined (organic removed) SSZ-33 was found to be in the range 1.46-1.63 g cm^{-3}. Triisopropylbenzene was used because of its large kinetic diameter. Although triisopropylbenzene adsorbs slowly into FAU crystals,[7] usually the kinetic diameter of triisopropylbenzene is large compared to the aperture of 12-ring pores. Thus, if it does diffuse into the void space of the crystals, it will do so very slowly. Also, accurate measurements of the density of microporous polycrystalline materials is often difficult because of the presence of small air bubbles trapped inside crystal aggregates and because impurities with small kinetic diameter in the liquid may diffuse inside the micropores affecting the value of the volume occupied by the crystals. We expect the former to be the most important source of error in the measurements and decided to use the higher value of the density to estimate the framework density (FD, number of T atoms per cubic nanometer). A FD of 16.9 T nm^{-3} was calculated assuming that the sample is formed of pure SiO_2. Comparison of this value with the FD of other zeolites of known structure (Table 4.1) is in agreement with the trends observed from the adsorption capacity data.

The FD of SSZ-33 is higher than the FD of three-dimensional 12-ring zeolites (BEA), but lower than mordenite (MOR) that contains intersecting 8- and 12-ring pores. This information led us to conclude that the pore system of SSZ-33 and SSZ-26 is probably formed of intersecting 10- and 12-ring or intersecting 12- and 12-ring pores.

The number of T atoms per unit cell can be estimated from the FD and the volume of the unit cell (3445 $Å^3$, *vide infra*). Although the data yield a total of 58 T atoms per unit cell, it is expected that the number of T atoms per unit cell is a multiple of 4 and most likely 8.[7] Therefore, we considered that a better estimate would be 56 T atoms per unit cell giving a corrected FD of 16.3 T nm^{-3}.

X-ray Powder Diffraction

SSZ-33 and SSZ-26 show similar XRD patterns. The differences in the XRD patterns (Fig. 4.2) suggest that there are at least long range structural differences between these two materials. The synchrotron XRD pattern of SSZ-33 shows sharp and broad features indicating the probable presence of stacking disorder in the structure. The sharp reflections were indexed on an orthorhombic unit cell with dimensions **a**=13.26 Å, **b**=12.33 Å, and **c**=21.08 Å. Except for the (0 1 0) reflection, the remaining reflections were of the form (h 3n l), n=0,1,2, which is indicative of shears associated with faulting of ± 1/3 **b.**

Electron Diffraction

The bright field transmission electron micrographs of SSZ-26 and SSZ-33 reveal that the crystal size of SSZ-26 is ~1 μm and that of SSZ-33 is about 5-6 μm long and 1-2 μm wide (Fig. 4.3). Diffraction patterns from individual crystals were recorded with a well-spread electron beam that minimized radiation damage to the zeolites. Electron diffraction patterns from individual crystals of SSZ-33 frequently showed sharp and streaking intensities for certain reflections (Fig. 4.4). The sharp spots occurred at columns of k=3n and the

streakings at columns of k=3n±1 (n=0, ±1, ±2, ...). This diffraction pattern is very similar to that of zeolite beta.[7] This characteristic intensity distribution is indicative of layer stackings with frequent faults. The occurrence of sharp spots for every 3rd column suggests that the relative displacement for successive layers is one-third of the intralayer spacing. This is also in agreement with a material in which two possible stacking sequences —ABAB... and ABCABC...— are present with frequent faulting between the two sequences. This observation is consistent with the XRD data, which shows mostly reflections of the form (h 3n l), n=0,1,2.

The unit cell of polymorph A was determined from ED by tilting the zeolite crystals through a large angle (30-40°). A simple orthorhombic lattice with cell parameters similar to the ones obtained from XRD was observed.

The major low-index zone electron diffraction patterns from polymorph A are shown in Fig. 4.5a-c. The following systematic absences have been observed from these patterns:

$$h\,k\,0: \quad h = 2n+1$$

$$h\,0\,l: \quad h+l = 2n+1$$

$$0\,k\,l: \quad \text{no conditions}$$

$$h\,0\,0: \quad h = 2n+1$$

$$0\,k\,0: \quad \text{no conditions}$$

$$0\,0\,l: \quad l = 2n+1$$

There are only two possible space groups which are consistent with the above systematic absences: P2na (No. 30) and Pmna (No. 53).

High resolution electron microscopy

HREM was carried out along the direction that gives the (0kl) diffraction pattern with the sharp spots and streakings (Fig. 4.4). Figure 4.6a shows that the surface of the SSZ-33 crystals consists essentially of many smaller crystallites with well-defined shapes and size of ~100 Å. The HREM image from one of these small crystallites is given in Figure 4.6b showing the intergrowth between polymorph A and B. The horizontal arrows lie along interface between the two polylmorphs. Enlarged images of polymorphs A and B are shown in Figures 4.7a and 4.7b with the corresponding digital diffractograms (power spectrum) illustrated in Figures 4.7c and 4.7d. The diffractograms show the coincidence of spots for columns of k=3n and a 1/3 shift of spot positions for columns of k=3n±1 (n=0, ±1, ±2, …). This results in both the sharp spots and streaking in the corresponding electron diffraction pattern (Fig. 4.4).

To reduce the image noise and extract high resolution structural information, a real-space averaging technique[6] was applied to the HREM images of SSZ-33. The averaged unit cells for polymorph A and B are shown in Fig. 4.8a and 4.8b. The image resolution is better than 2 Å as determined from the original image which was recorded near optimum defocus condition.[8] From the averaged unit cell, the large pores were easily identified as 10-rings. For polymorph A, a mirror plane was observed bisecting the 10-rings. This is due to the [001] a-glide plane since the image was recorded parallel to the glide plane and along the glide direction. Therefore, in projection the glide plane becomes a mirror.

Images in Fig. 4.8 contain valuable information about the zeolite structures because in addition to the 10-rings, other smaller rings surrounding the 10-ring are also clearly observed. It has been shown[9] that for thin zeolite samples and under the Scherzer or optimum focusing condition,[8] the projected potential in a zeolite crystal can be visualized by inverting the image contrast. In the projected potential map, bright regions correspond to high projected densities of T-atoms. As a result, the 2-D, 3-connected structure net can

be obtained and lead to the recognition of secondary building units (SBUs) in the structure. Figure 4.9 shows such a net (obtained from Fig. 4.8a), with the enlargement of each individual ring surrounding the 10-ring. It can be immediately seen that of these ten smaller rings, there are two 6-rings and eight 5-rings and that they are related by a horizontal mirror plane bisecting the 10-ring. Further quantitative analysis of the image intensities confirmed this conclusion.[9]

HREM image along the [010] direction of SSZ-26 was also recorded (Fig. 4.10). Large zeolite pores along with some secondary features (the zig-zag line between the large pores) can be seen in the image. The inset 2 is the image after noise reduction as mentioned above. Unlike the [100] HREM (Fig. 4.6b), it is not possible to obtain the 2-D, 3-connected structure net from such an image since the image resolution is only about 4 Å (not sufficient to resolve the shapes of individual rings). However, this image still provides some limited information of the structure in this projection.

4.3.2 Construction of the Framework of SSZ-33 and SSZ-26

Model building combined with the above experimental information was used as a basis to find the framework of SSZ-26 and SSZ-33. Three pieces of information suggested that the framework of SSZ-33 was related to zeolite beta:

a) One unit cell parameter of SSZ-33 was similar to the a unit cell parameter of the tetragonal polymorph A of zeolite beta (12.33 Å).

b) Although the material was heavily faulted, the faulting had no effect on the adsorption capacity, as observed in zeolite beta and unlike most cases of faulting in other zeolites.

c) The faulting of successive layers was 1/3 of the intralayer spacing. NU-86 also shows these three characteristics.[10]

As a starting point, we used a framework related to polymorph A and polymorph C of zeolite beta (see ref. 7 for details about the hypothetical polymorph C of zeolite beta). The projection along [0 1 0] of this hypothetical structure[11] (Fig. 4.11a) is the same as the projection along {1 0 0} of polymorph A of zeolite beta, and the projection along [1 0 0] is similar to the projection along {1 0 0} of polymorph C of zeolite beta. Next, the transformation shown in Figure 4.11b was carried out, and a model with orthorhombic symmetry and intersecting 10- and 12-ring pores was obtained. This model had the approximate unit cell dimensions expected for SSZ-33, it agreed with the experimental adsorption capacities and density, and qualitatively agreed with the information obtained from HREM. Similarly, a model based on the [110] projection of polymorph B of zeolite beta and the {1 0 0} projection of polymorph C of zeolite beta was obtained. After performing the same transformation (Fig. 4.11b), a model of monoclinic symmetry, also with intersecting 10- and 12-ring pores, was obtained. The cell dimensions of polymorph B are related to the cell dimensions of polymorph A by the transformation matrix (1 0 0; 0 1 0; 0 1/3 1).

The estimated atomic positions of the T atoms were derived from the physical models, and the oxygen atoms were added at the midpoints of the T atoms using the program KRIBER.[12] The atomic coordinates of the oxygen and T atoms were optimized using distance least-squares refinement (DLS-76).[13,14] An ORTEP representation of each polymorph is shown in Fig. 4.1. The effect of the ABAB... and the ABCABC... stacking sequence on the structure can be observed comparing the projection along the 10-ring pores of polymophs A and B (Fig. 4.1b and 4.1c).

4.3.3 Simulation of HREM Images and XRD Patterns

HREM images along the projection of the 10-ring and 12-ring pores have been simulated for each polymorph using the optimized atomic coordinates of the oxygen and silicon atoms

obtained from model building.[1]   The image simulations were carried out using the commercially available multislice programs of Molecular Simulations.   The image resolutions used in the simulations are 1.6 Å for the [100] and 4.0 Å for the [010] projections to be consistent with the experimental images. Other parameters used in the simulation are listed in Table 4.2. Figure 4.12a and 4.12b are simulated thickness/defocus image series along the 10-ring projection for polymorph A and polymorph B. The structure projection along the 12-ring for polymorph B is the same as for polymorph A giving idential images. The Scherzer defocus for the electron microscope used is about 500 Å. Fig. 4.13 is the similar thickness/defocus series along this projection.

From the simulated images, the best visual matches with experimental images were obtained for t=80 Å, Δf=-560 Å for the 10-ring projection (Fig. 4.8c and 4.8d), and t=75 Å and Δ=-800 Å for the 12-ring projection (inset 1 in Fig. 4.10). These simulated images are in excellent agreement with experimental images.

As indicated above, to describe quantitatively the effect of the presence of the ABABAB... and the ABCABC... stacking sequences in the structure, a faulting probability p was defined as the probability of the reversal in the direction of stacking. That is, if p=0.25, after an AB layer sequence, there is a 25% probability that the next layer will be in the A position and a 75% probability that the layer will be in the C position. The simulation of the XRD patterns incorporating the disorder was carried out using DIFFaX.[1,15]

The effect of faulting, i.e., a value of p different from 0 or 1, on the XRD pattern is to drastically reduce the intensity of the reflections that are not present in both the XRD patterns of polymorph A and polymorph B. Comparison of the experimental to the simulated XRD patterns for different fault probabilities indicates that SSZ-33 is an intergrowth of polymorph A and polymorph B with a fault probability p close to 30% (Fig. 4.14a). There is a predominance of polymorph B in SSZ-33 because p<0.5. Differences in the simulated XRD pattern for fault probabilities about 30% are relatively

small and therefore the value of p=0.3 is only approximate. Figure 4.14a shows very good agreement between the simulated XRD pattern with p=0.3 and experimental XRD pattern of SSZ-33. For SSZ-26, comparison of the simulated and experimental XRD patterns indicate that there is also a predominance of polymorph B in SSZ-26, but the faulting probability is close to 15% (Fig. 4.14b). There is some disagreement between the intensities of the simulated and experimental reflections at low angles, but this is likely to be the effect of adsorbed water molecules inside the zeolite pores.

4.3.4 Structural Relationships Between SSZ-26, SSZ-33 and Other Zeolites

The structure of SSZ-33 is related to the structures of zeolite beta and NU-86. These three materials are highly disordered because of the presence of stacking faults and share the property that the stacking faults are such that they do not block the pores of the zeolite. The tertiary building unit (TBU) responsible for these characteristics is shown in Fig. 4.15a. This TBU is formed of parallel double 5- and 6-rings with a repeating unit of 12.5 Å long. The oxygen atoms connecting the top and bottom layer of T atoms are equally spaced at about 4.1 Å. It is this similar separation that allows for the stacking disorder between the layers in zeolite beta, NU-86 and SSZ-33 with translations of ±1/3 **b**, and permits the formation of the orthorhombic or monoclinic polymorphs. The projection along **b** of this TBU is shown in Fig. 4.15b and a 2D illustration of the way this TBU is connected to the remainder of the structure in BEA, NU-86 and SSZ-33 is given in Fig. 4.15c. These conectivities are the main difference between the three structures.

The relationships between the structures of BEA, NU-86 and SSZ-33 can be appreciated further from the perspective of the Akporiaye-Price-Shannon formalism.[10] In this formalism, the zeolite frameworks are described in terms of a corrugated two-dimensional sheet and a number of stacking operators. Although beta, NU-86 and SSZ-33

are formed from different corrugated sheets, the stacking operators ($M_ZM_iM_ZM$ plus shear of $\pm 1/3$ **b**) that produce the unit cell are the same in the three frameworks. The two-dimensional sheet that forms the polymorph A of SSZ-33 is shown in Fig. 4.16.

The projection along the 12-ring pores of SSZ-33 is similar to the projection along **c** in the AFI structure. This projection is ubiquitous among many of the 12-ring aluminosilicate and high-silica zeolites, and it is also found in CAN, GME, OFF, BOG in addition to several aluminophosphate-based materials.[16] The relationship between SSZ-33 and boggsite[17] is particularly interesting because both materials have intersecting 10-ring and 12-ring pores and have similar projections along the 12-ring pores. The two structures also have the 4-4=1 secondary building unit among their structural units, but the manner in which these 4-4=1 building units are connected together is quite different. Figure 4.17 shows a comparison of related TBU, for SSZ-33 and BOG. In SSZ-33, the 4-4=1 SBUs are connected by three different Si—O—Si bridges. In contrast, the 4-4=1 SBUs of BOG share one of the edges of a 5-ring to effectively form a chain of 4-4=1 SBUs. SSZ-33 is the first synthetic zeolite that contains the 4-4=1 SBU. We find this very interesting because several common natural zeolites (STI, HEU) have been very difficult to synthesize under hydrothermal conditions in the laboratory. The synthesis of SSZ-33 may suggest the conditions to obtain this SBU. However, as with BOG, the 4-4=1 SBUs of STI and HEU are connected to form chains.[16]

4.3.5 Related Hypothetical Structures

In addition to the polymorphs A and B of zeolite SSZ-33, several other hypothetical structures can be formed by simple transformations on the models of polymorphs A and B. The space groups and approximate atom positions were obtained from these new models as before, and the atom positions were optimized using DLS-76. A list of the hypothetical structures and their space groups is given in Table 4.3. Several models show very good

convergence with DLS-76. The projection of all the models along the 12-ring pores is the same as the projection of the AFI structure along **c**. It seems that this projection plays the same role as the ferrierite projection down **c** in many 10-ring pore aluminosilicates as reported by Gramlich-Meier.[18] The ferrierite projection can be used for the formation of over a thousand hypothetical frameworks among which are many structures of known medium-pore zeolites (FER, TON, MFI, MEL, ZSM-48, MFS and SU–4). In particular, what we denote as structure C is obtained from the stacking of the layers of polymorph A in an AAA... stacking sequence. This model also contains intersecting 10- and 12-ring pores (Fig. 4.18) and it is the analogous SSZ-33 type structure to the polymorph C of zeolite beta.[7] Although no evidence has been obtained by XRD, HREM or ED for the presence of these hypothetical structures in SSZ-33 or SSZ–26, they may be achievable via modifications of the synthesis conditions.

4.3.6 Relationships Between Pore Geometry and the Geometry of the Organic Structure-directing Agent

Structure-direction is the process by which the organic structure-directing agent translates its geometrical characteristics into the pore-architecture of the zeolites.[19] As it will be shown below, the relationship between the structure-directing agent of SSZ-26 and the pore geometry of the zeolite originally proposed by Zones *et al.*,[2] and the minimum energy conformation of this molecule (**1**) inside the zeolite pores as calculated from energy minizations, are very similar. This indicates that the synthesis of SSZ-26 is the first clear example of a pore architecture formed by the *a priori* design of the organic-structure directing agent.

Experimentally, it has been observed that the structure-directing agent is intact inside the pores of SSZ-26.[2] Thermogravimetric analysis of as-synthesized SSZ-26 indicates that there are approximately two structure-directing molecules of **1** per unit cell.

This is the same as the number of pore intersections per unit cell in polymorphs A and B of SSZ-26. We carried out energy minimizations of **1** inside the pores of the polymorph B of SSZ-26.[20] The position of minimum energy (Fig. 4.19a) for **1** inside the zeolite pores closely relates to the original concept of structure-direction formulated by Zones and coworkers (Fig. 4.19b).[21] Although there is a close correspondence between the geometry of tetrapropylammonium and the pore structure of MFI, and also the geometry of the triquaternary ammonium cation used for the synthesis of MEI and the geometry of the cages of MEI,[19] these complementary relationships are not the result of an *a priori* synthesis of the organic molecule in order to obtain a pore architecture with the corresponding geometry.

4.4   Conclusions

SSZ-26 and SSZ-33 are two members of a family of materials with intersecting 10- and 12-ring pores. The proposed structures were obtained based on adsorption data, density data, and results from XRD, ED and HREM. The proposed structures agree very well with all the experiemental and simulated data. These materials fill a long existing gap in the type of molecular sieve materials available and are likely to have an important impact in the petroleum and refining industries. SSZ-26 and SSZ-33 are the first examples of molecular sieves whose multidimensional pore systems have been formed by the purposeful design of their organic structure-directing agents. The geometry of the organic molecule is the most important factor in obtaining a pore system intermediate in size to the zeolites ZSM-5 and beta. In addition to the novel pore system, the frameworks of SSZ-26 and SSZ-33 are the first high-silica molecular sieves to contain the 4–4=1 secondary building unit.

4.5   References and Notes

1.   R.F. Lobo, M. Pan, I. Chan, H.X. Li, R.C. Medrud, S.I. Zones, P.A. Crozier, M.E. Davis, *Science*, **1993**, *262*, 1543.

2.   S.I. Zones, M.M. Olmstead, D.S. Santilli, *J. Am. Chem. Soc.*, **1992**, *114*, 4195.

3.   S.I. Zones *et al.*, U.S. Patent 4,910,006 **1990.**

4.   S.I. Zones, U.S. Patent 4,963,337 **1990**.

5.   D.P. Shoemaker, C.W. Garland, J.W. Nibler, *Experiments in Physical Chemistry*, 5th Ed., Mc Graw Hill, 1989, p 17.

6.   M. Pan and P.A. Crozier, *Ultramicroscopy*, **1993**, *48*, 322.

7.   J.M. Newsam, M.M.J. Treacy,W.T. Koetsier, C.B. de Gruyter, *Proc. R. Soc. London Ser. A.* **1988**, *420*, 375.

8.   P.R. Bussek, J.M. Cowley, L. Eyring, *High-resolution Transmission `Electron Microscopy*, Oxford University Press: Oxford, 1988, p 22.

9.   M. Pan, P.A. Crozier, *Ultramicroscopy*, **1993**, *52*, 487.

10.   M.D. Shannon, in *Proceedings of the 9th International Zeolites Conference*, R. von Ballmoos, J.B. Higgins, M.M. Treacy Eds. Butterworth-Heinemann: Stoneham MA, 1993, Vol. 1, pp 389-398.

11.   This hypothetical structure is of orthorhombic symmetry (Pmma, No. 51) with unit cell parameters or approximately $a=23.69$ Å, $b=13.90$ Å and $c=12.71$ Å. The symmetry information and atomic positions of the asymmetric unit cell have been deposited as supplementary material with the journal.

12.   R. Bialek, *KRIBER*, Institut fuer Kristallografie und Petrografie, ETH, Zürich, **1991**.

13. The atomic possitions of the asymmetric unit cell of polymorphs A and B were reported in ref. 1. The weighted agreement values for polymorph A were R=0.0013, σ=0.007 and for polymorph B were R=0.001, σ=0.005. See ref. 1 for further details.

14. Ch. Baerlocher, A. Hepp, W.M. Meier, *DLS-76*, Institut für Kristallographie, ETH, Zürich, 1976.

15. M.M.J. Treacy, M.W. Deem, M.W. Newsam, *Proc. R. Soc. London Ser. A*, **1991**, *433*, 499.

16. W.M. Meier, D.H. Olson, *Atlas of Zeolite Structure Types* Butterworths-Heineman, Stoneham, MA, **1992**.

17. J.J. Pluth and J.V. Smith, *Am. Miner.* **1990**, *75*, 501.

18. R. Gramlich-Meier, *Z. Kristal.*, **1986**, *177*, 237.

19. M.E. Davis and R.F. Lobo, *Chem. Mater.* **1992**, *4*, 756.

20. The energy minimizations where carried out using the Crystal Packer option of Cerius 3.2 software, from Molecular Simulations. First, the geometry of the organic molecule (**1**) was optimized in free space and kept fixed during the energy minimizations. The zeolite framework was also kept rigid and only van der Waals interactions were allowed between the organic molecule and the zeolite framework.

21. S.I. Zones, D.S. Santilli, in *Proceedings of the 9th International Zeolites Conference*, R. von Ballmoos, J.B. Higgins, M.M. Treacy Eds., Butterworth-Heinemann: Stoneham, MA, 1993, Vol. 1, pp 171-179.

22. D.W. Breck, *Zeolite Molecular Sieves*, Robert E. Krieger Publishing Company: Florida, 1984, 618-619.
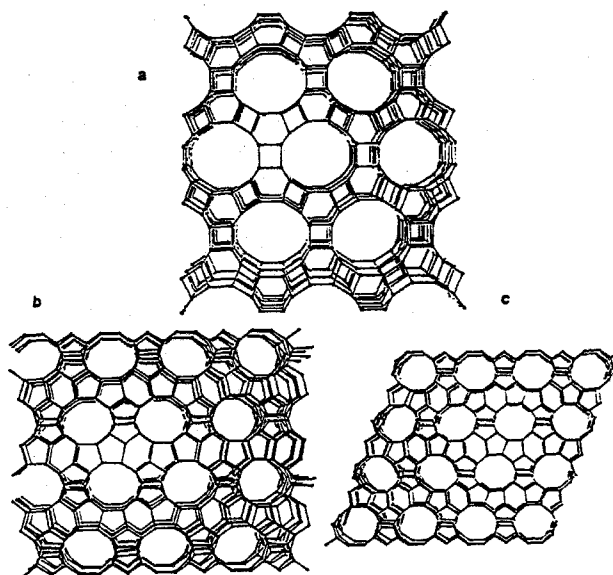
Figure 4.1   Framework structure of polymorph A viewed along the 12-ring pores (a)

and along the 10-ring pores (b) and framework structure of polymorph B viewed

along the 10-ring pores (c).
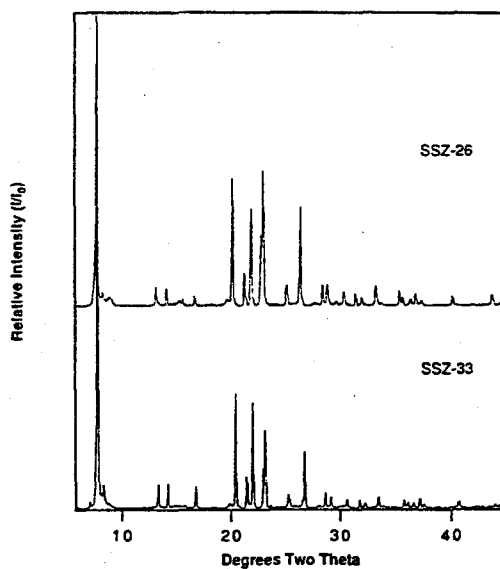
Figure 4.2   X-ray powder diffraction of SSZ-26 and SSZ-33, Cu-Kα radiation.
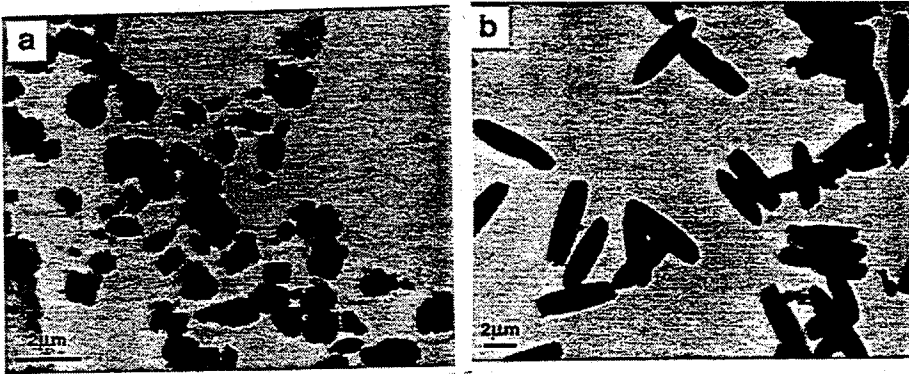
Figure 4.3   Low-magnification TEM images showing morphologies of (a) SSZ-33 and
(b) SSZ-26.
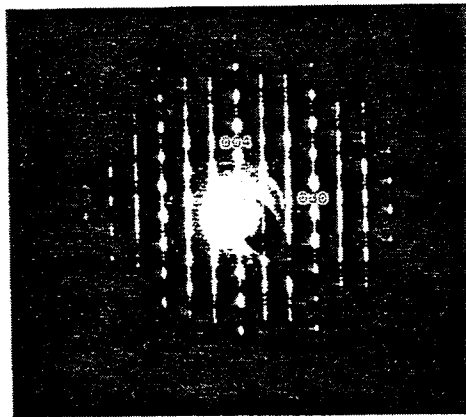
Figure 4.4   [100] electron diffraction pattern of SSZ-33 showing both sharp spots and
streaking intensities.
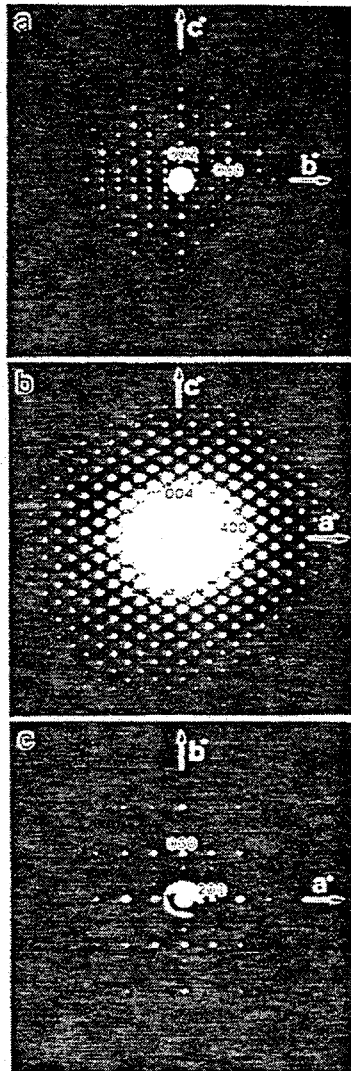
Figure 4.5   Major low-index zone electron diffraction patterns from SSZ-33. (a) (0kl),
(b) (h0l) and (c) (hk0).
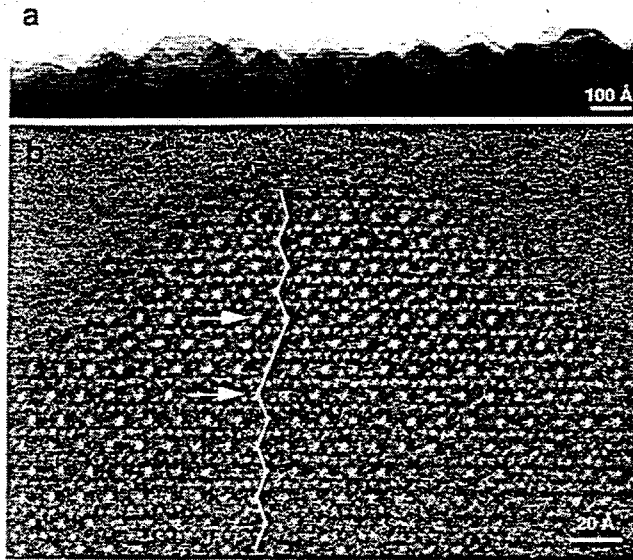
Figure 4.6   (a) Low-magnification image of SSZ-33 showing surface morphology; (b) HREM image of crystals in (a).
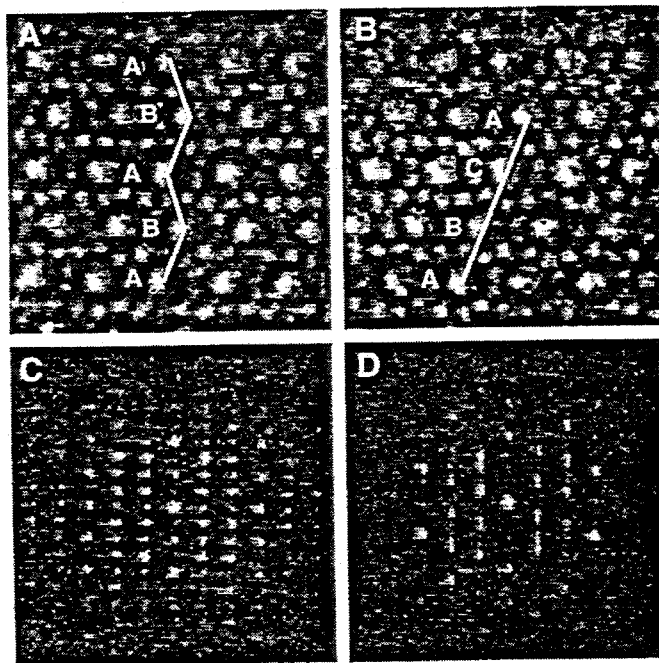
Figure 4.7   HREM images of polymorph A (a) and polymorph B (b) with corresponding digital diffractograms in (c) and (d).
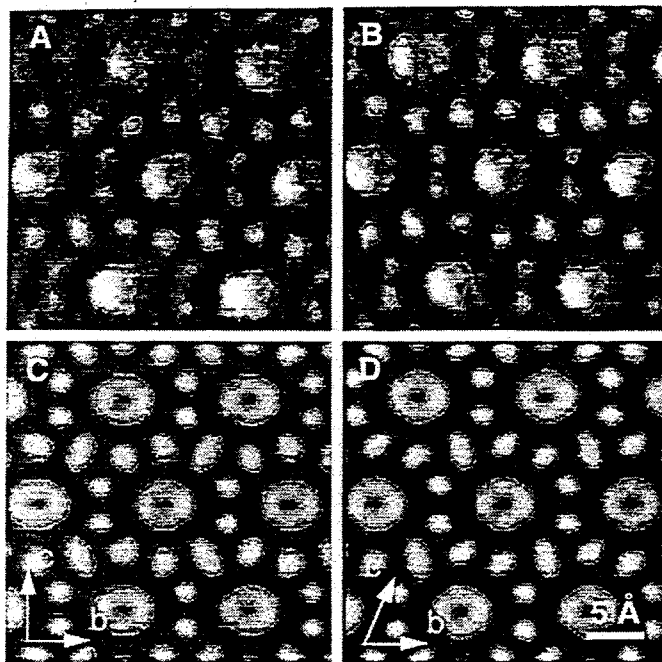
Figure 4.8   Real-space averaged unit cells of SSZ-33 along the 10-ring projection of (a)

polymorph A and (b) polymorph B with corresponding simulated images in (c) and

(d), respectively.
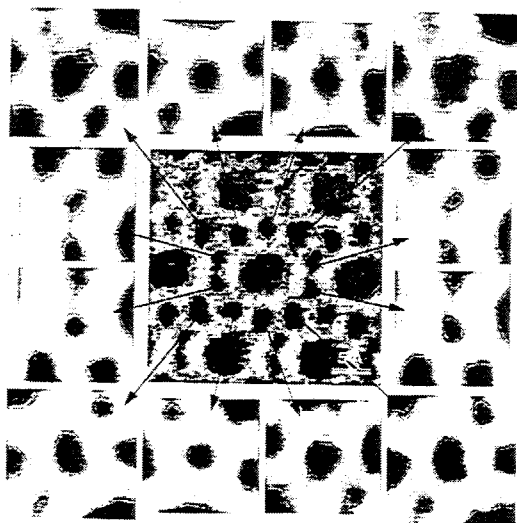
Figure 4.9   Contrast reversed image of real-space averaged unit cell of [100] polymorph

A with enlargements of surrounding smaller rings.
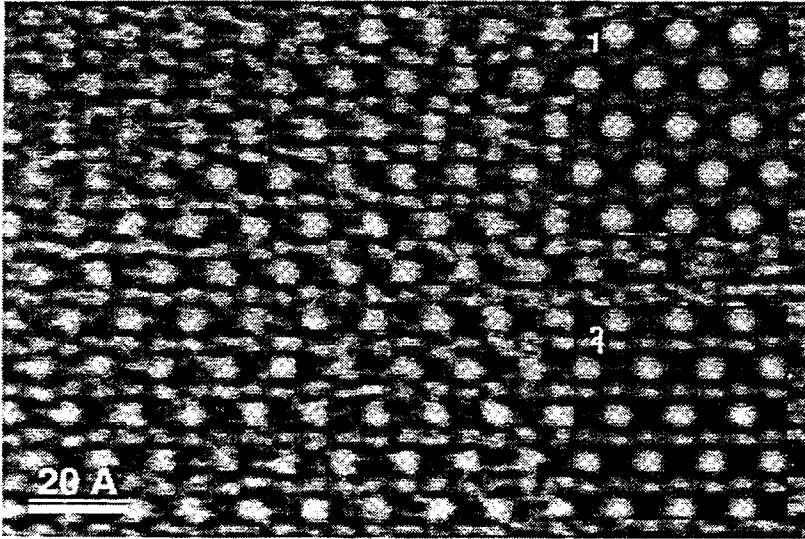
Figure 4.10   [010] HREM image of SSZ-26 showing large pores and secondary structural features with simulated image (inset 1) and processed image (inset 2).
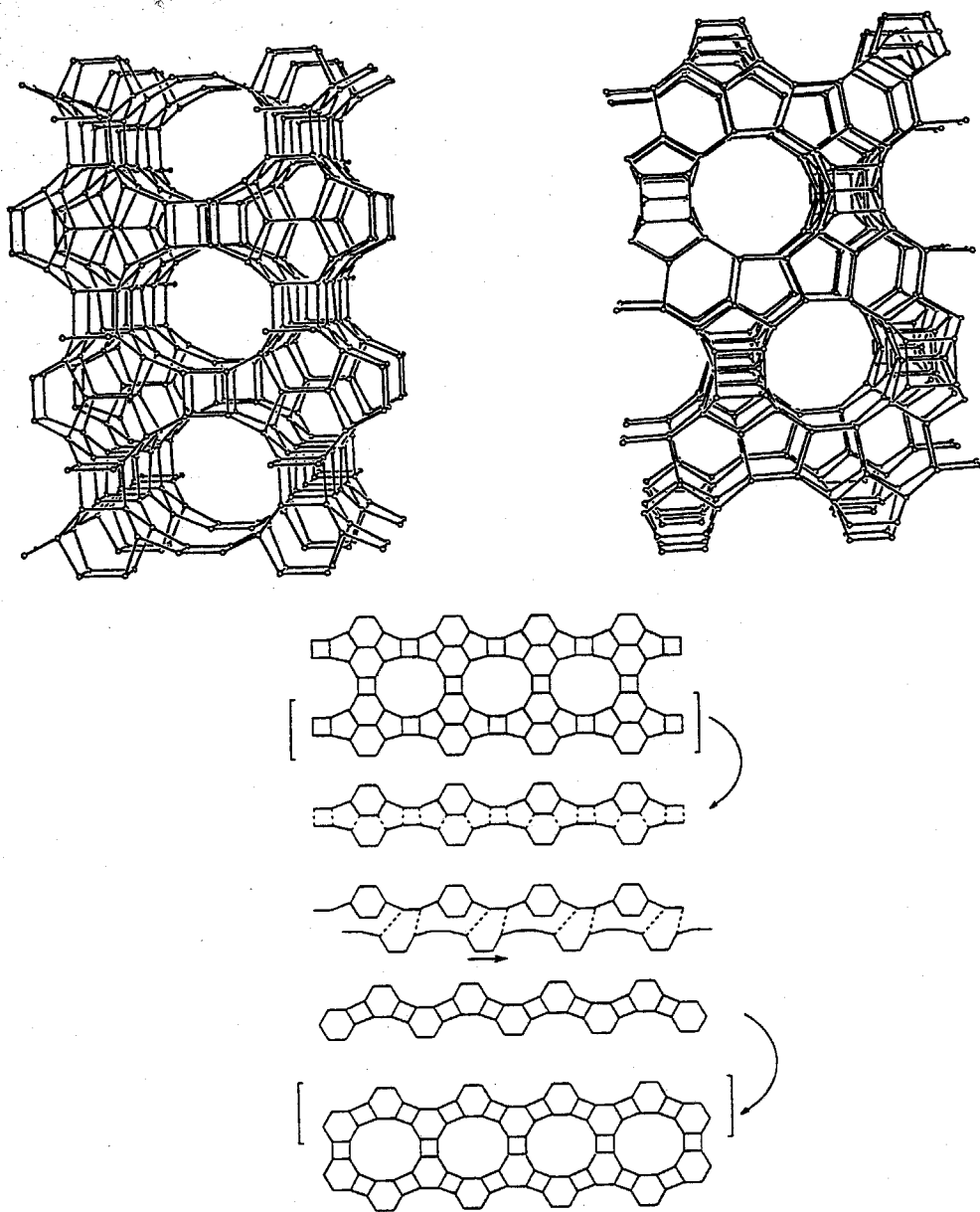
Figure 4.11   (a) ORTEP illustration of a hypothetical model related to the polymorph A and C of zeolite beta. The left drawing is the projection along [010], and the right drawing is the projection along [001]. (b) Formation of the framework structure of polymorph A of SSZ-33 based on a hypothetical model of polymorphs A and C of zeolite beta.[7]   The figures show how one layer of the hypothetical model of polymorphs A and C of zeolite beta (top) can be transformed into the layers that form polymorph A or B of SSZ-26 and SSZ-33 (bottom).
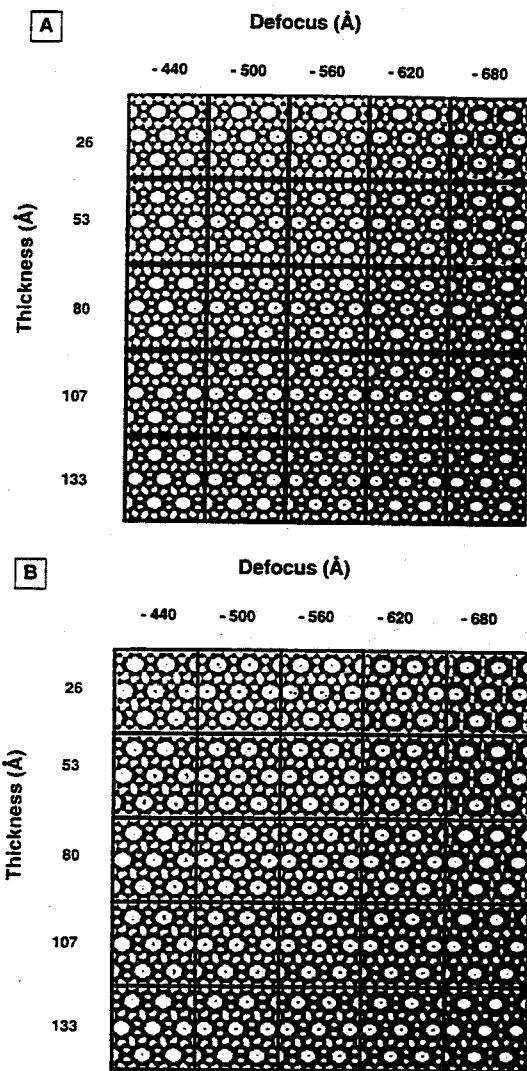
Figure 4.12   Simulated images along 10-ring pores of (a) polymorph A and (b) polymorph B.
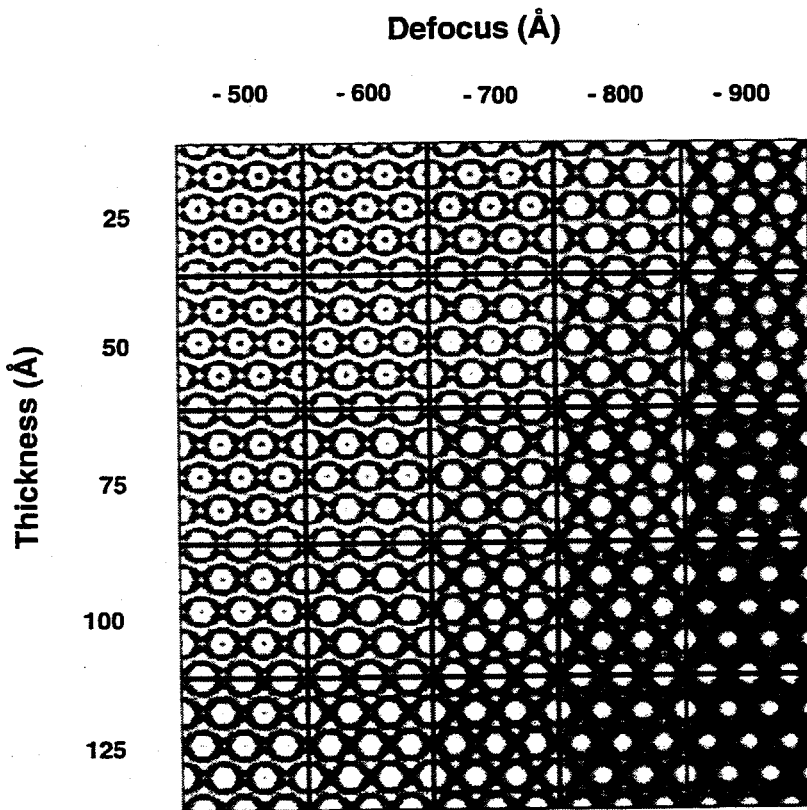
Figure 4.13   Simulated images along 12-ring projection of polymorphs A and B.
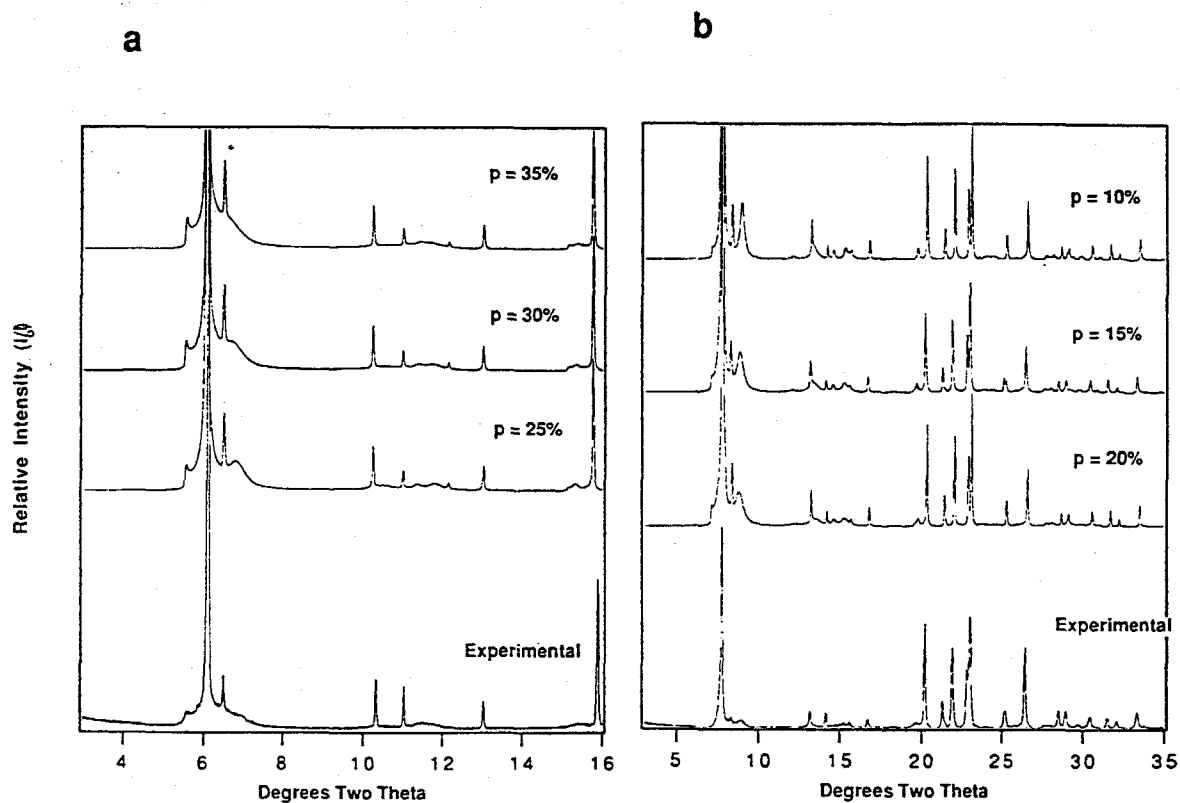
Figure 4.14   (a). Comparison of the calculated XRD patterns of the intergrowths of

polymorphs A and B with fault probabilities of p=25, 30 and 35% with the

experimental synchrotron XRD pattern of SSZ-33 (λ = 1.19505 Å). (b)

Comparison of the calculated XRD patterns of the intergrowths of polymorphs A

and B with fault probabilities of p=10, 20 and 25% with the experimental

synchrotron XRD pattern of SSZ-26 (λ = 1.5460 Å).
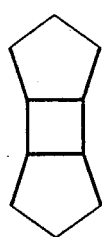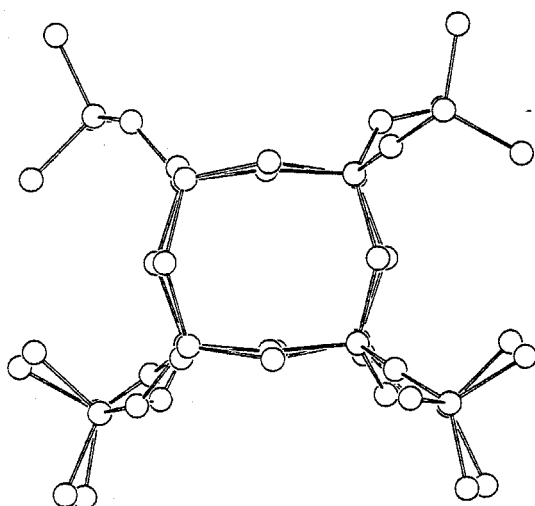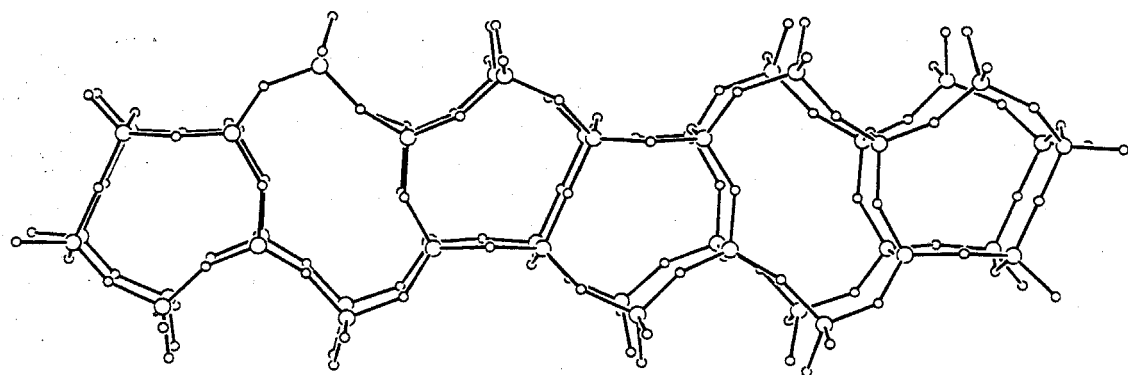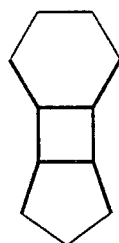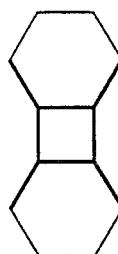
BEA   NU-86   SSZ-33

Figure 4.15   (a) TBU present in SSZ-33, zeolite beta and NU-86, (b) projection along **b** of the TBU shown in (a), and (c) Illustration of the different connectivities of this TBU with the rest of the framework in SSZ-33, zeolite beta and NU-86.
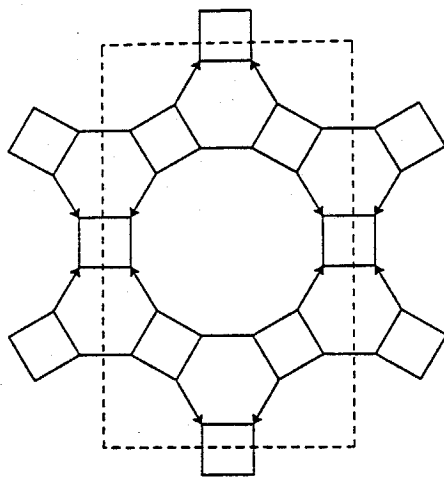
Figure 4.16   Two dimensional sheet used for the formation of polymorph A of SSZ-33 according to the Akporiaye-Price-Shannon formalism.
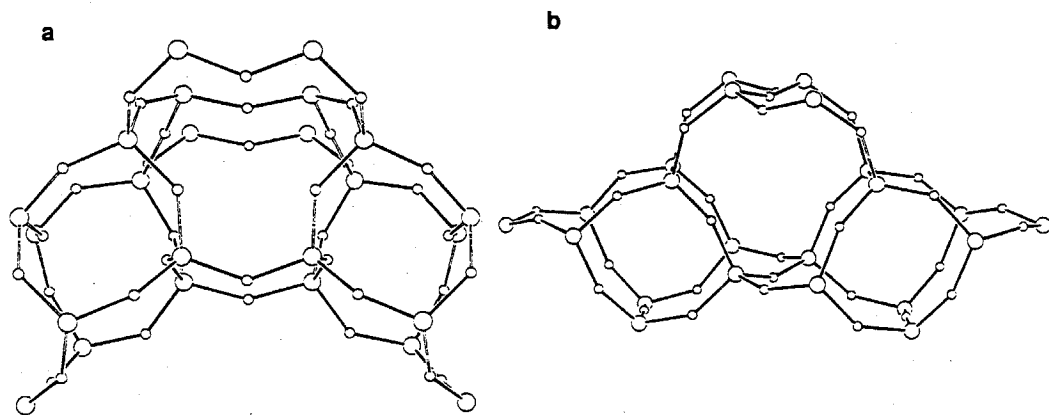
Figure 4.17   TBU's of SSZ-33 (a) and BOG (b) showing the presence of the 4-4=1 SBU in both frameworks. In SSZ-33 the 10-ring pores run horizontally and in BOG the 10-ring pores run vertically to the TBU.
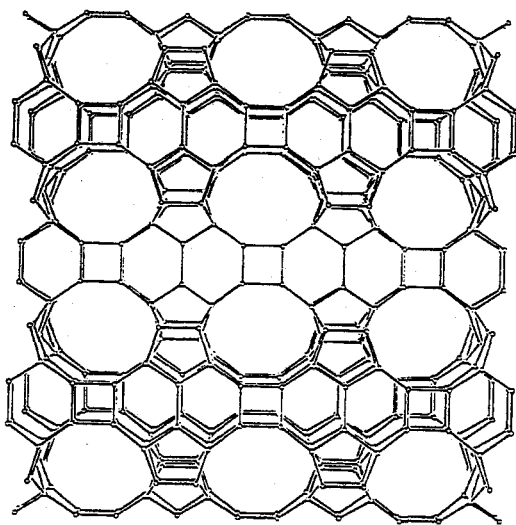
Figure 4.18   ORTEP representation of the hypothetical polymorph C of SSZ-33. View along the 10-ring pores.
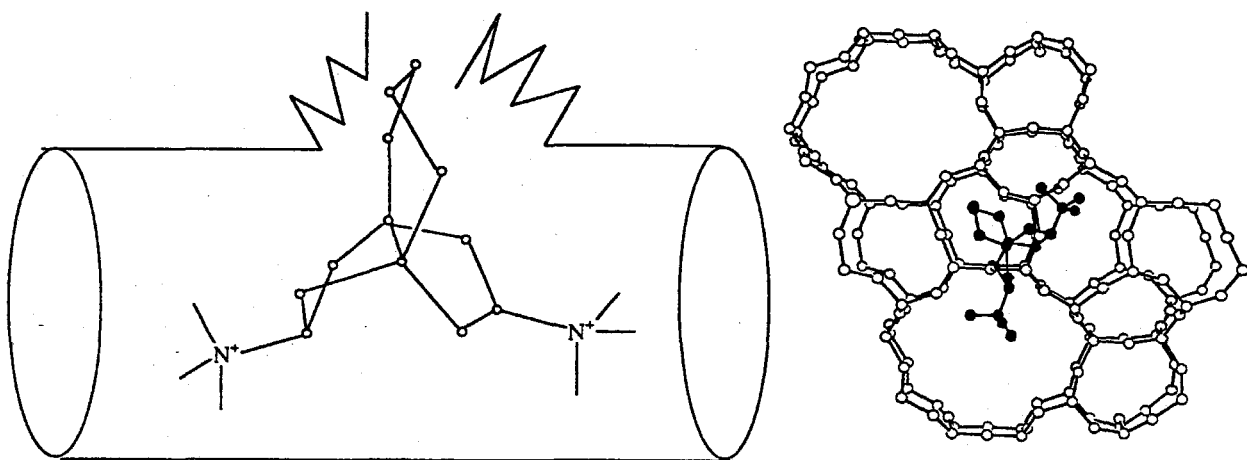
Figure 4.19   (a) Minimum energy position of molecule 1 inside the pores of polymorph B of SSZ-26. (b) Illustration of the effect of the geometry of molecule 1 as originally proposed by Zones et al..[2]

Table 4.1 Adsorption capacities and framework densities of molecular sieves.

Zeolite	Pore Dimensionality and ring size[a]	N_2 $(cm^3\ g^{-1})$	2,2-dimethyl-butane $(cm^3\ g^{-1})$	Framework Density[b] T atoms nm^{-1}
ZSM-5 (MFI)	3D, 10 x 10	0.14	$-$ [c]	17.9
SSZ-24 (AFI)	1D, 12	0.12	0.11	17.5
Mordenite (MOR)	2D, 8 x 12	0.15 [d]	0.09 [d,e]	17.2
SSZ-26	$-$	0.19	0.20	17.0 [f]
SSZ-33	$-$	0.21	0.19	16.9 [f]
Beta (BEA)	3D, 12 x 12 x 12	0.25	0.27	15.0
Y (FAU)	3D, 12 x 12 x 12	0.27	0.24	12.7

a nD indicates the channel dimensionality. The number following the channel dimensionality indicates the number of T atoms forming the rings of the channels.

b. From ref. 16.

c. ZSM-5 adsorbs 2,2-dimethylbutane very slowly at room temperature.

d. From ref. 22.

e. Adsorption capacity for neopentane.

f. From pycnometry measurements.

Table 4.2 Image simulation parameters.

Projection	C_S (mm)	E_0 (kV)	Convergence angle (mrad)	Focus spread (Å)	Resolution (Å)
10-ring	1.0	400	1.0	100	1.6
12-ring	1.0	400	1.0	100	4.0

Table 4.3 Hypothetical models based on polymorph A and B of SSZ-33.

Hypothetical Structure[a]	Space Group	Pore Dimensionality and Size	Weighted Agreement Values R[b]
C	Bmmm	2D, 12x10	1.2×10^{-3}
D	Bmmm	2D, 12x8	1.2×10^{-2}
E	Immm	1D, 12	8.5×10^{-3}
F	Bmmm	2D, 12x8	2.9×10^{-3}
G	Imma	2D, 12x8	2.4×10^{-3}
H	Bmmb	1D, 12	4.8×10^{-3}

a   The atomic positions of these hypothetical models have been deposited as supplementary material.

b   From DLS-76.

Chapter Five

CIT-1: A New Molecular Sieve with Intersecting Pores Bounded by 10- and 12-rings

[Raul F. Lobo and Mark E. Davis, to be submitted to *J. Am. Chem. Soc.*]

CIT-1: A New Molecular Sieve with Intersecting Pores Bounded by 10- and 12-rings

Raul F. Lobo and Mark E. Davis

Chemical Engineering

California Institute of Technology, Pasadena, CA 91125

Abstract

A new borosilicate molecular sieve, CIT-1, is synthesized using N,N,N-trimethyl-(-)-*cis*--myrtanylammonium (I) hydroxide as the organic structure-directing agent. The material is characterized by synchrotron X-ray powder diffraction (XRD), electron diffraction, solid-state NMR and IR spectroscopies, scanning electron microscopy and physical adsorption experiments. Rietveld refinement of the synchrotron XRD data (Rp=9.9%, Rwp=11.9%) shows that CIT-1 is essentially the pure polymorph B of the molecular sieve SSZ-33 (space group $C\ 2/m$, No. 12, a=22.6242 (10) Å, b=13.3503 (4) Å, c=12.3642 (6) Å and β=68.913 (4) Å). CIT-1 is the first synthetic molecular sieve to contain intersecting 10- and 12-ring pores that is not an intergrowth of two different polymorphs. The long-range ordering of CIT-1 is shown to be a direct consequence of the organic structure-directing agent. CIT-1 can be easily prepared and sequential treatments of the calcined form of CIT-1 with aqueous HCl and aqueous aluminum nitrate remove framework boron and insert aluminum into the structure, respectively. Aluminum-containing CIT-1 is a very active catalyst for the cracking of n-butane at 510 °C.

5.1 Introduction

Zeolites are technologically important materials that have found applications in a wide variety of chemical processes.[1-3] One of the appealing features of the materials is the existence of a direct relationship between the microsocopic structure of these crystalline solids and their macroscopic properties.[4] The rationalization of sorptive, catalytic and ion exchange properties in terms of molecular structure allows suggestions of new applications for these materials and drives the search for zeolites with novel structures. The synthesis of SSZ-33,[5,6] NU-87[7] (or SSZ-37),[8,9] and MCM-22[10] (or SSZ-25)[11] are recent successful examples of the synthesis of new zeolite structures.

New large pore zeolites, those with pores bounded by rings of 12 tetrahedral atoms (T-atoms, e.g., Si, Al, B), from now on denoted 12MR, are of current interest due to their pore size; ~7 Å. Zeolites Y and beta have intersecting 12MR pores and have found application in petrochemical processing as catalysts. Likewise, ZSM-5, an intersecting 10MR zeolite is used quite extensively in shape-selective catalysis, e.g., production of p-xylene. It is likely that zeolites with intersecting 10MR and 12MR pores will offer a unique combination of reaction activity, selectivity and stability not found in other zeolites.[12]

Recently, we reported the structures of SSZ-33 and SSZ-26,[13] the first materials to contain a multidimensional pore system formed by intersecting 10MR and 12MR pores that provides access to the crystal interior through both pore sizes. The structure of SSZ-33 and SSZ-26 can be thought of as members of a family of materials in which the two end members (denoted polymorph A and B) are formed by the stacking of layers in an ABAB... sequence or an ABCABC... sequence. The framework formed by the ABAB... stacking sequence (polymorph A) is of orthorhombic symmetry while the framework formed by the ABCABC... stacking sequence (polymorph B) is of monoclinic symmetry.

In between these two end member polymorphs, there is a whole family of materials that can be characterized by a fault probability p. The fault probabilities of p=0% and p=100% represent the end members polymorph B and polymorph A, respectively. The aluminosilicate SSZ-26 and the borosilicate SSZ-33 are members of this family of materials with fault probabilities of approximately 15% and 30%, respectively.[14]

Like zeolite beta, SSZ-26 and SSZ-33 are likely to show interesting catalytic properties that will not be easily correlated to structural parameters since all three materials are intergrowth structures. A pure phase would greatly assist the determination of structure-catalytic property relationships for this new class of zeolites (with intersecting 10MR and 12MR pores). Here we report the first pure phase zeolite with intersecting 10MR and 12MR pores that provides molecular access to the crystal interior through the 12MR and 10MR pores. We denote this new material as CIT–1 for California Institute of Technology–1.

In this chapter, we present the synthesis and initial characterization of CIT-1, a novel molecular sieve that has been identified as the ordered polymorph B of the SSZ-33 and SSZ-26 molecular sieves. Unlike the structure-directing agents used to prepare SSZ-33 and SSZ-26, that require significant synthetic steps in their synthesis, the structure-directing agent of CIT-1 can be obtained from suppliers of organic compounds or can be easily prepared from β-pinene. CIT-1 is characterized using synchrotron X-ray powder diffraction (XRD), scanning electron microscopy (SEM), physical adsorption experiments, solid-state NMR spectroscopy, IR spectroscopy and electron diffraction (ED). The ED data and a Rietveld refinement of the XRD data from a calcined sample are used to confirm the proposed structure of CIT-1. The catalytic properties of CIT-1 for the cracking of n-butane are compared to the properties of other high-silica zeolites, e.g., ZSM-5 and zeolite beta.

5.2 Experimental Section

5.2.1 Synthesis of the Organic Structure-Directing Agents

Synthesis of N,N,N-trimethyl-(-)cis-myrtanylammonium (I) hydroxide: A typical synthesis of N,N,N-trimethyl-(-)cis-myrtanylammonium is carried out as follows: 10g (65.4 mmol) of (-)-*cis*-myrtanylamine ((1S)-[1α, 2β, 5α]-2-methanamine-6,6-dimethyl-bicyclo[3.1.1]heptane, from Aldrich) were dissolved in 100 ml of methanol. To this solution, 27 g of K_2CO_3 (3 meq) and 55 g of methyliodide (2 meq) were added. The mixture was stirred for a few minutes and then kept static for 12 h at room temperature in the absence of light. The reaction mixture was filtered and the solid filtrate was washed with additional 50 ml of methanol. The combined methanol solutions were heated at about 323 K in a rotavapor. A white solid is formed in the flask which is then extracted with 2 portions of 100 ml of $CHCl_3$. The combined $CHCl_3$ solutions, that now contain the trimethylmyrtanylammonium, were filtered again and were heated in a rotavapor until the $CHCl_3$ was evaporated. Often, a very viscous oily liquid was obtained after evaporation of the $CHCl_3$. In this case, the ammonium salt can be easily crystallized by the addition of 50 ml of diethyl ether. After the solid was formed, the crystals were washed with 200 ml of additional ether. The ether was then allowed to evaporate from the solid at room temperature in a hood. The recovered solids were recrystallized in a 9:1 tetrahydrofuran:methanol solution. 16.9 g (80% yield) of completely white crystals of the iodide salt of **I** were recovered. Expected ($C_{13}H_{26}NI$): C, 48.3; N, 4.3; H, 8.04; I, 39.3. Found: C, 47.9; N, 4.25; H, 8.16; I, 39.21. ^{13}C NMR: δ = 23.2, 23.7, 25.6, 27.2, 31.5, 35.6, 38.2, 40.2, 47.6, 53.8, 76.9 ppm.

The exchange of the iodide salt into a hydroxide was accomplished as follows: 4.2 g of the iodide salt of **I** (13 mmol) were dissolved in 60 ml of distilled water and passed through a 100 ml column of Amberlite IRA-400 OH anion exchange resin (140 mmol exchange capacity). The collected solution was concentrated to a total volume of 50 ml in a rotavapor at 343 K. The conversion of iodide to hydroxide was 96% based on titration of the resultant solution.
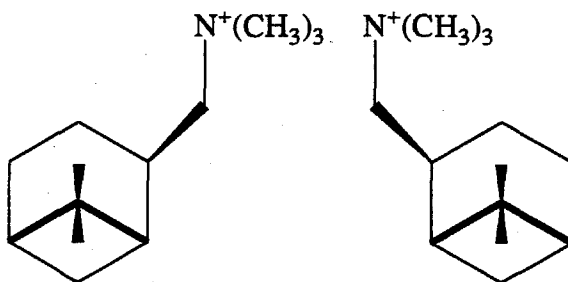
I   **II**

Synthesis of N,N,N-trimethyl (+)-cis-myrtanylammonium (**II**) *hydroxide:* The synthesis of N,N,N-trimethyl (+)-*cis*-myrtanylammonium (**II**) was carried out by reacting (+)-*cis*-myrtanylamine with methyliodide as described above for **I**. (+)-*cis*-myrtanylamine was prepared via hydroboration of β-pinene following the procedure of Brown et al.[15] However, in this case (+)-β-pinene ((1R)-6,6-dimethyl-2-methylene-bicyclo[3.1.1]heptane, from Fluka) was used as starting reagent rather than (-)-β-pinene. The yield for the crude amine was 48%. After reaction with iodomethane and recrystallization, the iodide salt (7 g, 66% yield) of **II** was exchanged to the hydroxide form as described above. (+)-*(cis)-myrtanylamine* ^{13}C NMR δ = 20.3, 23.3, 26.2, 28.1, 33.4, 38.7, 41.6, 43.9, 45.6, 48.4 ppm.

Synthesis of N,N,N-trimethyl-(1S,2S,3S,5R)-isopinocampheylammonium (**III**) hydroxide: (1S,2S,3S,5R)-isopinocampheylamine ([1α,2β,3β,5α]-2,6,6-trimethyl-3-

amine-bicyclo[3,1,1]heptane) was first synthesized from (+)-α-pinene by hydroboration.[15] The preparation was carried out using hydroxylamine-O-sulfonic acid in diglyme. Specifically, trimethyl-isopinocampheylammonium was synthesized here by reacting (1S,2S,3S,5R)-isopinocamphenylamine as was done to yield trimethylmyrtanylammonium and exchanged to the hydroxide form as described above. Expected ($C_{13}H_{26}NI$): C, 48.3; N, 4.3; H, 8.04; I, 39.3. Found: C, 48.4; N, 4.12; H, 8.05. *Isopinocampheylamine* ^{13}C NMR δ= 20.9, 23.3, 28.0, 34.0, 38.3, 39.6, 42.0, 48.1, 48.7, 50.7 ppm. *Trimethylisopinocampheylammonium* ^{13}C NMR: 23.1, 24.1, 26.8, 29.3, 30.9, 36.8, 38.3, 40.5, 48.2, 51.5, 73.9 ppm.

N,N,N-trimethyl-tricyclo[5.2.1.0^{2,6}]decaneammonium (**IV**): The tricyclo-decane derivative (**IV**) was supplied by S.I. Zones and Y. Nakagawa of Chevron Research and Technology Company, Richmond, California.
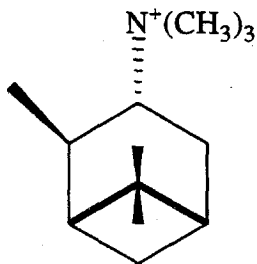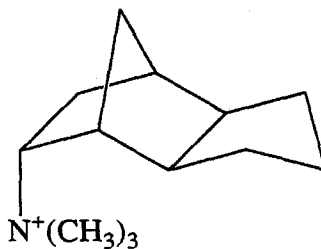
III   **IV**

5.2.2 Zeolite Synthesis

The borosilicate molecular sieve CIT-1 was synthesized from reaction mixtures of composition:

$$50\ SiO_2 : x\ B_2O_3 : 10\ ROH : 5\ NaOH : y\ H_2O$$

where R is N,N,N-trimethyl-(-)-*cis*-myrtanylammonium (I), with 0.8 < x <1.7 and 2500< y <10000. A typical synthesis of CIT-1 was carried out with x=1 and y=3000 (SiO_2/B_2O_3 ratio of 50 and a H_2O/SiO_2 ratio of 60). For this composition, 0.2 g of sodium borate decahydrate ($Na_2B_4O_7 \cdot 10H_2O$) and 0.2 of NaOH were dissolved in a solution obtained by combining 29 ml of a 0.35 M solution of ROH and 26 ml of distilled water. After the solids were completely dissolved, 3 g of fumed silica (Cab-O-Sil grade M-5) were added and the mixture blended until an homogeneous gel was obtained. The mixture was sealed in pure-silica glass tubes (25 mm I.D., 100 mm long approximately 85% filled with the gel) and heated statically in convection ovens at 423 K for 3-5 weeks. After the crystallization, the solid product was recovered by filtration and was dried in air at room temperature. To remove the organic molecules occluded inside the zeolite pores, the sample was heated at a rate of 5 K min^{-1} to 923 K in air and kept at this temperature for 4 hours. Treatment of the calcined sample of CIT-1 with 0.01 N HCl (solid/liquid ratio of 1g/100 ml) for 24 h removes the B that is incorporated in the framework.[16] Insertion of aluminum into the framework positions was accomplished by reflux of the HCl treated sample in an Al(NO3)3 solution (CIT-1: Al(NO3)3 $\cdot$ 9H2O : H2O ratio = 1 : 2 : 50 by weight)[17] for 12 h. The CIT-1 samples treated with Al(NO3)3 will be denoted Al-CIT-1.

5.2.3 Analytical

X-ray powder diffraction (XRD) patterns were collected on a Scintag XDS 2000 diffractometer using Cu-Kα radiation and a solid-state Ge detector. The diffraction profiles were scanned over the range of 2°<2Θ <50° in steps of 0.02° with a count time of 15 s at

each point. Fluorophologopite mica (Standard Reference Material 675, National Bureau of Standards) was used as an external standard. Fourier-Transform infrared (FTIR) spectroscopy was carried out on a Nicolet System 800. The samples were prepared using the KBr pellet technique. Thermogravimetric analyses (TGA) were performed in air on a DuPont 951 thermogravimetric analyzer with a heating rate of 5 K min^{-1}. Nitrogen adsorption isotherms were collected at 77 K on an Omnisorp 100 analyzer. The scanning electron micrographs (SEM) were recorded on a Camscan series 2-LV scanning electron microscope. Elemental analyses were performed at Galbraith Laboratories Inc., Knoxville, Tennessee.

Liquid ^{13}C NMR spectra were collected on a GE 300 NMR QE Plus spectrometer. Solid-state NMR spectra were obtained on a Bruker AM 300 spectrometer equipped with a Bruker cross-polarization, magic angle spinning (CP/MAS) accessory. All samples were packed into ZrO_2 rotors. The ^{13}C MAS and CP/MAS NMR spectra (75.5 MHz) were recorded with a pulse length of 4 μs and a spinning rate of 3 kHz and were referenced to an adamantane standard (downfield resonance at 38.4 ppm). ^{29}Si NMR spectra (59.63 MHz) were collected using MAS and CP/MAS with a spinning rate of 2.2-3 KHz, and were referenced to a tetrakis(trimethylsilyl)silane standard (TMS, downfield resonance at -10.05 ppm). The sample used for ^{29}Si MAS NMR was steamed at 1023 K for 3 days in air. The air stream was bubbled in a 0.1 M NH_4F aqueous solution at room temperature before contact with the zeolite sample. The ^{13}C and ^{29}Si NMR spectra are reported referenced to TMS. The ^{27}Al MAS NMR spectra (78.2 MHz) were recorded using MAS at a spinning rate of 5 kHz and were referenced to a 1M aqueous aluminum nitrate solution (resonance at 0 ppm). The ^{11}B MAS NMR spectra (96.3 MHz) were obtained at a spinning rate of 4 kHz and were referenced to an aqueous solution of 1M boric acid (resonance at 0 ppm).

Synchrotron X-ray powder diffraction data (λ=1.30042(2) Å) were collected at Brookhaven National Laboratory at the X7A beam line. The diffraction profile was

scanned over the range of $2° < 2\Theta < 60°$ in steps of $0.01°$ with a count time of ~2 s at each point. Before recording the XRD pattern, the CIT-1 sample was calcined at 923 K, treated with HCl (*vide supra*) and exposed to a flowing stream of N_2 containing $SiCl_4$ vapors (see Li et al.[18] for details of this procedure) at 823 K. The sample was dried at 473 K before packing in a 1mm O.D. glass capillary.

5.2.4 Catalysis

The acidic properties of Al-CIT-1, ZSM-5 and zeolite beta were characterized using temperature programmed desorption (TPD) of ammonia. The experiments were carried out on a flow-type apparatus equipped with a fixed-bed and thermal conductivity detector. Approximately 300 mg of the sample were activated in a helium flow at 773 K for 1h. Pure ammonia, with a flow rate of 50 cm^3 min^{-1} was then passed through the sample at 423 K for 30 min. The sample was subsequently purged with He at the same temperature for 1.5 h to remove the physisorbed ammonia. The TPD was performed under helium flow of 100 cm^3 min^{-1} from 423 K to 873 K with a heating rate of 10 K min^{-1}.

The catalytic activity of zeolite samples in the n-butane cracking reaction was carried out in a flow type system equipped with a fixed-bed reactor. Prior to the cracking experiments, 200 mg of the sample were dehydrated *in situ* in the reactor system in a helium flow of 5 l h^{-1} at 873 K, after heating from room temperature at a heating rate of 5 K min^{-1}. A gaseous mixture of n-butane and helium (20% vol. n-butane) was used. The reaction was conducted at 783 K and atmospheric pressure with a total gas flow of 2 l h^{-1}. The reactant and products were analyzed with an on-line gas chromatograph using a flame ionization detector and a 50 m capillary column that contained cross-linked methyl silicone gum as stationary phase.

5.3 Results and Discussion

5.3.1 Structure of CIT-1

Using a borosilicate synthesis gel and N,N,N-trimethyl-(-)-*cis*--myrtanylammonium (I) as structure-directing agent resulted in the formation of a new molecular sieve that we have denoted as CIT-1.[19] The XRD pattern of a calcined sample of CIT-1 (Si/B=16) (Fig. 5.1a) reveals many similarities to the XRD pattern of SSZ-33 (Fig. 5.1b) indicating that it may be closely related to the structure of SSZ-33. However, the pattern of CIT-1 shows more reflections than the SSZ-33 pattern. The additional reflections could be the result of a higher degree of long-range order in the structure of CIT-1 than in the structure of SSZ-33, or it could be the result of the presence of other crystalline phases in the product. The SEM of CIT-1 (Fig. 5.2a) shows the morphology and size of CIT-1 crystals (typically 3 μm $\times$ 3 μm $\times$ 6 μm). The morphology is somewhat similar to the morphology of SSZ-33 crystals (Fig. 5.2b) although the CIT-1 crystals have sharper edges and on average are larger than SSZ-33 crystals. Many of the CIT-1 crystals are also twinned, in contrast to SSZ-33 samples that normally do not reveal this behavior. However, no other morphologies other than those shown here can be detected in the samples of CIT-1. Thus, it does not appear that CIT-1 is a physical mixture of more than one crystalline phase because multiple crystal morphologies are not detected. Therefore, the additional peaks in the XRD pattern of CIT-1 are more likely an indication of a higher degree of long-range order in the structure of CIT-1 compared to the structure of SSZ-33. Using results from our previous work on the structure solution of SSZ-33 and the related aluminosilicate SSZ-26, it appeared that the XRD pattern of CIT-1 was very close to the simulated XRD pattern of polymorph B of SSZ-33.[13]

All the peaks of the XRD pattern of calcined CIT-1 could be indexed with a monoclinic unit cell (Table 5.1). The optimized unit cell lattice parameters (a=22.620(8) Å, b=13.281(5) Å, c=12.371(5) Å, β=68.88(3)°) agree very well with the calculated unit cell parameters of polymorph B of SSZ-33 (a=22.62 Å, b=13.26 Å, c=12.33 Å, β=68.7°).[13] Additionally, the systematic absences are in agreement with the highest topological symmetry of the framework proposed for polymorph B (*C 2/m*, No. 12). However, these data would be also consistent with space groups *Cm* or *C2*.

Single-crystal ED patterns confirm the monoclinic unit cell derived from the XRD pattern. The C-centering (*h+k=2n*) is clearly observed in Figure 5.3a. We were unable to find, by electron diffraction methods, streaks along the [0 1 0] direction. The streaks are ubiquitous along this axis direction in the samples of SSZ-33, and they are a manifestation of the heavy stacking faults present in the SSZ-33 materials.[14] Although the absence of streaks in the ED pattern of CIT-1 does not prove that faults are completely absent, it is a strong indication that the faulting is infrequent (*vide infra*). Thus, electron diffraction data are in agreement with the postulate that CIT-1 is polymorph B of SSZ-33.

5.3.2 Rietveld Refinement of CIT-1

The sample used to obtain the synchrotron X-ray powder pattern, after treatment with HCl, presented in the ^{29}Si MAS and CP/MAS NMR spectra (not shown) a peak assigned to Q^3 silicon ((Si–O)$_3$–Si–OH) that was not found in the original sample. This new peak is in agreement with the premise that silanol groups are formed upon extraction of the B atoms. To reduce the number of silanol groups, the sample was then contacted with $SiCl_4$ vapors in a N_2 stream in attempts to implant Si atoms into the framework positions vacated by B. The intensity of the Q^3 peak was reduced by this treatment (not observed in the ^{29}Si MAS NMR spectrum), but it was still observable in the ^{29}Si CP/MAS NMR spectrum. These

NMR data indicate that the $SiCl_4$ treatment did indeed reduced the number of silanol groups present in the sample, but did not completely eliminate them.

The General Structure Analysis System[20] (GSAS) was used for the refinement of the CIT-1 sample. The refinement was initiated using the atomic positions obtained from the distance least-squares optimization of polymorph B of SSZ-33 and SSZ-26 (DLS-76)[21] using Si in all T atom positions and using the maximum topological symmetry of the framework ($C\ 2/m$, No. 12). Other crystallographic data for the refinement are summarized in Table 5.2. At the initial stage of the refinement, only the background coefficients and scale factors were optimized. In following stages, lattice parameters and then peak shape function parameters were also included in the refinement. After convergence of the refinement, the resulting residuals were Rp=14.8%, Rwp=22.6%. Analysis of the difference pattern showed that some peaks had smaller widths than others; the sharper peaks were systematically of the form ($h\ k\ 3n$). One possibility that could explain this anisotropic broadening is that, despite the ED data, there is some small amount of faulting present in the sample.

To test the effect that a small probability of faulting (p) has upon the XRD pattern, a series of simulated XRD patterns were produced using the program DIFFaX[22], the atomic coordinates obtained from DLS-76[13] and small values of p (see Fig. 5.4). The results from the simulations show that there is a clear effect in the width of several reflections for faulting probabilities even as low as 1%. To account for this effect in the refinement, the anisotropic broadening axis option of the GSAS program was used. A sublattice formed by the ($h\ k\ 3n$) reflections, which is not affected by the broadening effect, was defined. A new parameter characterizing the differences in the peak widths between the full lattice and the sublattice was optimized. After including this new variable, the values of the residuals dropped to Rp=12.6% and Rwp=16.4%.

In the next stage of the refinement, the atomic positional parameters of Si and O atoms were optimized. Soft geometrical constrains were placed on the Si–O bond distances (1.61 Å). The isotropic thermal parameters (U) were not optimized at this stage of the refinement and were fixed at a value of 0.015 $Å^2$ and 0.03 $Å^2$ for the Si and O atoms, respectively. The weight of the geometric constrains was gradually reduced, and in the final refinement, the isotropic thermal parameters of all Si atoms (refined as one variable) and of all O atoms (also refined as one variable) were optimized. The final values of the residuals were Rp=9.9% and Rwp=11.9%. The atomic positional parameters and thermal parameters are presented in Table 5.3, and the experimental, calculated and difference XRD patterns are shown in Figure 5.5. A stereo plot of the crystal structure of CIT-1 along [0 1 0] and along [0 0 1] is presented in Figure 5.6. The final residual electron density from a difference Fourier map was generally low (less than 1 e $Å^{-3}$), and no scattering matter that could be associated with atoms in the pores was found.

All the Si—O distances (Table 5.4) are within 2σ of the expected 1.61 Å and for each Si atom, average bond distances are in very good agreement with this value (differences are less than 0.05 Å). The minimum, maximum and average Si—O bond distances are 1.55 Å, 1.66 Å and 1.608 Å, respectively. The T—O—T angles (Table 5.4) range from 125 ° to 170° with an average of 155°. These values are within the ranges normally reported for Rietveld refinement of zeolites.[23] It is important to note that most of the long Si—O bond distances are associated with oxygen atoms placed along the mirror plane of *C2/m* (O(8), O(15), O(18), O(22) and O(23), marked with an asterisk in Table 5.4). This result most possibly indicates that the real symmetry of CIT-1 does not contain this mirror plane. If the mirror planes are removed, these oxygen atoms would move away from the mirror planes to form shorter Si—O bond distances (symmetry reduced to at least *C2*). Fyfe et al.[24] have shown that ^{29}Si MAS NMR can help to resolve issues regarding different alternatives of space groups that agree with the diffraction data. However, our

attempts to use ^{29}Si MAS NMR of a steamed sample to resolve the different crystallographic sites in CIT-1 were not successful (Fig. 5.7). Although the Q^3 resonance in the spectrum has been eliminated and a small shoulder at -116 ppm can now be observed, no insights into the number of T-sites could be obtained. Reduction of the symmetry to the space group $C2$ would increase the number of structural parameters to 134. Therefore, no attempts were made to lower symmetry in the refinement because only 17 uniquely defined reflections (out of 1085) can be observed in the XRD pattern. Similar limitations have been reported for other molecular sieves.[25]

The free diameters (maximum and minimum) for the 12MR channel are 6.8 Å $\times$ 6.4 Å (calculated from O(11)—O(11) and from O(18)—O(22) with an oxygen radius of 1.35 Å)[26] and for the 10RM channel are 5.1 Å $\times$ 5.1 Å (O(12)—O(21), O(9)—O(9)). These values are somewhat smaller than those observed in multidimensional 12MR pore materials like zeolite beta (7.6 Å $\times$ 6.4 Å) and faujasite (7.4 Å) and multidimensional 10MR pore materials like ZSM-5 (5.6 Å $\times$ 5.3 Å).[26] However, it is expected that combination of both pore sizes should give special catalytic properties to CIT-1.

The results from the Rietveld refinement of zeolite CIT-1 confirms the proposed topology of this material. CIT-1 is essentially the pure polymorph B of the disordered zeolite SSZ-33. The results of the refinement also indicate that CIT-1 is not completely fault-free. The overall stacking sequence of a CIT-1 crystal contains a small probability of faulting, probably close to 1%. Analysis of the Si—O bond distances also suggest that the real symmetry of the zeolite is probably lower than $C\ 2/m$, but no further refinement of the data was carried out in space groups of lower symmetry for reasons discussed above.

5.3.3 Synthesis of CIT-1

Pure samples of CIT-1 can be crystallized using a range of temperatures and chemical compositions. The temperature has a strong effect on the crystallization time. Fully crystalline product can be obtained in 8-10 days at 448 K and in 21-35 days at 423 K. However, there is a lack of reproducibility in the syntheses at 448 K, with large amounts of kenyaite (layered silicate)[27] often found in the final product. It is possible that at 448 K, the Hoffmann degradation of I is faster than at 423 K, and that the degradation products interfere with the synthesis of CIT-1. Most of the CIT-1 syntheses were therefore conducted at 423 K and all the characterization data given in this paper are from samples prepared at this temperature.

Comparison of the ^{13}C CP/MAS NMR spectrum of the as-synthesized sample of CIT-1 with the liquid ^{13}C spectrum of I indicates that I is occluded intact inside the pores of the zeolite. No other peaks are observed in the spectrum besides the ones assigned to I. The ^{11}B MAS spectrum of as-synthesized CIT-1 show only one peak at -3 ppm, consistent with the presence of only tetrahedrally coordinated boron in the product.

FTIR spectra of the as-synthesized CIT-1 and SSZ-33 are essentially identical, except for small differences in the region of 1400–1500 cm^{-1} (Fig. 5.8). These spectral features are due to differences in the IR spectra of the structure-directing agents I and IV. FTIR spectra of the calcined forms of the two zeolites show a band at 1400 cm^{-1}. This band is often found in the calcined form of borosilicate molecular sieves[28] and it is assigned to trigonal boron formed during the calcination process. Additionally, bands at 907 cm^{-1} in the as-synthesized CIT-1 and SSZ-33 are in agreement with the presence of boron in tetrahedral coordination[29] as observed in the ^{11}B MAS NMR spectrum. After calcination, both bands shift to ~927 cm^{-1} in a manner similar to other borosilicates such as B-SSZ-24 and B-ZSM-5.[28] The shift in this band from the as-synthesized to the calcined

samples is probably due to differences in the water coordination environment of the framework boron atoms.

CIT-1 can be synthesized from gels with SiO_2/B_2O_3 ratios between 30 and 60. The SiO_2/B_2O_3 ratios of the calcined products are 32 and 72, respectively. If higher SiO_2/B_2O_3 ratios are used, the product often contains small amount of SSZ-31.[30] No crystalline materials are obtained if B is absent from the synthesis gel. The formation of SSZ-31 at high SiO_2/B_2O_3 ratios is in agreement with results of Nakagawa[30] and Zones and Nakagawa,[31] who have shown that several structure-directing agents that form SSZ-33 zeolites at SiO_2/B_2O_3 ratios of 30 also form SSZ-31 at high SiO_2/B_2O_3 ratios. At SiO_2/B_2O_3 ratios below 30, CIT-1 forms, but is contaminated with layered oxide impurities. The layered, sodium silicate, kenyaite was clearly observed in the XRD pattern of all the samples that were synthesized with SiO_2/B_2O_3 ratios of 25. The formation of layered silicates for syntheses using sodium borate as source of boron have been observed for other high-silica materials.[17,31] Sodium borates with SiO_2/B_2O_3 ratios below 25 were not investigated. We were also unable to synthesize any crystalline product if the borate was substituted by sodium aluminate or by aluminum nitrate when I was used as the structure-directing agent (even after several months of heating). Similar results have been reported by Zones and Nakagawa[31] for the synthesis of SSZ-33.

The presence of a small amount of sodium is necessary for the synthesis of CIT-1. If boric acid is used instead of sodium borate and no other source of sodium is added to the synthesis gel, no crystalline material is formed. $SiO_2/NaOH$ ratios of 5-10 are typical for most of the syntheses. Higher sodium concentrations, as it has been observed for zeolite ZSM-12,[32] promote the nucleation of layered materials. Only small amounts of Na (less than 0.4%) are detected in the calcined samples.

Small amounts of as-synthesized B-zeolite beta (borosilicate analogue of zeolite beta) are found to promote the nucleation of CIT-1. The B-zeolite beta is a better promoter

than the seed crystals of CIT-1. The reasons for this behavior are not understood at this time.

It is important to emphasize that none of the effects discussed above—temperature, sodium or boron concentration and the use of CIT-1 or zeolite beta as nucleation promoters— have any noticeable effect on the fault probability (as observed by X-ray powder diffraction). This is an indication that the long-range order observed in CIT-1 is related primarily to the structure-directing agent I and not to any of the other inorganic components in the synthesis gel.

What is special about I that allows it to form the ordered polymorph B of SSZ-33? First, a test to see whether the selectivity is related to the chirality of I was performed. To do so, the enantiomorph of I, namely II, was prepared and the following two syntheses were carried out: one using only II and a second with equimolar amounts of I and II (racemic). The products of these two syntheses are indistinguishable —by XRD— from the CIT-1 sample prepared using I. The results from the first experiment are not surprising and imply that the selectivity of I towards the formation of polymorph B is not correlated with chirality. This is expected because neither polymorph A or B of SSZ-33 is chiral and therefore their interactions with each enantiomorph of the organic structure-directing agent (I or II) should be the same. The result from experiment two indicates that intermolecular interactions between organic molecules are probably <u>not</u> involved in the step(s) that define the layer ordering in CIT-1. If this were the case, then interactions between two molecules of I (or two of II) should be different than interactions between a molecule of I and II. A second possibility for the structure-directing effect of I on CIT-1 is that the selectivity for an ordered layer sequence in CIT-1 is related to the myrtanyl, polycyclic group. If this were the case, it is expected that III, an isomer of I, would also form CIT-1. The product of a zeolite synthesis using III at similar conditions to those used above gives neither CIT-1, or SSZ-33, but SSZ-31. Zeolite SSZ-31 has been prepared with a variety of organo-

cations of approximately cylindrical shape.[30] The crystallization of SSZ-31 using **III** is then understandable in terms of the geometry of this organic molecule. In **III**, the trimethylammonium group is diagonally opposite to the two methyls of the cyclobutane ring of the pinane group. Thus, the molecule is approximately cylindrical in shape and can thus direct the formation of SSZ-31. This result indicates that the selectivity of **I** is not due to the shape of the polycyclic myrtanyl group alone. The geometry of the complete molecule is required to achieve the long-range order observed in CIT-1.

Further insight into the structure-directing effects of **I** can be obtained by comparing the molecules that form SSZ-33 to those that form CIT-1. SSZ-33 can be synthesized using a variety of structure-directing agents that have a wide diversity of shapes. Although SSZ-33 is normally synthesized using the tricyclo[5.2.1.0^{2,6}]decane derivative **IV**,[5] the synthesis of SSZ-33 has also been reported using molecules **V-VIII**.[31] Thermogravimetric analyses of SSZ-33 synthesized with **IV** show two stages of weight loss: one stage between 298-573 K at 0.4% which is assigned to water desorption, and a second stage between 573-923 K with a weight loss of 18.2% that is assigned to the pyrolysis and combustion of **IV**. The second weight loss corresponds to 3.9 molecules of **IV** ($C_{13}H_{26}N$) per unit cell of SSZ-33. The TGA of CIT-1 also shows two stages of weight loss. For CIT-1, the weight loss between 298-573 K is 1.5% and between 573-923 K is <u>only</u> 14.5% (**I**:$C_{13}H_{26}N$). The high-temperature weight loss from CIT-1 corresponds to 2.9 molecules of **I** per unit cell. Given the similarity in the chemical composition of **I** and **IV**, this difference is significant. The TGA results indicate that for CIT-1 the geometry of **I** is such that the molecule cannot adopt a conformation inside the void space that completely fills the pores (*vide infra*). This is unlike **IV**, which seems to adopt a conformation that fill the pores more completely. The very small water loss (only 0.4%) of SSZ-33 prepared with **IV** is also in agreement with a very efficient packing of **IV** inside the void space.

The differences in weight loss at high temperature between SSZ-33 and CIT-1 are not the result of differences in void volume or pore sizes between these two structures. The n-hexane adsorption capacity of CIT-1 is 0.18 ml g^{-1}(P/P$_0$=0.3) very similar to the cyclohexane adsorption capacity reported for SSZ-33 (0.20 ml g^{-1}). Additionally, physical adsorption isotherms of N_2 at 77 K for both materials are very similar (Fig. 5.9), but are different from the isotherms obtained for multidimensional 12MR zeolites (zeolite beta) and multidimensional 10MR zeolites (ZSM-5).
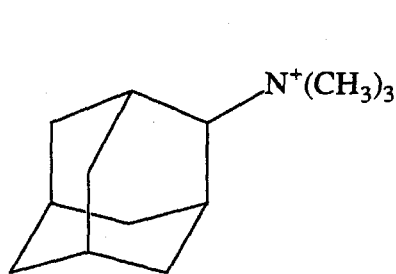
V
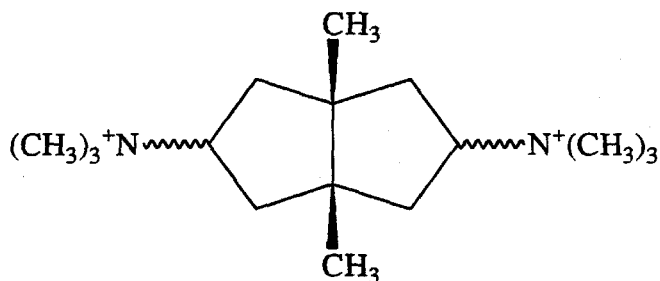
VI
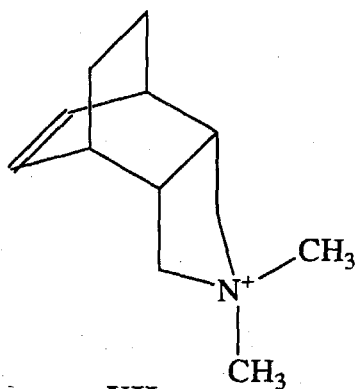
VII
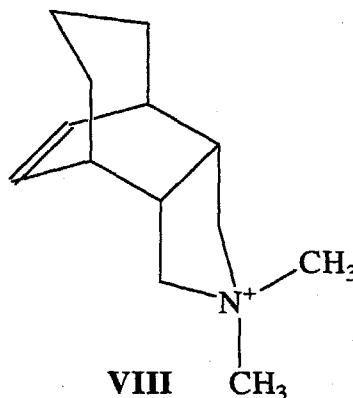
VIII

De Ruiter et al.[29] have previously indicated that for B-substituted ZSM-5 and β zeolites, there appears to be an approximate one-to-one correspondence between the number of positive charges of the organic cations per unit cell and the negative charges

introduced to the silicate by the isomorphous substitution of B^{3+} for Si^{4+}. Similar to the results observed by de Ruiter et al. for other borosilicates,[29] it is found here for CIT-1 from chemical analysis that there are 3.3 B atoms per unit cell, in rough agreement with the 3 molecules of **I** per unit cell derived from TGA. The chemical analysis of SSZ-33 indicates that there are 3.8 B atoms per unit cell which is also in correspondence with the results derived from TGA for the number of organic molecules per unit cell.

To test further the relationships betwen CIT-1 and SSZ-33, syntheses were carried aout using two structure-directing agents (**I** and **IV**). Five different preparations were investigated using mixtures of **I** and **IV** in the molar ratios of 100:0, 75:25, 50:50, 25:75 and 0:100. The XRD patterns of the calcined samples (Fig. 5.10a) show that there is a continuous change in the faulting probability from p=30% (SSZ-33) synthesized using only **IV** to p~0% for materials synthesized with **I** (CIT-1). These XRD patterns correlate very well with simulations using fault probabilities of p=30, 22.5, 15, 7.5 and 0% (Fig. 5.10b), and indicate that the fault probability changes linearly with the relative concentrations of the structure-directing agent (**I**). ^{13}C CP/MAS NMR of the as-synthesized samples (Fig. 5.11) also show a continous change in the NMR spectrum of **I** to the NMR spectrum of **IV**. This change, however, did not correlate linearly with the amounts placed in the synthesis gels (^{13}C CP/MAS NMR of physical mixtures of CIT-1 and SSZ-33 (not shown) were used for comparison). The nonlinear change in the amount of **I** and **IV** may be due to the preferential occlusion of **IV** over **I**, as found in the TGA experiments of pure SSZ-33 and CIT-1. Thus, it is clear that molecule **I** controls the ABC... stacking se nce fo polymorph B.

5.3.4 Energy Minimization Calculations

Energy minimizations of molecules **I** and **IV** in the pores of polymorph A and B of SSZ-33 were calculated to gain some insights into the structure-directing effects of molecule **I** and **IV** on the formaiton of CIT-1 and SSZ-33, respectively. The objective of the energy minizations is to find *i*) the most favorable conformation of these molecules in the zeolite pores, and *ii*) to determine the reasons why the trimethylmyrtanylammonium cation directs the crystallization of only polymorph B and not polymorph A. The minimizations were carried out using Cerius 3.2 software using the crystal packer module. We limited our modeling strictly to van der Waals interaction energies between organic molecules and pure-silica frameworks. Electrostatic interaction energies were not used because we do not have enough information about charge distribution in the organic molecules, the distribution of water in the pores and the distribution of B framework atoms in the zeolite to form a realistic model. We do, however, expect that the key to the selectivity of **I** over **IV** for the formation of polymorph B will be captured by short-range interactions between the organic molecule and the framework. The simulations treat the zeolite framework and the organic molecule as rigid units. This is not a severe limitation for the organic molecules which, in this case, are fairly rigid. It is, nevertheless, a source of error for the framework because it has been previously shown that the framework of zeolite structures adapts to the shape and size of adsorbed organic molecules with small displacive transitions.[33-35] It is noteworthy to say that the geometrical differences between the pore shapes of both polymorphs are rather small. They consist mainly of differences in the positions of the O atoms that bound the 10-ring pores.

To find the energy minima, the organic molecules (one per unit cell) were placed randomly in the zeolite pores in 20 different positions. Then, the energy minimization program translated and rotated the molecule until it reached an energy minimum. The results of the minimizations are shown in Table 5.5. No difference between the interaction

energies are observed for polymorphs A and B and for molecules **I** and **IV** along the 12MR pores. Minimum energies along 10MR pores were consistently of lower stability for both molecules than the minimum energies along the 12MR pores. This indicates, as expected, that the organic molecules will reside along the large pores instead of along the medium ones. The interaction energy of **I** with the framework along the 10-ring pores is substantially less negative than the equivalent interaction of **IV**. Indeed, it was difficult to find a minimum energy conformation for **I** along the 10MR because the minimization routines would translate it to the 12MR pores (in contrast with **IV** for which there were several minima along the 10MR pores). This result is in agreement with the TGA of CIT-1, which indicates that the packing of **I** in the zeolite pores is more constrained than the packing of **IV**. Further diffraction investigations of **I** inside the CIT-1 pores will be necessary to unravel the geometrical relationships of molecule **I** with the architecture of these zeolites.

5.3.5 Catalytic Properties of CIT-1

After treatment with the aluminum nitrate solution, the ^{27}Al MAS NMR spectrum of Al-CIT-1(Si/Al=35) showed two peaks at 56 and 0.5 ppm with relative areas of 6.5:1, respectively. These two peaks are assigned to Al in tetrahedral and octahedral coordination, respectively. The ^{27}Al NMR spectrum reveals that Al is incorporated in the framework (in tetrahedral coordination) and it is expected to form a strong acid site upon activation.

Ammonia TPD of Al-CIT-1 is compared to a ZSM-5 sample (Si/Al=31) in Figure 5.12. The TPD curves of both samples are characterized by two desorption peaks. The relative acidity of the strong acid sites (peak at 675 K) of Al-CIT-1 is slightly smaller than the acidity of the strong acid sites in ZSM-5 (peak at 725 K). It can also be observed that

the relative amount of weak acid sites (peak at about 550 K) to the amount of strong acid sites in Al-CIT-1 is larger than in ZSM-5.

Al-CIT-1 was found to be very active for the n-butane cracking reaction. The conversion of the sample of Al-CIT-1 after 6 h of reaction time was 31%, slightly better than the conversion of zeolite beta. Additionally, AL-CIT-1 showed an slower rate of deactivation than zeolite beta. Zeolite ZSM-5 showed a higher conversion than the other 12-ring zeolites (80%), and also showed a very small deactivation rate. The higher activity may be related to the realtive acidity of the catalytic sites inside the ZSM-5 pores and the very small deactivation rate is probably due to the smaller pores of the ZSM-5 zeolite. The smaller pores would inhibit the formation of the intermediates that are responsible for the deactivation process. The catalytic results shown here indicate that Al-CIT-1 presents similar catalytic activity than related high-silica molecular sives. Further studies are necessary to test the selectivity of this novel material.

5.4   Conclusions

A new borosilicate molecular sieve, CIT-1, has been synthesized. Rietveld refinement of the synchrotron XRD of CIT-1 confirms that this zeolite is essentially the pure polymorph B of the disordered zeolite SSZ-33. The presence of long range order in CIT-1 is a direct consequence of the structure-directing agent (N,N,N-trimethyl (-)-*cis*-myrtanylammonium (**I**)) and does not depend on temperature or the relative concentration of the inorganic components in the synthesis gel.

The fault probability of the SSZ-33 type of materials can be controlled using mixtures of structure-directing agents **I** and **IV**. The results from preliminary energy minimization calculations of **I** inside the polymorph A and polymorph B of SSZ-33

revealed no conclusive information. No preference for the incorporation of **I** inside either of the two polymorphs was detected. Treatment of CIT-1 with aluminum nitrate transforms CIT-1 into a very active catalyst for the cracking of n-butane.

5.5 References

(1) I.E. Maxwell and W.H.J. Stork, In *Stud. Sur. Sci. Catal.* H. van Bekkum, E. M. Flanigen and J. C. Jansen, Eds., Elsevier: Amsterdam, 1991, pp 571-630.

(2) L. Moscou, In *Stud. Sur. Sci. Catal.* , H. van Bekkum, E. M. Flanigen and J. C. Jansen, Eds., Elsevier: Amsterdam, 1991, pp 1-12.

(3) M.E. Davis, *Ind.Eng. Chem. Res.* **1991**, *30*, 1675-1683.

(4) J.M. Newsam, In *Solid State Chemistry: Compounds*, A. K. Cheetham and P. Day, Eds., Oxford University Press: New York, 1992, Vol. 2.

(5) S.I. Zones, U.S. Patent 4963337, 1990.

(6) S.I. Zones *et al*, U.S. Patent 4910006, 1990.

(7) M.E. Shannon, L.J. Casci, P.A. Cox, S.J. Andrews, *Nature* **1991**, *353*, 417-420.

(8) Y. Nakagawa, U.S. Patent 5,254,514, 1993.

(9) Y. Nakagawa, In *Stud. Sur. Sci. Catal.*, Elsevier: Garmisch-Partenkirchen, Germany, 1994, pp 323-330.

(10) M.E. Leonowicz, J.A. Lawton, S.L. Lawton, M.K. Rubin, *Science* **1994**, *264*, 1910-1913.

(11) S.I. Zones, European Pat. Appl. EP 231,019, 1987.

(12) M.E. Davis and R.F. Lobo, *Chem. Mater.* **1992**, *4*, 756.

(13) R.F. Lobo, M. Pan, I. Chan, H.X. Li, R.C. Medrud, S.I. Zones, P.A. Crozier, M.E. Davis, *Science* **1993**, *262*, 1543-1546.

(14) R.F. Lobo, M. Pan, I. Chan, R.C. Medrud, S.I. Zones, P.A. Crozier, M.E. Davis, *J. Phys. Chem.* in press.

(15) H.C. Brown, K.-W. Kim, M. Srebnik, B. Singaram, *Tetrahedron* **1987**, *43*, 4071-4078.

(16) R. de Ruiter, A.P.M. Kentgens, J. Grootendorst, J.C. Jansen, H. van Bekkum, *Zeolites* **1993**, *13*, 128-138.

(17) R.A. Van Nordstrand, D.S. Santilli, S.I. Zones, In *Synthesis of Microporous Materials*, M. L. Occelli and H. Robson, Eds., Van Nostrand Reinhold: New York, 1992, Vol. 1, pp 373.

(18) H.X. Li, C.Y. Chen, M.J. Annen, J.P. Arhancer, M.E. Davis, M. E. *J. Mater. Chem.* **1991**, *1*, 79-85.

(19) R.F. Lobo and M.E. Davis, U.S. Patent Application, 1993.

(20) A.C. Larson and R.B. Von Dreele *General Structure Analysis System*, Los Alamos National Laboratory: Los Alamos, NM, 1994.

(21) C. Baerlocher, A. Hepp, W.M. Meier, *DLS-76*, In Institut für Kristallographie et Petrographie, ETH: Zurich, 1976.

(22) M.M.J. Treacy, M.W. Deem, J.M. Newsam, *Proc. R. Soc. London A* **1991**, *433*, 499.

(23) I. Petrovic, A. Natvrotsky, S.I. Zones, M.E. Davis *Chem. Mater.* **1993**, *5*, 1805-1813.

(24) C.A. Fyfe, H. Gies, G.T. Kokotailo, C. Pasztor, H. Strobl, D.E. Cox *J. Am. Chem. Soc.* **1990**, *111*, 2470-2474.

(25) Kennedy, G. J., Higgins, J. B., Ridenour, C. R., Li, H. X., Davis, M. E. *J. Magnetic Resonance,* in press.

(26) Meier, W. M., Olson, D. H. *Atlas of Zeolite Structure Types,* 3rd ed., Butterworth-Heinemann: Stoneham, MA, 1992.

(27) K. Beneke and G. Lagaly *Am. Miner.* **1983**, *68*, 818-826.

(28) R.F. Lobo and M.E. Davis *Microporous Mater.* **1994**, *in press.*

(29) R. de Ruiter, J.C. Jansen, H. van Bekkum *Zeolites* **1992**, *12*, 56-62.

(30) Y. Nakagawa, S.I. Zones, In *Synthesis of Microporous Materials*, M. L. Occelli and H. Robson, Eds., Van Nostrand Reinhold: New York, 1992, Vol. 1, pp 222-239.

(31) S.I. Zones, Y. Nakagawa, *Microporous Mater.* **1994**, *2*, 543-555.

(32) Goepper, M., Li, H. X., Davis, M. E. *J. Chem. Soc., Chem. Commun.* **1992**, 1665-1666.

(33) van Koningsveld, H., van Bekkum, H., Jansen, J. C. *Zeolites* **1987**, *7*, 564-568.

(34) van Koningsveld, H., Tuinstra, F., van Bekkum, H., Jansen, J. C. *Acta Crystallogr., Sect. B* **1989**, *45*, 423-431.

(35) van Koningsveld, H., Jansen, J. C., van Bekkum, H. *Zeolites* **1990**, *10*, 235-242.
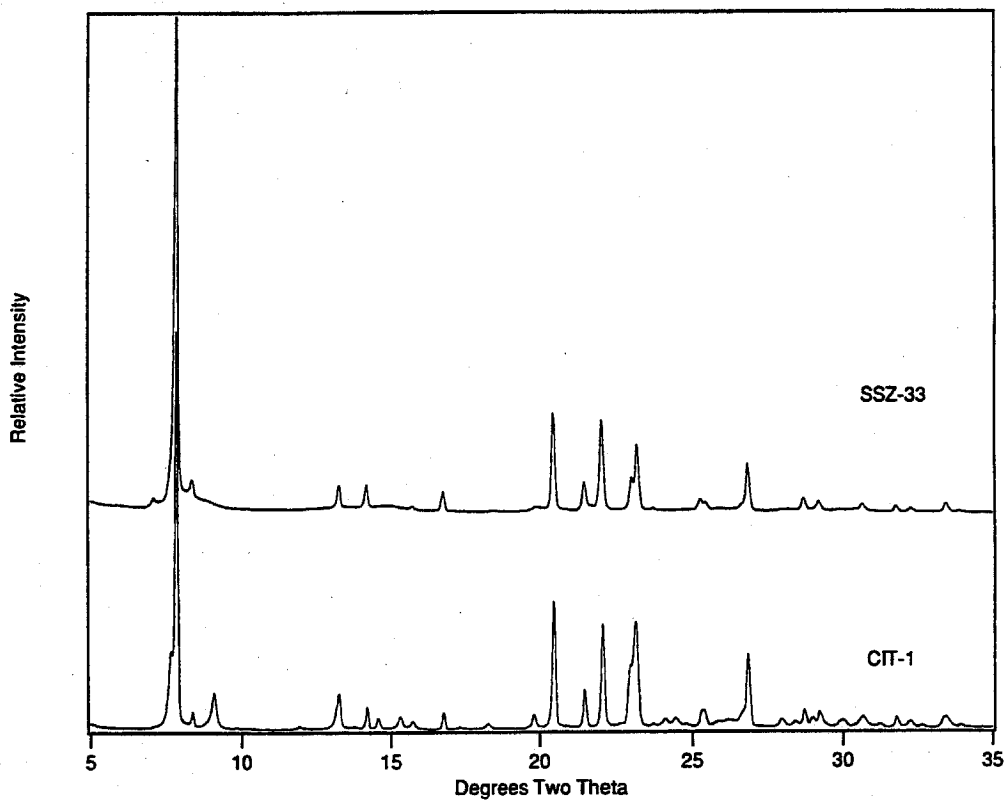
Figure 5.1　X-ray powder diffraction patterns of zeolites SSZ-33 and CIT-1 (Cu Kα radiation, λ=1.5460 Å).
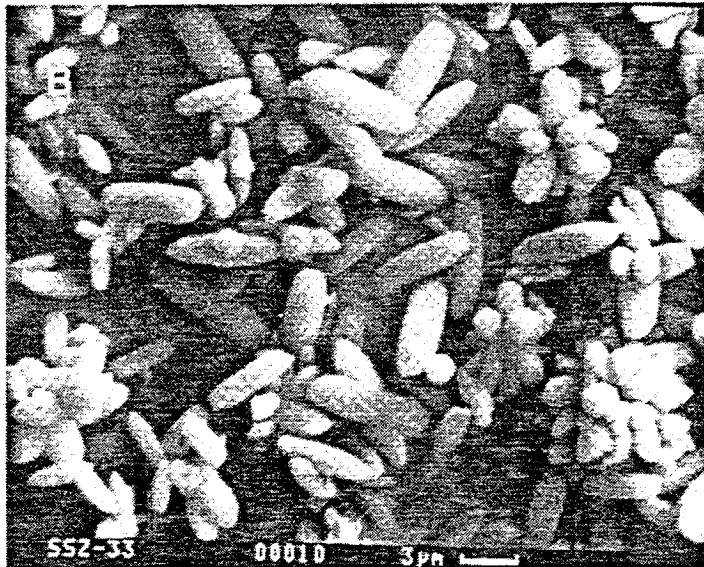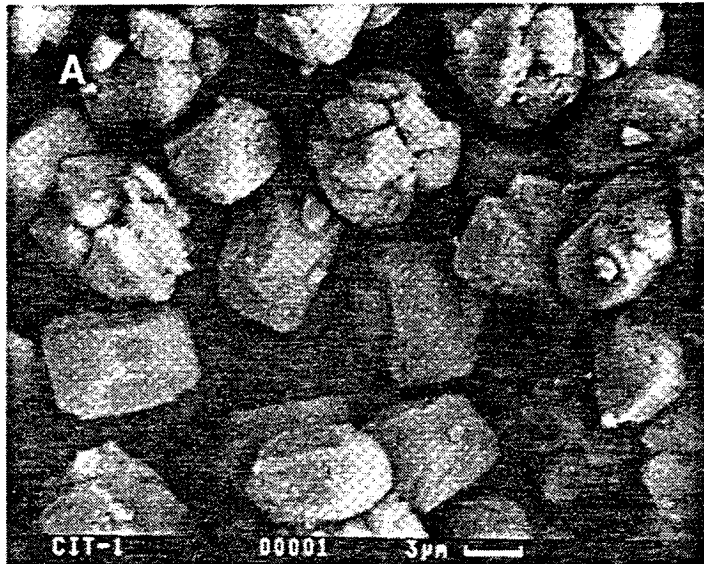
Figure 5.2   Scanning electron micrograph of zeolite CIT-1 (a) and of zeolite SSZ-33 (b).
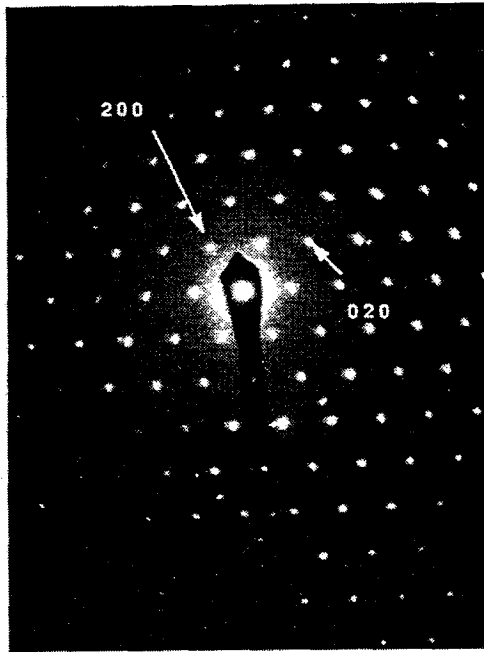
Figure 5.3   Electron diffractogram of zeolite CIT-1 along [0 0 1].
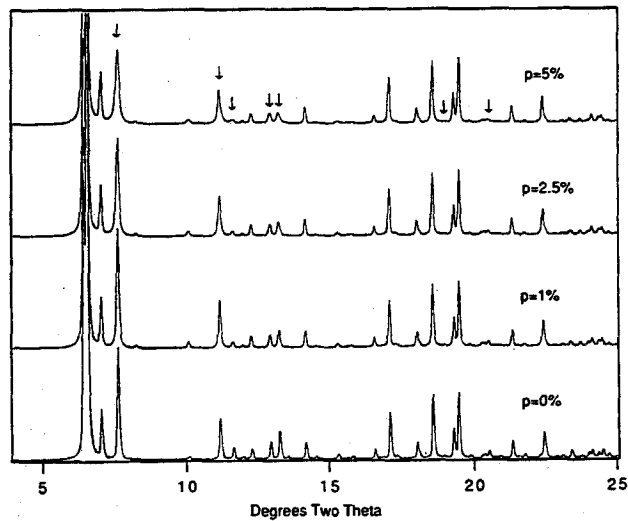
Figure 5.4   Effect of small values of the faulting probability p on the simulated XRD

patterns of polymorph B of zeolite SSZ-33 (λ=1.3004 Å).
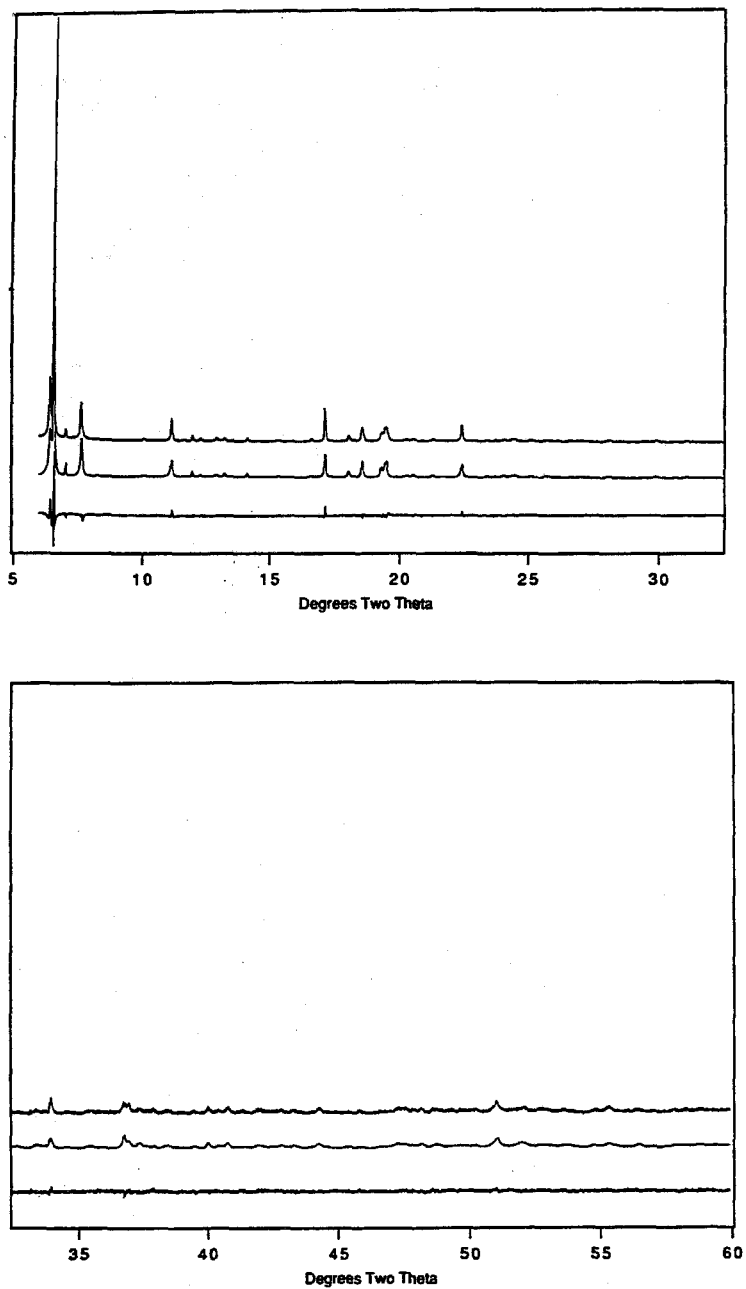
Figure 5.5   Observed (upper), calculated (middle) and difference (lower) profiles for synchrotron XRD patterns of zeolite CIT-1 (λ=1.3004 Å). The intensity scale has been increased 8 times for the section between 32-60 ° 2Θ.
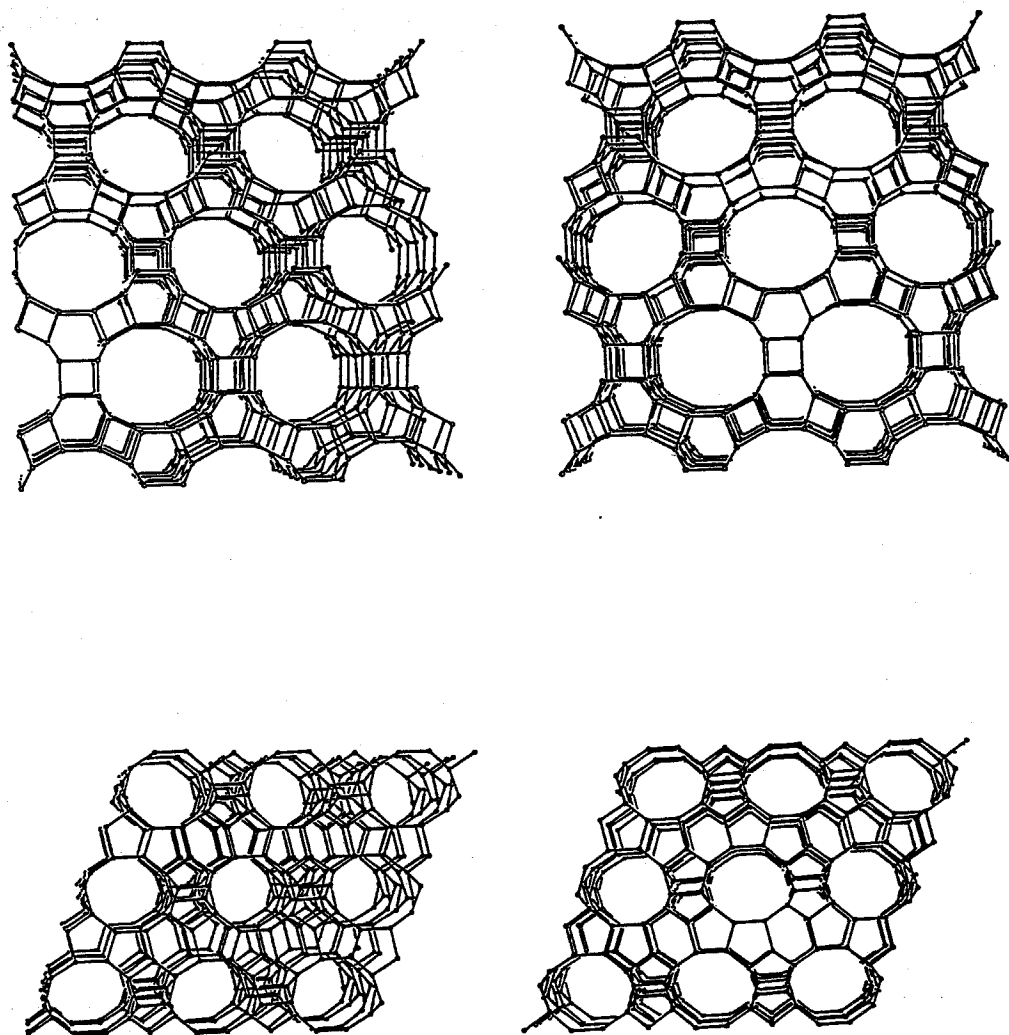
Figure 5.6   Stereoplot of the framework structure of CIT-1 view along [0 0 1], i.e., the
              12MR channels (top), and viewed along [0 1 0], i.e., the 10MR channels
              (bottom). The oxygen atoms have been omitted for simplicity.
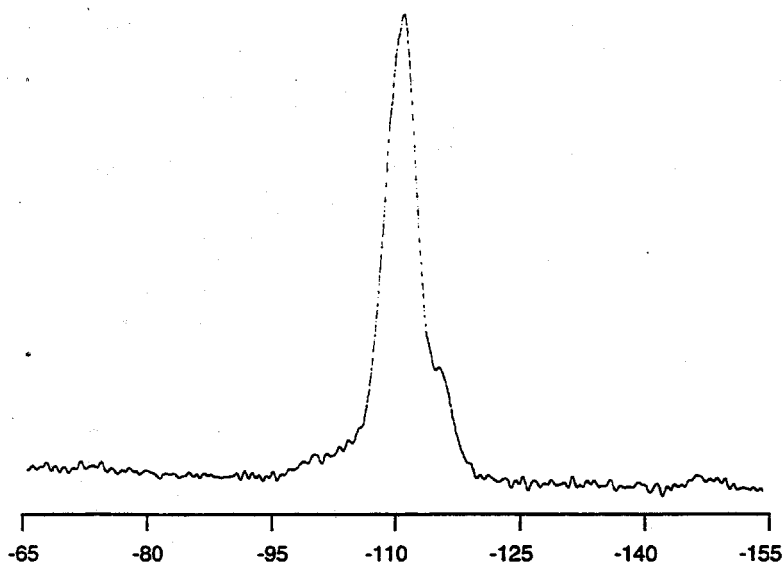
Figure 5.7 ^{29}Si MAS spectrum of CIT-1 after steaming.
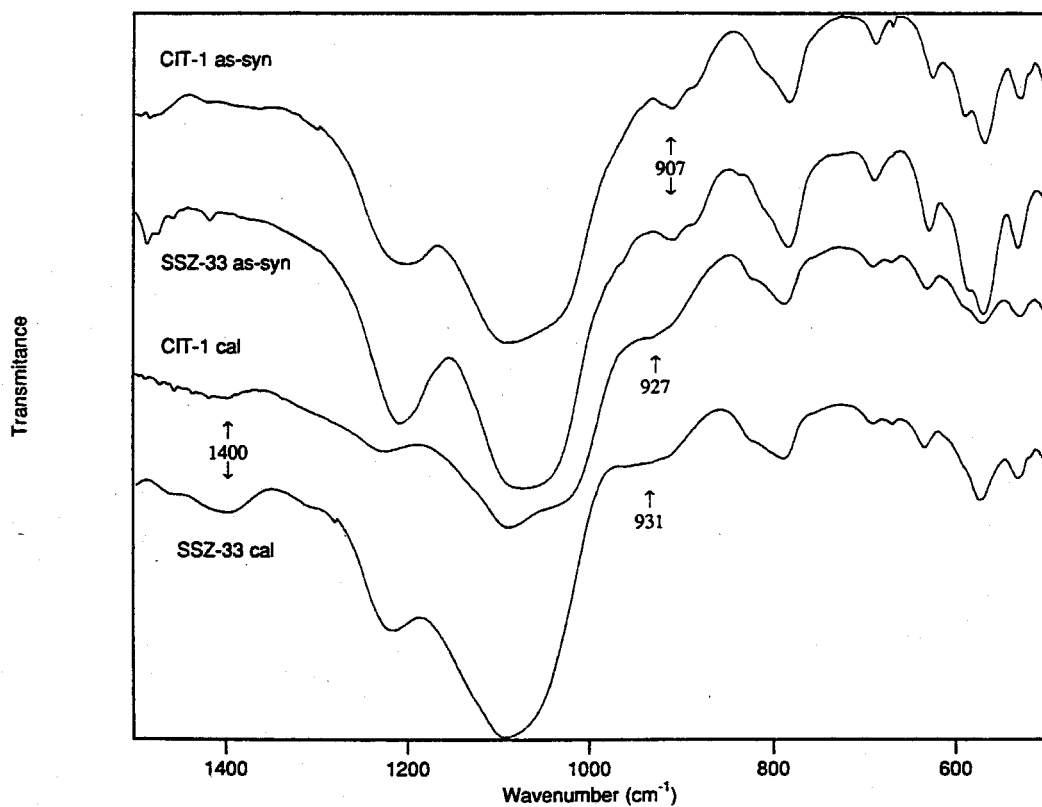
Figure 5.8   FTIR spectra of as-synthesized samples of CIT-1 and SSZ-33 (top) and the

calcined samples of CIT-1 and SSZ-33 (bottom).
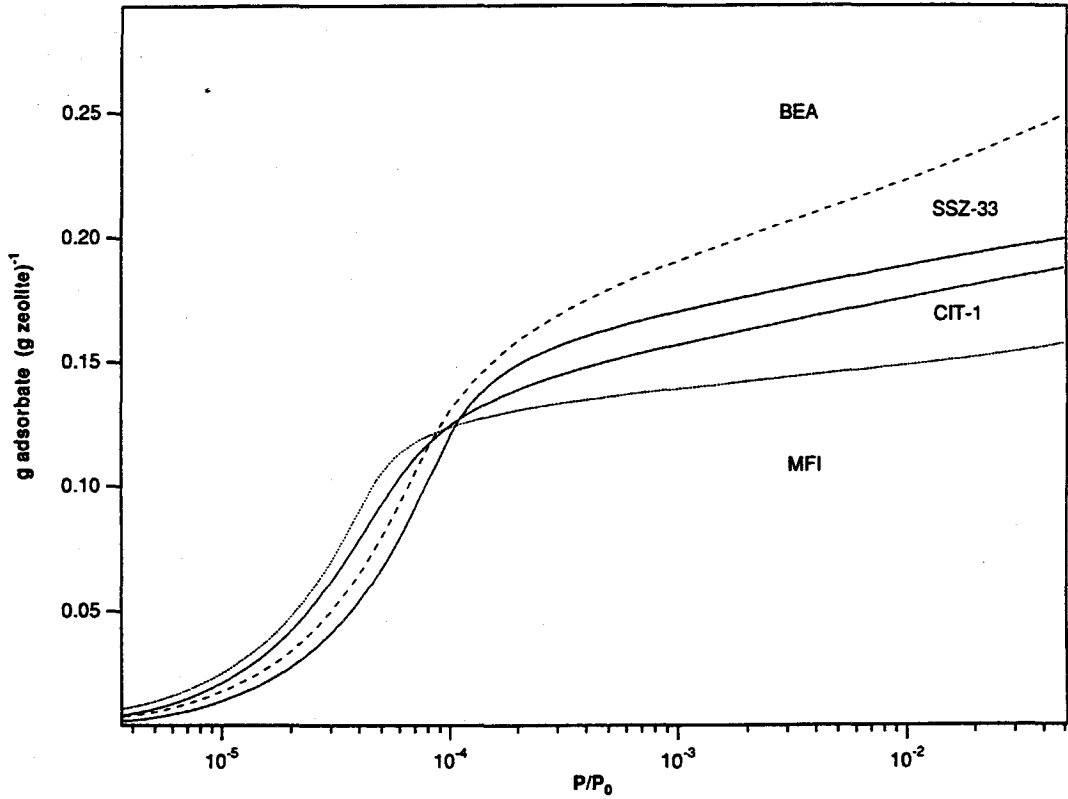
Figure 5.9   Physical adsorption isotherms of N_2 at 77 K for CIT-1, SSZ-33, ZSM-5

and zeolite beta.
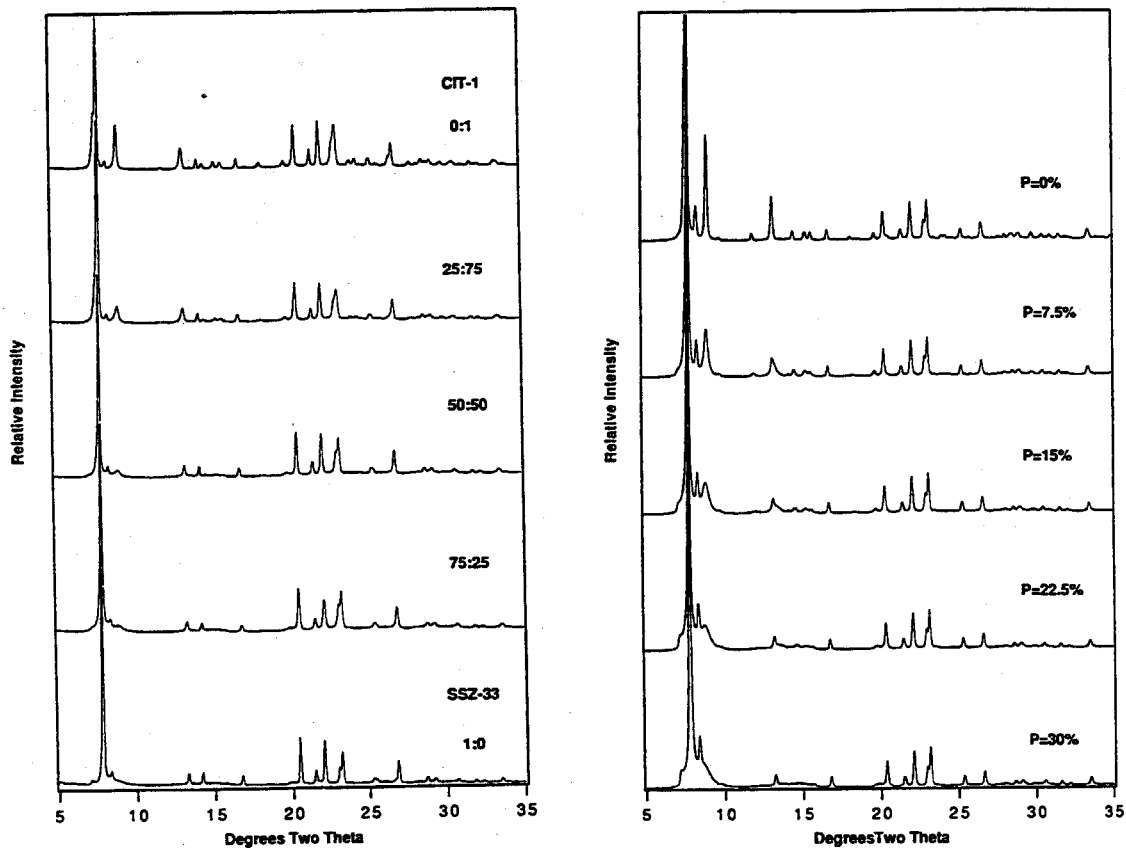
Figure 5.10   (a) Experimental XRD patterns of zeolite samples prepared using mixtures of molecules **I** and **IV**. (b) Simulated XRD patterns of materials with 0, 7.5, 15, 22.5 and 30% fault probabilities.
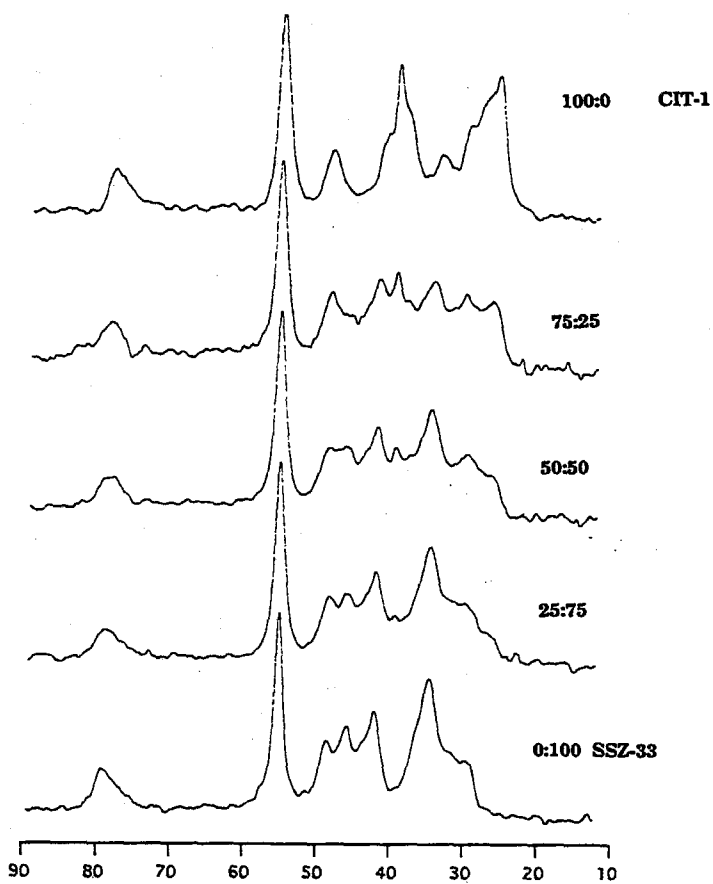
Figure 5.11 ^{13}C CP/MAS NMR spectra of zeolite samples prepared using mixtures of molecules **I** and **IV**.
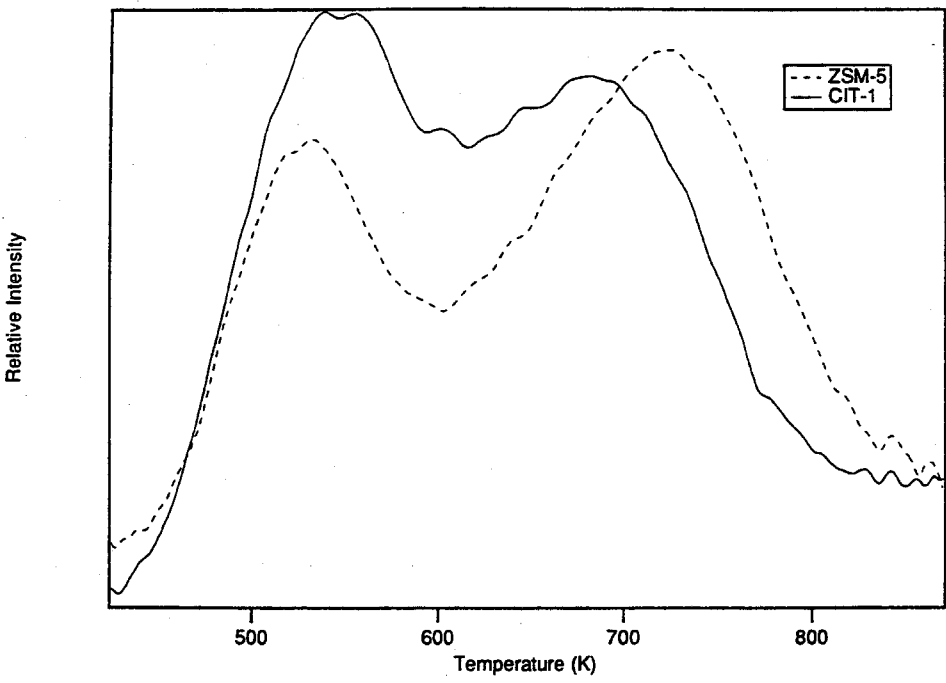
Figure 5.12   Ammonia TPD profile of Al-CIT-1 and ZSM-5.

Table 5.1   d-spacing and indexing for a calcined CIT-1 sample.

d/(Å)	I/I$_0$[a]	h	k	l
11.50	66	0	0	1
11.26	100	1	1	0
10.57	10	2	0	0
9.75	26	2	0	1
7.38	2	1	1	-1
6.69	3	2	0	-1
6.64	12	0	2	0
6.39	2	3	1	1
6.22	7	3	1	0
6.06	4	2	0	2
5.77	7	0	0	2
5.62	3	4	0	1
5.28	6	4	0	0
5.11	22	3	1	2
4.86	3	4	0	2
4.48	21	2	2	2
4.33	53	1	3	0
4.13	18	4	2	0
4.02	44	5	1	0
3.87	49	3	1	3
3.84	55	4	0	3
3.75	1	3	3	0
3.69	5	2	2	-2
3.64	6	6	0	2
3.59	2	4	2	-1
3.51	12	2	2	3
3.45	3	5	1	-1
3.34	15	4	0	-2
3.32	27	0	4	0
3.19	4	0	4	-1
3.14	18	2	4	1
3.11	7	6	2	0
3.08	4	2	0	4
3.05	15	5	3	0

a   Calculated as the ratio of the peak area and the peak area of the 1 1 0 reflection.

Table 5.2   Crystallographic data

Data collection temperature	298 K
Wavelength	1.30042(2) Å
Profile Range	6-60 °
Step Scan Increment	0.01 °
Space Group	$C\,2/m$ (No. 12)
a	22.6240 (1) Å
b	13.3503 (4) Å
c	12.3642 (6) Å
β	68.913 (4) °
No. Observations	5417
No. Reflections	1085
No. Uniquely defined reflections	17
No. Profile Parameters	12
No. Structural Parameters	68
Rwp	11.9 %
Rp	9.9 %

Table 5.3 Refined atomic positional parameters in space group $C\,2/m$ (No. 12) and e.s.d. in parentheses. The isotropic thermal parameters of the Si and O atoms converged to $U_i=0.0187(24)$ Å^2 and $U_i=0.018(4)$ Å^2, respectively.

Atom	Site	x	y	z
SI(1)	8j	0.0677(11)	0.1102(20)	0.4914(26)
SI(2)	8j	0.1567(13)	0.1889(19)	0.2510(27)
SI(3)	8j	0.0734(13)	0.1204(18)	0.7390(23)
SI(4)	8j	0.2879(12)	0.1171(19)	0.1026(24)
SI(5)	8j	0.2770(11)	0.1141(21)	0.8607(23)
SI(6)	8j	0.0738(14)	0.1195(19)	0.1043(30)
SI(7)	8j	0.1480(13)	0.1898(21)	0.8835(26)
O(8)	4i	0.0763(23)	0.0000	0.4256(55)
O(9)	8j	0.0784(22)	0.1380(29)	0.6085(37)
O(10)	8j	0.1205(20)	0.1669(31)	0.3814(35)
O(11)	4h	0.0000	0.1458(41)	0.5000
O(12)	8j	0.2185(17)	0.1200(34)	0.2009(37)
O(13)	8j	0.1097(21)	0.1569(30)	0.1860(43)
O(14)	8j	0.1728(19)	0.3005(28)	0.2109(40)
O(15)	4i	0.0852(27)	0.0000	0.7309(51)
O(16)	8j	0.0003(20)	0.1379(29)	0.8223(43)
O(17)	8j	0.1271(18)	0.1859(29)	0.7717(35)
O(18)	4i	0.3045(25)	0.0000	0.1272(62)
O(19)	8j	0.2721(17)	0.1330(31)	0.9904(36)
O(20)	8j	0.3442(18)	0.1888(30)	0.0983(42)
O(21)	8j	0.2102(19)	0.1217(35)	0.8382(39)
O(22)	4i	0.3046(29)	0.0000	0.8219(57)
O(23)	4i	0.0873(28)	0.0000	0.1087(70)
O(24)	8j	0.0837(17)	0.1783(30)	0.9900(35)

Table 5.4 Interatomic distances (Å) and angles with e.s.d.'s in parentheses.

Si(1)—O(8)	1.659(33)*		Si(5)—O(14)	1.628(35)	
O(9)	1.596(35)		O(19)	1.59(4)	
O(10)	1.637(33)		O(21)	1.635(34)	
O(11)	1.570(24)*		O(22)	1.651(29)*	
mean	1.615		mean	1.626	
Si(2)—O(10)	1.55(4)		Si(6)—O(13)	1.59(4)	
O(12)	1.601(35)		O(16)	1.612(35)	
O(13)	1.60(4)		O(23)	1.628(25)*	
O(14)	1.571(31)		O(24)	1.56(4)	
mean	1.581		mean	1.598	
Si(3)—O(9)	1.59(4)		Si(7)—O(17)	1.61(4)	
O(15)	1.626(23)*		O(20)	1.655(33)	
O(16)	1.62(4)		O(21)	1.597(35)	
O(17)	1.662(34)		O(24)	1.579(34)	
mean	1.624		mean	1.610	
Si(4)—O(12)	1.602(33)				
O(18)	1.661(27)*				
O(19)	1.567(34)				
O(20)	1.58(4)				
mean	1.602				

Si(1)—O(8)—Si(1)	125.0(5)*
Si(1)—O(9)—Si(3)	154.9(3)
Si(1)—O(10)—Si(2)	155.0(4)
Si(1)—O(11)—Si(1)	145.0(5)*
Si(2)—O(12)—Si(4)	142.0(4)
Si(2)—O(13)—Si(6)	170.0(4)
Si(2)—O(14)—Si(5)	151.0(4)
Si(3)—O(15)—Si(3)	162.0(5)*
Si(3)—O(16)—Si(6)	162.3(3)
Si(3)—O(17)—Si(7)	133.7(3)
Si(4)—O(18)—Si(4)	140.0(5)*
Si(4)—O(19)—Si(5)	156.6(3)
Si(4)—O(20)—Si(7)	135.5(3)
Si(5)—O(21)—Si(7)	136.6(3)
Si(5)—O(22)—Si(5)	135.0(5)*
Si(6)—O(23)—Si(6)	157.0(5)*
Si(6)—O(24)—Si(7)	126.3(3)
mean	155.4

*   Distances and angles associated with an oxygen atom in a special position.

Table 5.5   Minimum energies (kJ) of **I** and **IV** in the pores of polymorph A and B of SSZ-33.

Molecule	Polymorph A		Polymorph B	
	12-ring pores	10-ring pores	12-ring pores	10-ring pores
I	-104	-38	-104	-41
IV	-104	-66	-104	-72

Chapter Six

Characterization of As-Synthesized High-Silica Zeolites by Energy Minimization Calculations and Variable Temperature ^{1}H MAS NMR Spectroscopy

Characterization of As-Synthesized High-Silica Zeolites by Energy Minimization Calculations and Variable Temperature ^{1}H MAS NMR Spectroscopy

Raul F. Lobo

Chemical Engineering, California Institute of Technology

Pasadena, CA 91125

Abstract

The one-dimensional pure-silica zeolites SSZ-24 and ZSM-12 are used as probes to understand the selectivity observed for the nucleation of one zeolite framework over another. Energy minimization calculations of five structure-directing agents inside the pores of zeolites SSZ-24 and ZSM-12 suggest that repulsive steric interactions between the molecules and the pores of the framework of ZSM-12 and favorable dispersive interactions of the molecules with the SSZ-24 framework are responsible for the selectivity observed for the nucleation of the SSZ-24 framework for these organic molecules. The simulations also reveal that the coulombic interaction is an essential part of the energetic interaction of the zeolite frameworks and the organocation molecules. Variable temperature ^{1}H MAS NMR experiments indicate that, for pure-silica zeolites, there is a deprotonated silanol group that acts as charge balancing counter ion for the positive charge of the structure-directing agent. Additionally, there are protonated silanol groups and several water molecules inside the zeolite pores. Water molecules have a higher degree of motion than the structure-directing agents and silanol groups in the zeolite structure. It is clear that to carry out molecular dynamic and energy minimization calculations of zeolite frameworks

and structure-directing agents with physical and chemical relevance, all these interactions need to be considered simultaneously.

6.1   Introduction

Structure-direction can be defined as a process in which geometrical information about the size and shape of structure-directing agent is transferred to the topology of the silicate framework.   Implicit in this process, there is an energetic interaction that drives the formation of microporous crystalline materials.   In this chapter, this energetic interaction will be investigated using a combination of molecular energy minimization techniques and solid-state NMR spectroscopy.

First, energy minimizations of different structure-directing agents inside zeolite pores are carried out to attempt to understand the selectivity observed for the nucleation of one zeolite framework over another.   The simulations are carried out with the zeolites ZSM-12 (MTW)[1] and SSZ-24 (AFI).[2] Zeolites ZSM-12 and SSZ-24 are two high-silica zeolites with a one-dimensional large pore system.   Both zeolites can be synthesized in the "pure" silica form, i.e., no other tetrahedral (T) elements besides Si are purposely added to the synthesis gel.   Additionally, both ZSM-12 and SSZ-24 can be synthesized using the same experimental conditions—gel composition, reactant sources, temperature and pressure— except for the use of different structure-directing agents.

Table 6.1[3] shows a summary of the structure-directing agents that have been used to synthesize ZSM-12 and SSZ-24.   Comparison of the diameter of the structure-directing agents for ZSM-12 and SSZ-24 syntheses reveals that the length of the shortest dimension of each molecule is smaller for the structure-directing agents used in ZSM-12 syntheses than in SSZ-24 syntheses.   The projection of the framework topology of ZSM-12 and

SSZ-24 (Fig. 6.1) indicates that the diameter of the pore opening of ZSM-12 (6.2 Å x 5.5 Å) is smaller than the opening of SSZ-24 (7.3 Å).[4] Thus, it can be argued that the selectivity of molecules VI–X in Table 6.1 towards the formation of SSZ-24 is a consequence of favorable short-range interactions for the structure-directing agents in the bigger pores of SSZ-24 and, at the same time, of unfavorable steric interactions of the structure-directing agents with the oxygen atoms that surround the pores of the ZSM-12 framework.

This energetic interaction can be studied using empirical molecular dynamics and energy minimization calculations. In this chapter the energy minimizations of structure-directing agents II and VI–IX inside the pores of ZSM-12 and SSZ-24 are carried out. Because of our limited understanding of the coulombic interactions between the structure-directing agent and the zeolite framework, the minimization calculations are carried out only on the basis of van der Waals interactions. The results suggest that indeed that larger size of molecules VI–IX compared to II is the responsible agent for the nucleation of the SSZ-24 framework instead of the ZSM-12 framework. However, the calculations also indicate that to achieve a complete understanding of the structure-directing effect in this pure-silica material, it is necessary to include the long-range coulombic interactions and the presence of defects.

In addition to the energy minimization calculations, ^{1}H magic angle spinning (MAS) NMR spectroscopy is used to characterize the defects and the coulombic forces that act between the structure-directing agents and the zeolite framework. ^{1}H NMR spectroscopy in solids has found a relatively small number of applications because of the peak broadening created by the large dipolar interaction between hydrogen nuclei.[5] In some cases, this broadening can be of the order of hundreds of kHz. The dipolar interaction scales as r^{-6} and therefore is very sensitive to changes in intermolecular

distances. Thus, fortunately in zeolites, the intermolecular dipolar interaction is greatly reduced because the organic molecules are partially isolated from each other by the zeolite framework. However, the intramolecular dipolar interactions are still present and create peak broadening of about ~30 kHz. The MAS technique[5] average some of the dipolar interactions and reduces even more the peak broadening, but because the peak broadening of the spectrum is larger than the spinning rate (4-8 kHz in our case), the ^{1}H MAS NMR spectra of the samples present spinning side bands that complicate the analysis of the NMR results. Despite this limitation, useful chemical information can be obtained from the ^{1}H spectra of structure-directing agents.

Variable temperature MAS NMR spectra of the structure-directing agents has been carried out so that, in addition to the chemical information that can be obtained from the MAS NMR spectra, qualitative information about the molecular motion of the organic molecules inside the zeolite pores can also be obtained.

6.2   Methods

6.2.1 Energy Minimizations

The energy minimization were carried out using the program Discover 2.9 and Catalysis 3.0 from Biosym Technologies Inc. The minimizations were carried out excluding the coulombic portion of the total energy of interaction between the atoms. The energy of the empty zeolite framework (E_1) and the energy of the organic molecule (E_2) were first optimized in free space. Independently, the position and geometry of the organic molecule inside the zeolite framework was optimized (E_3) and the energy of interaction between the framework and the organic structure-directing agent was calculated as

$$\Delta E = E_3 - (E_2 + E_1)$$

ΔE gives the energy gain (or loss) obtained from the process of transferring the organic molecules for outside the crystal to its interior. For each molecule (II, VI–IX) the minimization was carried out inside the pores of ZSM-12 (MTW) and SSZ-24 (AFI).

$$\Delta\Delta E = \Delta E_{AFI} - \Delta E_{MTW}$$

is then the difference of the stabilization energy of the structure-directing agent in the pores of MTW and AFI. A negative energy indicates that the interaction is more favorable with the AFI framework than with the ZSM-12 framework.

The minimization calculations were carried out *i*) allowing the unit cell lattice parameters to increase or decrease and *ii*) with the unit cell (u.c.) lattice parameters fixed at the values reported from the structure of the calcined zeolite.[1,2] These two alternatives were considered because small differences in unit cell size and space group symmetry have been observed between the structure of the as-synthesized and calcined materials.[6-8]

As a basis for the energy minimization, the u.c. of SSZ-24[2] along the c axis was doubled (to about 16 Å) to be able to accommodate the structure-directing agents inside the pore without large interaction between two adjacent organic molecules. The u.c. of ZSM-12 (C-centered)[1] contains 4 channels per cell. To form the u.c. basis for the energy minimization, first the u.c. of ZSM-12 was changed to a primitive setting (P-1) to reduce the number of pores to 2 per u.c; and second, 3 u.c. along b (~15.5 Å total) were added together and taken as the basis u.c. for the energy minimization. The energy minimizations of the organic molecule inside the pores of ZSM-12 were carried out using two structure-directing agents per basis u.c.—i.e., one in each pore. The energies reported for this case are the energy of interaction of two organic molecules with the framework instead of one.

It is important to recognize that implicit in the minimization, there is a spatial correlation of the structure-directing agents between adjacent zeolite pores. There is no

experimental evidence for this kind of translational correlation in the as-synthesized zeolites. However, there are no apparent reasons that indicate that this correlation should produce important error for the energy of interaction between the zeolite framework and the structure-directing agent.

6.2.2 Solid-State NMR Spectroscopy

Solid-state NMR spectra were obtained on a Bruker AM 300 spectrometer equipped with a Bruker solid-state cross-polarization, magic angle spinning (CP/MAS) accessory. All samples were packed into ZrO_2 rotors. The ^{1}H MAS NMR spectra (300 MHz) were recorded with a spinning rate of 4-8 kHz. For each sample 16 scans were recorded. The spectra were referenced to a tetrakis-(trimethylsilyl)silane standard (TMS). The variable temperature ^{1}H MAS NMR spectra were taken at 295 K, 310 K, 330 K, 350 K and 370 K. The samples were slowly heated at about 5 K min^{-1} and were kept at the final temperature for at least 15 min before the spectra were recorded.

The as-synthesized zeolite sample of ZSM-12 was prepared according to Goepper et al.[9] using bis(dimethylpiperidinium)trimethylene hydroxide (II). A sample prepared by Annen and coworkers[2] of pure-silica SSZ-24 with trimethyl-1-adamantylammonium hydroxide (VI) —denoted as Ada-SSZ-24— and a sample of pure-silica SSZ-24 synthesized with N(16) methylsparteinium hydroxide[6] (IX)—denoted Spa-SSZ-24— were used to obtain the ^{1}H MAS NMR spectra of the SSZ-24 samples. The sample of ZSM-5 was prepared in the pure-silica form using tetrapropylammonium hydroxide as the structure-directing agent. The samples of the borosilicates CIT-1 and SSZ-33 were prepared as in Chapter 5 using molecules XI and XIII as the structure-directing agents, respectively. The sample of the aluminosilicate SSZ-26 was provided by S.I. Zones. This SSZ-26 sample was prepared using the diquaternary ammonium molecule XII.

$N^+(CH_3)_3$

XI

$-N^+(CH_3)_3$

$N^+(CH_3)_3$

XII

$N^+(CH_3)_3$
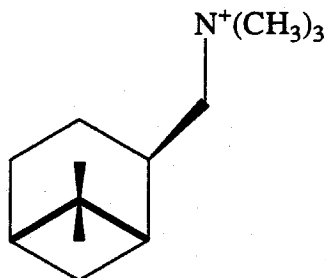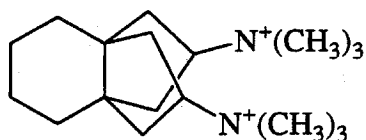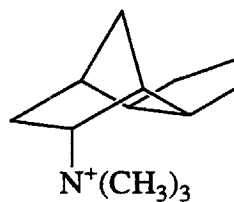
XIII

6.3 Results and Discussion

6.3.1 Energy Minimizations

The results from the energy minimization calculations are presented in Table 6.2 for fixed u.c. parameters and in Table 6.3 for the energy minimizations carried out with variable u.c. parameters. The results from the energy minimizations with fixed u.c. parameters give interaction energies (ΔE) in agreement with the expected values. That is, ΔE_{AFI} for molecules VI-IX is more negative than the corresponding ΔE_{MTW}; but ΔE_{AFI} for II is less negative than ΔE_{MTW}. From the values of the $\Delta\Delta E$, it is clear that the structure-directing agent that promotes the crystallization of the AFI zeolite have a lower (in some cases repulsive) energy of interaction with the ZSM-12 framework. Note however, that the

total minimum energy for the organic molecules and the framework are all large positive values. This is a consequence of the exclusion of the coulombic interaction between the atoms when carrying out the energy calculations. The result from these calculations have to be valued carefully because the constrain on the u.c. lattice parameters is not in agreement with the changes observed experimentally in zeolite frameworks between the as-synthesized and the calcined form (between 2-3% difference in the u.c. volume).[6,8] Small changes in u.c. lattice parameters may have significative effect on the values from the energy calculations.

The effects of the exclusion of the coulombic interaction in the calculations is clearly observed for the energy minimizations carried out with variable u.c. parameters (Table 6.3). The total energy of the empty frameworks is reduced at the expense of an increase of the u.c. parameters and an increase in the u.c. volume of 11-12%. The increase of the u.c. parameters also increases the size of the zeolite pores, and this change has a large effect on the energy of interaction of the structure-directing agent and the framework. In this case, the ΔE_{AFI} is less negative than the ΔE_{MTW}. This change in u.c. size is unrealistically large, and therefore, the values from the energy minimization calculations do not have a real physical meaning. These calculations do show that to perform realistic simulations of the as-synthesized zeolite, coulombic forces need to be carefully taken into account.

From the results of the energy minimization calculations, we can tentatively conclude that the selectivity of the structure-directing agents VI-IX towards the crystallization of SSZ-24 is due to unfavorable steric energetic interactions of the organic molecules with the small pore of the ZSM-12 structure, in addition to the favorable dispersive energetic interactions of the molecules with the SSZ-24 framework. However, the simulations also reveal that the coulombic interaction is an essential part of the energetic interaction of the zeolite frameworks and the organocation molecules.

Thus, how is the positive charge of the structure-directing agent balanced? In the synthesis gel the only kind of anions present are OH⁻, but these are very unstable species in isolation and would be expected to be coordinated to several water molecules in the zeolite pores. ^{29}Si MAS NMR spectra of as-synthesized clathrasils and zeolites (see Chapter 1) indicates that there are silanol species present in the framework. Deprotonated silanol groups (Si—O⁻) may be the species that are balancing the positive charge in the zeolite framework. As with the OH⁻, deprotonated silanol groups are unstable in isolation and would be expected to be coordinated to several water molecules or to other protonated silanol groups. Further characterization of these defect sites is presented in the next section.

6.3.2 Characterization of Defect Sites in As-synthesized High-silica Zeolites by ^{1}H MAS NMR Spectroscopy

The ^{1}H MAS NMR spectrum of Ada-SSZ-24 (Fig. 6.2) shows 5 resonances at 2, 2.4, 3, 5-6 and 10 ppm. The resonance at 3.0 ppm is assigned to the hydrogen atoms of the methyl groups of the structure-directing agent and the two resonances at 2.4 and 2 ppm are assigned to the hydrogen atoms from the adamantyl group. The resonances at ~10 and ~5 ppm are also present in the Spa-SSZ-24 (Fig 6.3), BIP-ZSM-12 (Fig. 6.4) and TPA-ZSM-5 (Fig. 6.5). In contrast, the samples synthesized with boron-containing gels (CIT-1 and SSZ-33, Figs. 6.6 and 6.7, respectively) as well as the samples synthesized with aluminum-containing gels (SSZ-26, in Fig. 6.8) do not show the resonance at ~10 ppm. This is a strong indication that this resonance is from the (protonated) silanol groups in the as-synthesized zeolites of pure-silica materials.

The resonance at ~5-6 ppm, present in all the samples, is probably from water molecules. This resonance is relatively broad and may indicate that *i*) the water molecules are tightly bound by hydrogen bonding and/or coulombic interactions to the organic

structure-directing agents or the framework, or *ii*) that there are several spectroscopically different water molecules in the defect sites. The resonances at ~5 ppm in BIP-ZSM-12 (Fig. 6.4) and TPA-ZSM-5 (Fig. 6.5) are clearly asymmetrical, suggesting that there are different water environments in the zeolite pores.

The broadening of this ~5 ppm resonance in Figures 6.3-6.5 can be compared to the sharp peak at 4.8 ppm in the spectrum of TPA-ZMS-5 (Fig. 6.5). This resonance is assigned to the protons of weakly bonded water molecules in the ZSM-5 pores. In Figure 6.5 it can also be observed that at 370 K, the chemical shift of this resonance moves to 4.2 ppm, in contrast to the chemical shift of the other resonances which is almost not affected by the change in temperature. This change in the chemical shift of this resonance is in agreement with its assignment to the protons of weakly bonded water molecules in the zeolite pores. Unfortunatelly, it is not possible to determine the number of water molecules and silanol groups per structure-directing agent because of the presence of spinning side bands.

6.3.2 Characterization of the Motion of Structure-directing Agents in As-Synthesized High-silica Zeolites by ^{1}H MAS NMR Spectroscopy

The dipolar broadening of each hydrogen atoms in the ^{1}H MAS NMR spectrum depends on their motional properties. The most mobile hydrogens will have a lower dipolar broadening than the rigid ones, and this difference will be manifested in the relative contributions of each hydrogen atom to the sideband resonances. More rigid atoms will have a greater contribution to the intensity of the spinning sidebands. Therefore, from the position of the spinning sidebands, it is concluded that the most rigidly held hydrogen atoms are the ones attached to the polycyclic groups of the structure-directing agents. In Figure 6.2, a spinning sideband has been plotted shifted from its original position

according to the spinning rate (5.1 kHz, i.e. 17 ppm). This sideband is centered at ~2 ppm indicating that the sideband results from contributions from partially averaged resonances from the hydrogen atoms attached to the adamantyl group of the structure-directing agent. The spinning sideband associated with the silanol (Si—OH) groups can only be clearly observed in Figures 6.3 and 6.5, in part due to the relatively small number of silanol groups in the samples. The presence spinning sidebands from the silanol groups indicate that, also, the silanol groups are relatively rigidly attached to the zeolite framework.

In contrast to the resonances from hydrogens from the structure-directing agents and from silanol groups, the resonance from H atoms of the water molecules is not observed in the spinning sidebands. The spectrum of BIP-ZSM-12 is remarkable in regards to this characteristic with a stronger 5 ppm signal than the one at 3 ppm (due to the H atoms attached to the N-methyl groups). From the position of the spinning sidebands, it can be concluded that there is only a small contribution from the protons of water molecules to the spinning sidebands. The H atoms of water molecules are therefore more mobile than the H atoms of the silanol groups and of the structure-directing agents.

Further insight on the motion of the structure-directing agents can be obtained from comparison of ^{1}H MAS NMR spectra at different temperatures for the same sample. For Ada-SSZ-24 in Figure 6.2, it can be observed that at 370 K, the resonance at 3 ppm is stronger than at 295 K. The motion of the methyl groups of the molecule increases faster from 295 to 370 K than the motion of the rest of the molecule. This difference is reflected in the shape of the spinning sidebands, which at 370 K show a shoulder in the left side of the band. Some of the magnetization present in the spinning sidebands has been transferred to the central resonance due to the faster motion of the methyl groups. The background in the Ada-SSZ-24 sample is also much smaller than the background of the other one-dimensional pore zeolites (Figs. 6.3, 6.4). This difference suggests that the

trimethyladamantyl-ammonium molecule is rotating along the zeolite pores faster than the methylsparteinium and the bipiperidinium molecules. This difference is also noted in the width of the spinning sidebands which is smaller in Figure 6.2 than in Figures 6.3 and 6.4.

The spectra of the methylsparteinium molecule inside the SSZ-24 pores (Fig. 6.3) are the ones most influenced by temperature. The relative intensity of the spinning sidebands is greatly reduced with temperature, and a resonance at ~15 ppm, clearly observed at 295 K, is not detected in the spectrum at 370 K. The reduction of the relative intensity of the spinning sidebands is likely to be due to the onset of rotation of the methylsparteinium cation inside the zeolite pores between 295-370 K. The assignment of the 15 ppm resonance is unclear. One possibility is that this resonance comes from silanol groups associated by hydrogen bonding to the tertiary amine of the methylsparteinium cations (N --- **HO**—Si). This is the only sample that shows this resonance, and it is the only sample that contains a tertiary amine in the structure-directing agent. Additionally, this assignment would also be in agreement with the reduction of the intensity of this resonance with higher temperature because the rotation of the organic molecule inside the zeolite pores would disrupt the N --- H interaction.

The resonances of the hydrogen atoms of the bipiperidinium cation (Fig. 6.4) also show an increase in their relative intensity with an increase in the temperature. This increase is not as marked as with the trimethyladamantammonium molecule and suggests that the motion of the structure-directing agent in ZSM-12 is not large enough as to rotate along the elongated 12-ring pores of the ZMS-12 zeolite.

In contrast to the one-dimensional pore zeolites, the effect of the temperature on the resonances of the hydrogen atoms of the structure-directing agents in the multidimensional pore zeolites is small. For TPA-ZSM-5 (Fig. 6.5), there is almost no change in the relative size of the spinning sidebands as in the width of the resonance of the tetrapropylammonium hydrogen atoms between the spectra of the 295 K and 370 K. This result is in agreement

with X-ray crystallographic studies of as-synthesized ZSM-5 that show that there is a very tight fit between the organic molecule and the geometry of the pore intersections in the MFI topology. Similar results can be inferred from the spectra of the trimethyl-myrtanylammonium cation in CIT-1 (Fig. 6.6), where almost no change is observed between the spectra at 295 and 370 K. It is interesting to note the presence of a shoulder at ~1 ppm (actually two resonances at 1 and 1.2 ppm) in these two spectra (Fig. 6.6). These resonances are assigned to the two methyl groups in C(6) of the myrtanyl group. These methyl groups are rapidly rotating along the C—C bond and this rotation greatly averages the dipolar interaction between the H atoms of the methyl groups. The bicyclo[3.1.1]heptanyl group, on the other hand, is not rotating and only the broad signal at ~3 ppm can be observed. Similar results can be observed for XII and XIII in the pores of SSZ-26 and SSZ-33 (Figs. 6.7 and 6.8). It is noteworthy that the intensity of the H atoms assigned to water molecules is higher in CIT-1 than in SSZ-33, as it was observed in the thermogravimetric experiments of Chapter 5.

The results from the ^{1}H MAS NMR experiments indicate that for pure-silica zeolites associated with each structure-directing cation, there is a deprotonated silanol group that act, as charge balancing counter ions in the material. Additionally, there are protonated silanol groups and several water molecules that show different degrees of hydrogen bonding with the silanol groups. It is expected that these groups will be mutually coordinated by hydrogen bonding. Further investigations are needed to elucidate the detailed structure of these defect sites, but it is clear that to carry out molecular dynamic and energy minimization calculations of the interaction between zeolite frameworks and structure-directing agents with physical relevance, all these interactions need to be considered simultaneously.

6.4   Conclusions

Energy minimization calculations of structure-directing agents inside the pores of zeolites SSZ-24 and ZSM-12 suggest that repulsive steric interactions between the molecules VI-IX and the pores of the framework of ZSM-12, and favorable dispersive interactions of the molecules with the SSZ-24 framework control the observed selectivity for the crystallization of SSZ-24 in the presence of these molecules. However, the simulations also reveal that the coulombic interaction is an essential part of the energetic interaction of the zeolite frameworks and the organocation molecules.

The ^{1}H MAS NMR experiments indicate that, for pure-silica zeolites, there is a deprotonated silanol group that acts as charge balancing counter ion for the positive charge of the structure-directing agent. Additionally, there are protonated silanol groups and several water molecules that show different degrees of hydrogen bonding with the silanol groups. It is expected that these groups will be mutually coordinated by hydrogen bonding. Water molecules have a higher degree of motion than the structure-directing agents and silanol groups in the zeolite structure. Further investigations are needed to elucidate the detailed structure of these defect sites.

It is clear that to carry out molecular dynamic and energy minimization calculations of zeolite frameworks and structure-directing agents with physical and chemical relevance, all these interactions need to be considered simultaneously. It is also shown that ^{1}H MAS NMR is a useful technique for the characterization of as-synthesized zeolites.

6.5 References

(1)   C.A. Fyfe, H. Gies, G.T. Kokotailo, B. Marler, D.E. Cox, *J. Phys. Chem.* **1990**, *94*, 3718-3721.

(2)   R. Bialek, W.M. Meier, M.E. Davis, M.J. Annen, *Zeolites* **1991**, *11*, 438-442.

(3)   R. Szostak, *Handbook of Molecular Sieves*; Van Nostrand-Reinhold: New York, 1992.

(4)   W.M. Meier and D.H. Olson *Atlas of Zeolite Structure Types;* 3rd ed.; Butterworth-Heinemann: Stoneham MA, 1992.

(5)   R.K. Harris, *Nuclear Magnetic Resonance Spectroscopy;* 2 ed.; Longman Scientific & Technical: Essex, 1986, pp 146-150.

(6)   Lobo, R. F. and Davis, M. E. *Microporous Mater.* **1994**, *in press.*

(7)   H. van Koningsveld, H. van Bekkum, J.C. Jansen, *Zeolites* **1987**, *7*, 564-568.

(8)   H. van Koningsveld, J.C. Jansen, H. van Bekkum, *Zeolites* **1990**, *10*, 235-242.

(9)   M. Goepper, H.X. Li, M.E. Davis, *J. Chem. Soc., Chem. Commun.* **1992**, 1665-1666.
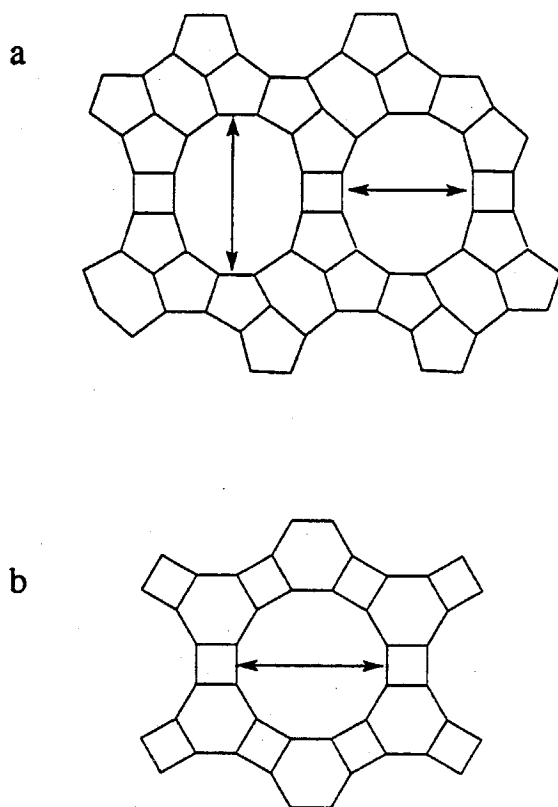
Figure 6.1   Projection along the pore direction of the structure topologies of ZSM-12 (top) and SSZ-24 (bottom).
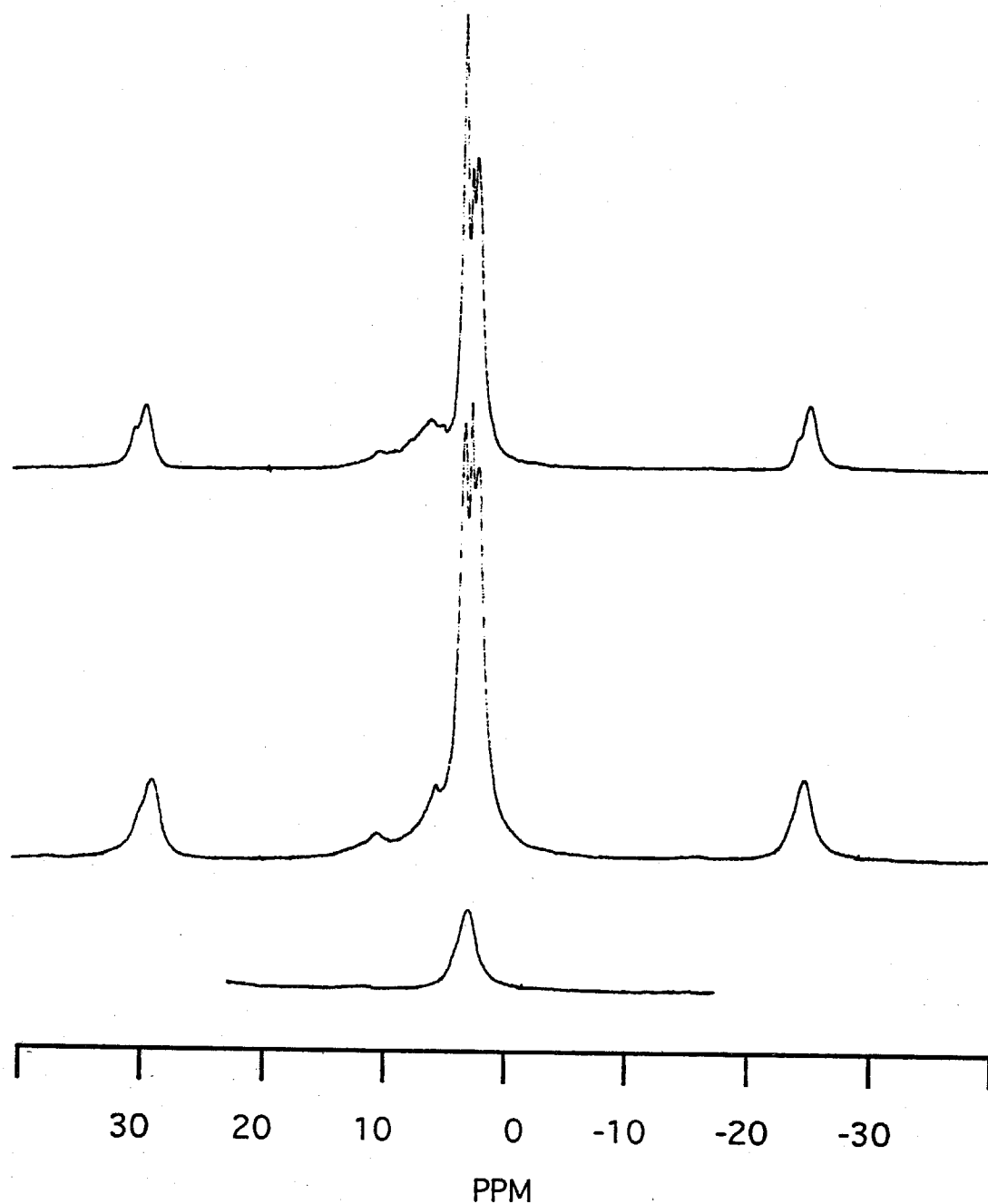
Figure 6.2 ^{1}H MAS NMR spectra of SSZ-24 synthesized using **VI** as structure-directing agent. The spectra were recorded at 295 K (middle), 370 K (top). A spinning sideband shifted by 5.1 kH is shown in the bottom profile.
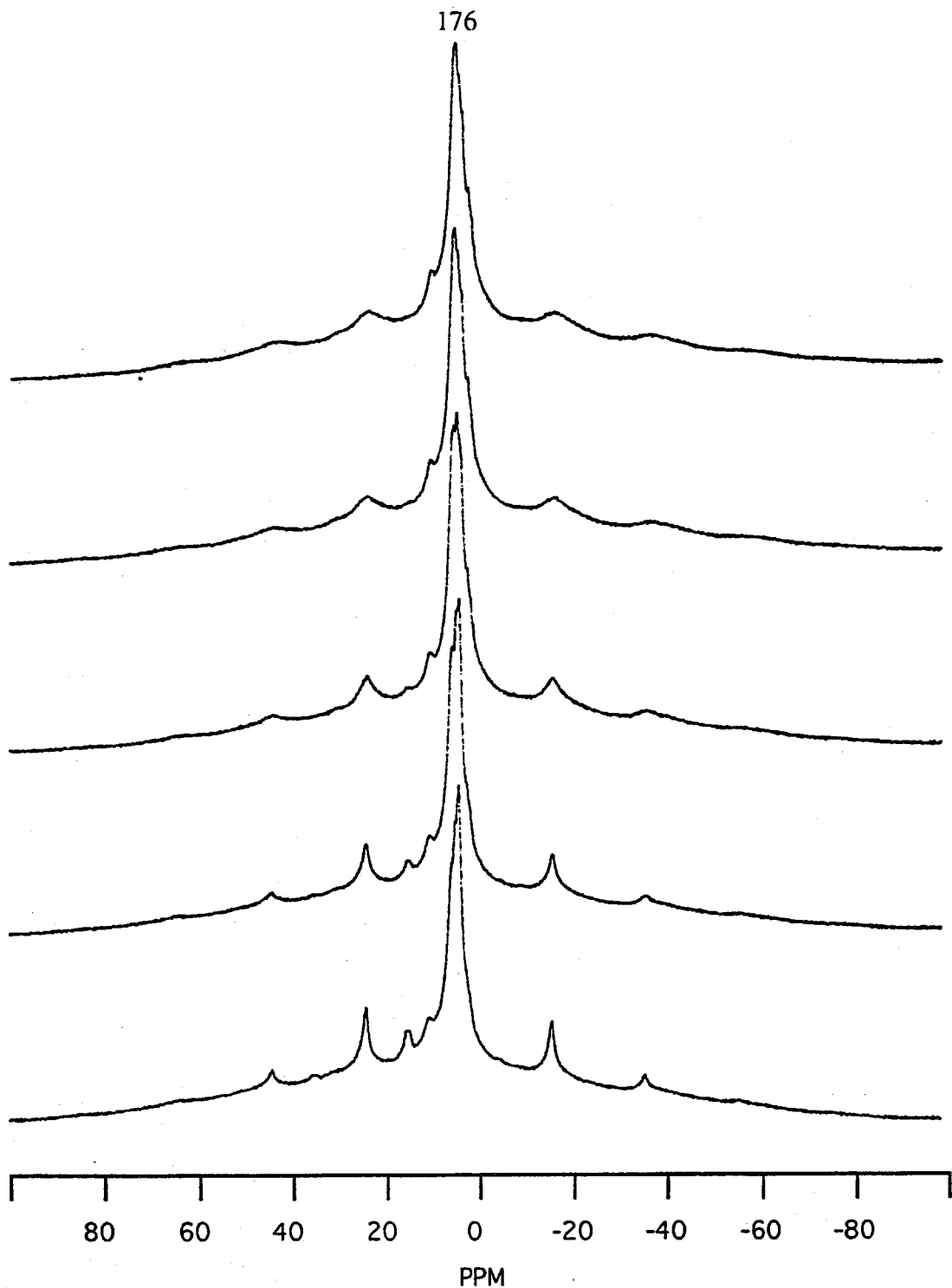
Figure 6.3   Variable temperature ^{1}H MAS NMR spectra of SSZ-24 synthesized using
IX as structure-directing agent (T=295 K (bottom), 310 K, 330 K, 350 K
and 370 K (top)).
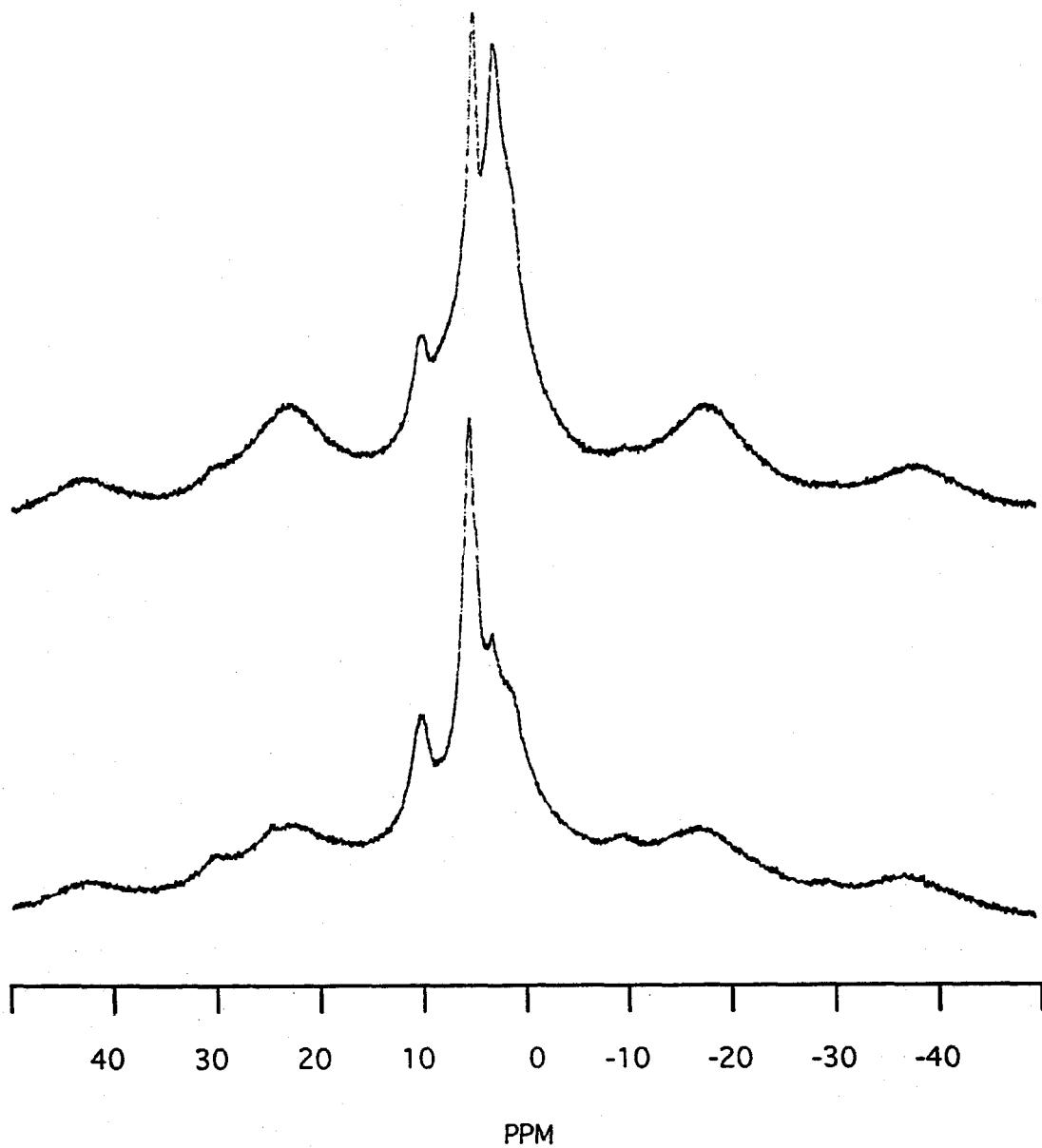
Figure 6.4 ^{1}H MAS NMR spectra of ZSM-12 synthesized using **II** as structure-directing agent (T= 295 K (bottom), 370 K (top)).
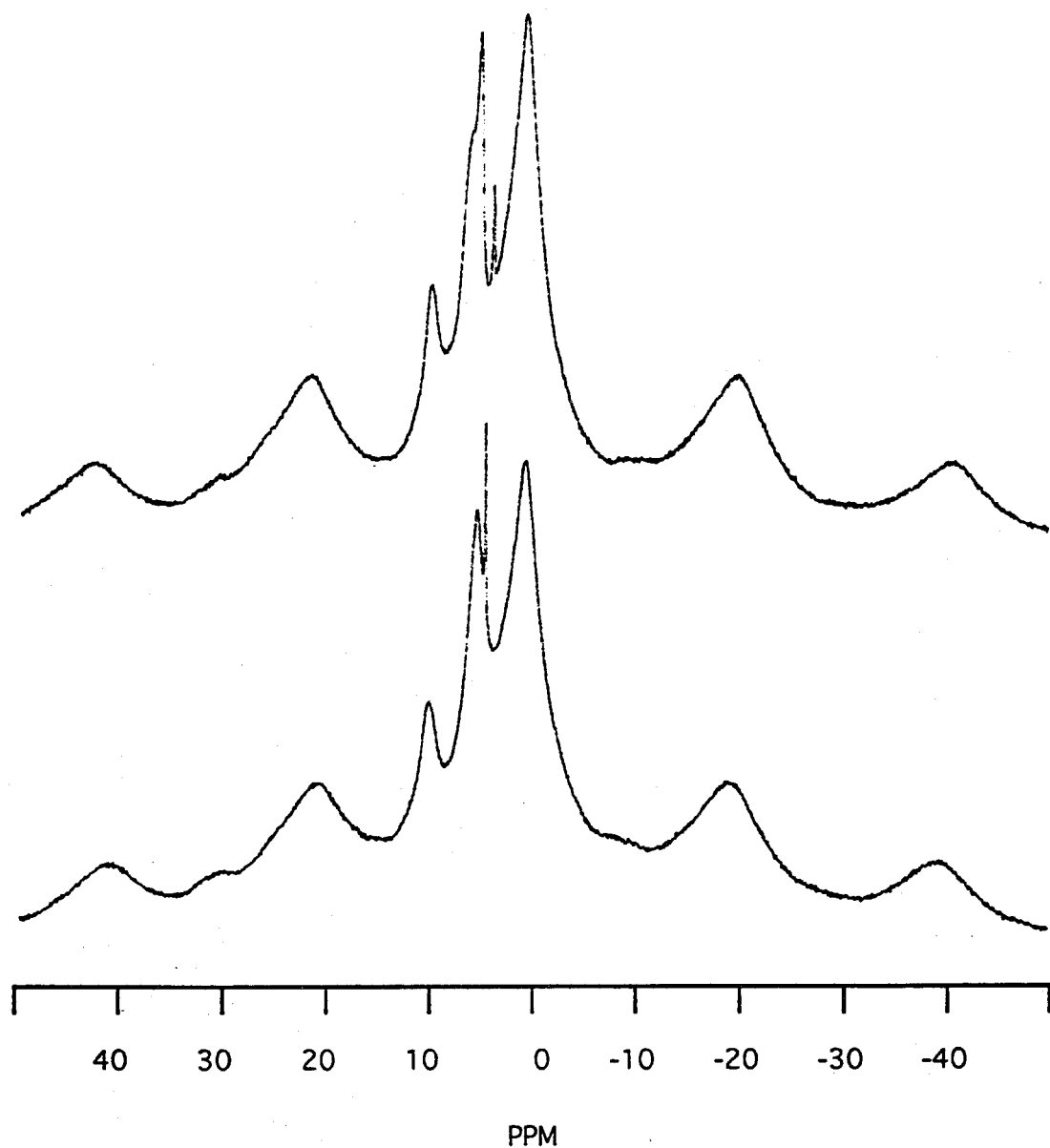
Figure 6.5 ^{1}H MAS NMR spectra of ZSM-5 synthesized using tetrapropylammonium hydroxide as structure-directing agent (T= 295 K (bottom), 370 K (top)).
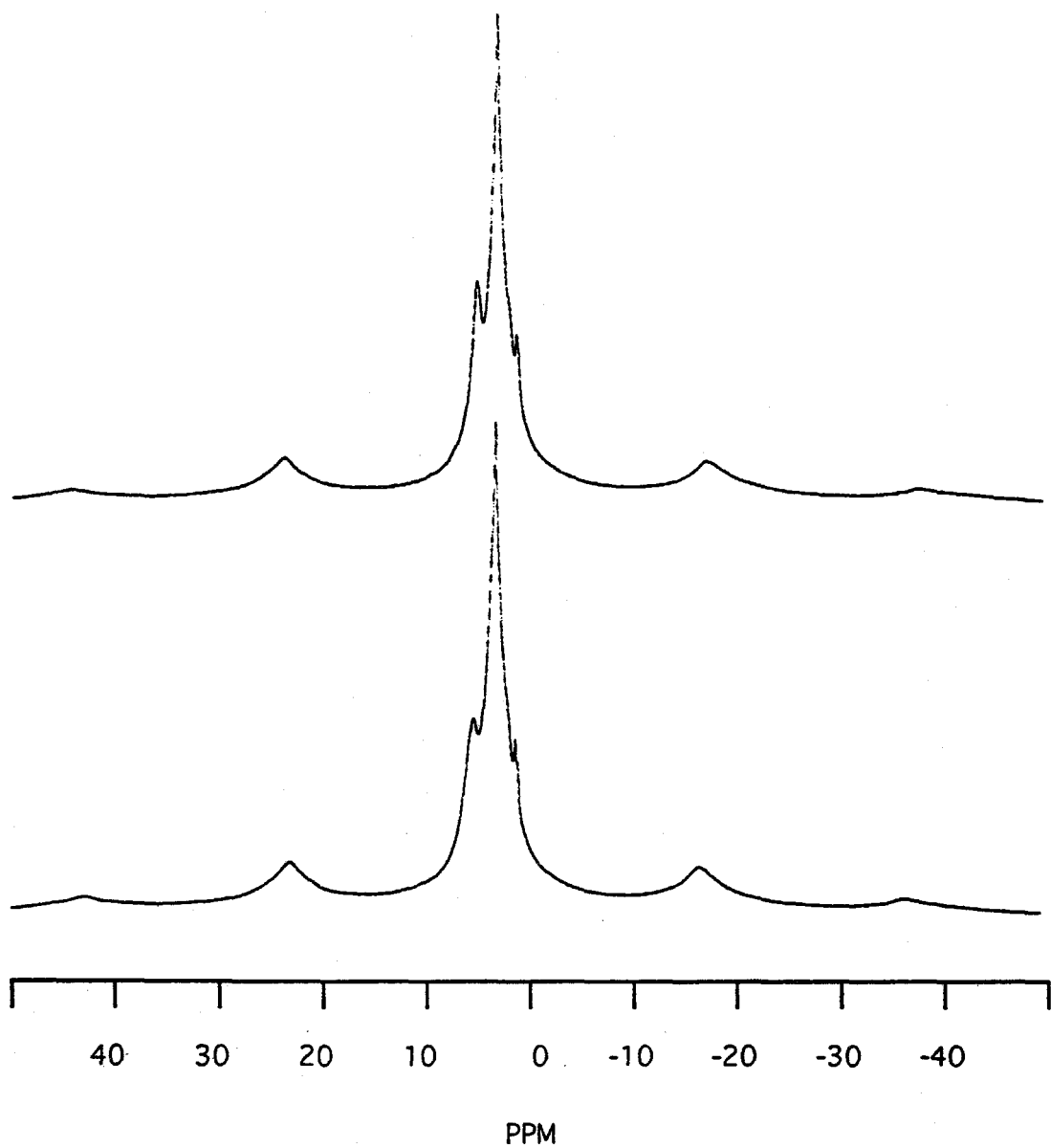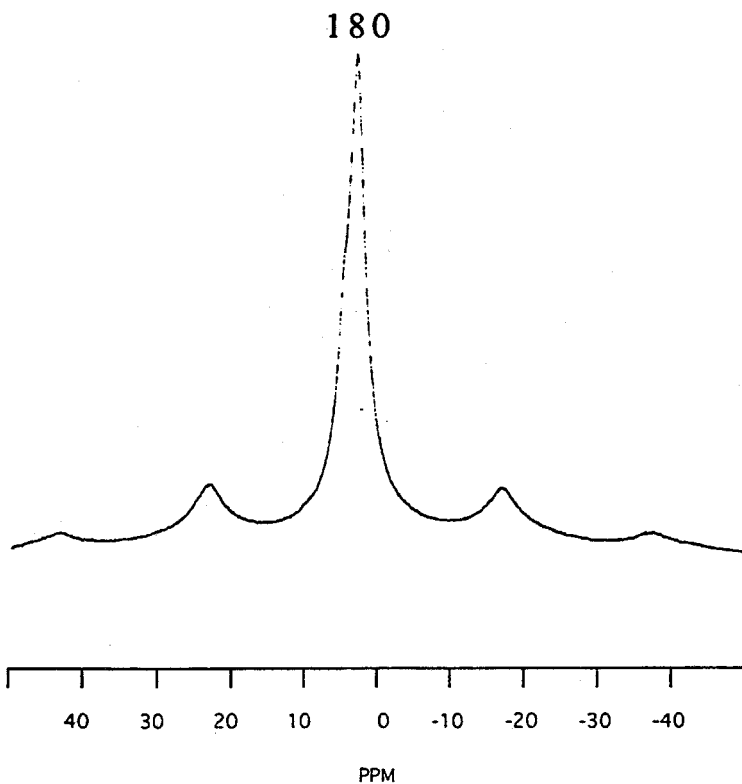
Figure 6.6 ^{1}H MAS NMR spectra of CIT-1 synthesized using **XI** as structure-directing agent (T= 295 K (bottom), 370 K (top)).

180

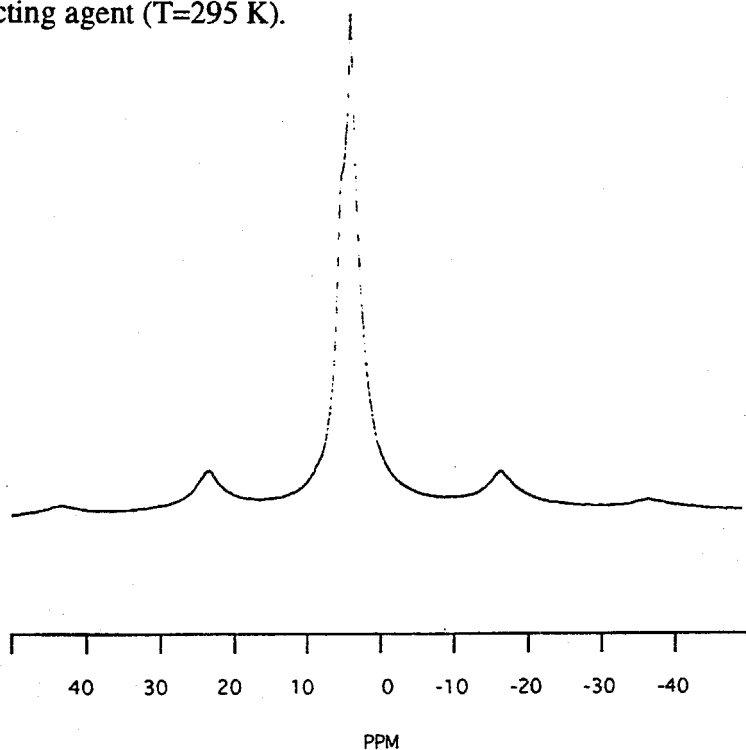Figure 6.7 ^{1}H MAS NMR spectrum of SSZ-26 synthesized using **XII** as structure-directing agent (T=295 K).
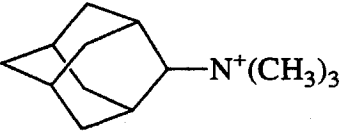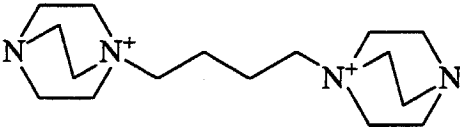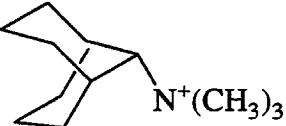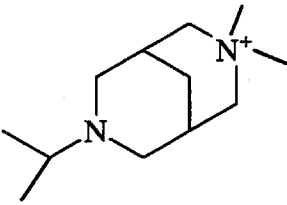
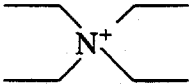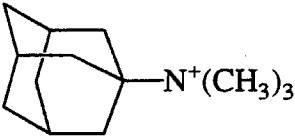Figure 6.8 ^{1}H MAS NMR spectrum of SSZ-33 synthesized using **XIII** as structure-directing agent (T= 295 K).

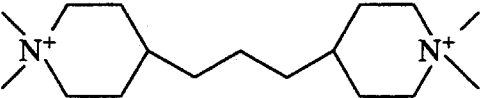**Table 6.1** Structure-directing agents used for the synthesis of ZSM-12 and SSZ-24.[3]

Structure-Directing Agents ZSM-12	Structure-Directing Agents SSZ-24
I	VI
II	VII
III	VIII
IV	IX
V	X

Table 6.2 Energy minimization of organic structure-directing agents in zeolites SSZ-24 (AFI) and ZSM-12 (MTW). Minimization calculations carried out with fixed unit cell parameters.

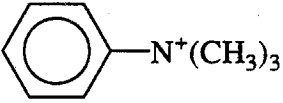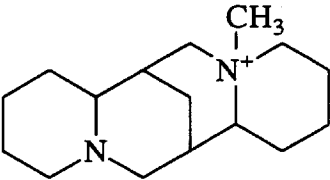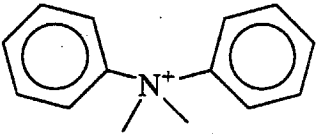| Energy	Organic Structure-Directing Agents				
(kJ)	**VI**	**VII**	**IX**	**VIII**	**II**
E_2	67.7	69.5	89.4	59.9	56.2
E_1 AFI	116.1	116.1	116.1	116.1	116.1
E_3 AFI	169.5	161.9	188.2	145.1	145.8
ΔE_{AFI}	-14.3	-23.7	-17.3	-32.9	-26.5
E_1 MTW	227.6	227.6	227.6	227.6	227.6
E_3 MTW	351.6	363	409.71	360.9	256.1
ΔE_{MTW}	-5.7	-1.8	1.65	6.7	-42.9
$\Delta\Delta E$	-8.6	-21.9	-18	-35.7	16.4

Table 6.3 Energy minimization of organic structure-directing agents in zeolites SSZ-24 (AFI) and ZSM-12 (MTW) with variable unit cell parameters.[a]

Energy (kJ)	Organic Structure-Directing Agents				
	VI	**VII**	**IX**	**VIII**	**II**
E_2	67.68	69.50	89.35	59.89	56.24
E_1 AFI	52.48	52.48	52.48	52.48	52.48
E_3 AFI	95.21	123.77	139.47	101.3	98.36
ΔE_{AFI}	-24.9	1.8	-2.4	-11.1	-10.4
E_1 MTW	47.22	47.22	47.22	47.22	47.22
E_3 MTW	114.16	123.25	160.58	106.27	49.47
ΔE_{MTW}	-34.2	-31.5	-33.0	-30.4	-55.1
$\Delta\Delta E$	9.7	29.3	30.6	19.3	44.7

a   The unit cell volume of the empty frameworks increased by ~12% for the AFI framework and by ~11% for the MTW framework when the u.c. lattice parameters were included in the optimization. The addition of the structure-directing agents did not change the u.c. volume from the already expanded value in any of the two zeolite frameworks.

Chapter Seven

Conclusions and Recommendations for Further Investigation

Conclusions and Recommendations for
Further Investigation

The overview of the synthesis of high-silica zeolites indicates that the concepts of structure-direction provide a basis for the understanding of many reported phenomena on these materials. In particular, for pure-silica molecular sieves and clathrasils, it has become more evident that the hydrophobic hydration of the structure-directing agent favors the interactions between the organic structure-directing agents and the soluble silicate species. It is through this interaction that the organic molecule influences the structure of the material that crystallizes in the reactor. Other factors, such as the motion of the organic structure-directing agent, the concentration of the mineralizing agent and the presence of relatively small amounts of trivalent (B, Al, Ga, etc.) and divalent cations (Zn) in the gel, also compete with the organic structure-directing agent for interactions with the silicate species and also affect the structure of the zeolite that is formed.

The synthesis of SSZ-24 using the chiral molecule N(16)methylsparteinium hydroxide provides an example of one of these effects. Although the organic structure-directing agent is chiral, the structure that is formed is not only not chiral but very symmetric. ^{1}H MAS NMR of the as-synthesized material indicates that the organic molecule is spinning inside the zeolite pores. The thermal motion of the molecule averages the geometry to what is effectively a cylinder. The rapid motion of the molecule then explains why a chiral molecule forms the SSZ-24 zeolites.

In addition, SSZ-24 prepared using N(16)methylsparteinium as structure-directing agent is the first example of the synthesis of the SSZ-24 zeolite where the isomorphous substitution of boron for silicon in the zeolite framework is accomplished using sodium

borate as the source of boron atoms. This result greatly simplifies the incorporation of aluminum into the zeolite framework compared to previous procedures. The aluminum treated form of SSZ-24 forms an active material for acid catalysis.

The geometrical relationship proposed by Zones and coworkers between the polycyclic diquaternary ammonium ion used in the synthesis of SSZ-26 and the geometry of the pore intersections of SSZ-26 is confirmed using energy minimization calculations. During this process, the structures of the zeolites SSZ-26 and SSZ-33 were solved. These zeolites are the first synthetic molecular sieves to contain an intersecting pore system formed by 10- and 12-ring pores. This novel pore system is likely to show a combination of catalytic activity, selectivity and stability not found in any other zeolite. The geometry of the organic molecule is the most important factor to obtain a pore system intermediate in the size of the zeolites ZSM-5 and beta. The frameworks of SSZ-26 and SSZ-33 are the first high-silica molecular sieves to contain the 4-4=1 secondary building unit. This unit has only been found in natural zeolites prior to the synthesis of SSZ-26, and suggest that other molecular sieves with this unit (like boggsite), can also be synthesized in the laboratory.

The concepts of structure-direction have been extended to show that the organic structure-directing agent can be used to control the stacking sequence of zeolites form by different staking of layers. This was accomplished by the synthesis of the new zeolite CIT-1, the ordered polymorph B of the disordered zeolites SSZ-26 and SSZ-33. A Rietveld refinement of the synchrotron X-ray powder diffraction data of CIT-1 confirms the proposed structure. It is also shown that the structures of SSZ-26 and SSZ-33 are closely related to the structure of zeolite beta. The fact that the stacking sequence of SSZ-26 and SSZ-33 can be controlled to give CIT-1, supports the idea that the stacking sequence of zeolite beta can also be controlled. One of the ordered polymorphs of zeolite beta, polymorph A, is chiral and its synthesis may give the first heterogeneous catalyst with the chiral catalytic activity. Comparison of the structures of CIT-1 and zeolite beta indicate that

larger structure-directing agents than the one used in the synthesis CIT-1 will be necessary to synthesize and ordered polymorph of zeolite beta. This quaternary ammonium ion may contain as many as 18 to 22 carbon atoms per molecule.

The investigation of as-synthesized high-silica molecular sieves reveals that in the as-made material, there are other species present inside the zeolite pores besides the structure-directing agent. This species are most likely deprotonated and protonated silanol groups, and water molecules. Energy minimization calculations of the organic structure-directing agent inside the zeolite pores also indicates that to understand the interaction of these organic molecules with the zeolite framework, all these different species. Despite the large amount of information available about the characterization of the calcined form of many zeolites, comparatively very little work has been carried out on the as-synthesized form of high-silica zeolites. To improve our understanding of the energetic interaction of organic structure-directing agents and zeolite frameworks, further work on the characterization of as-synthesized zeolites needs to be carried out.

One possibility is to complete the series of ^{1}H MAS NMR spectra carried out in Chapter Six to other silicate structures. The spectra of Nonasil, SSZ-31 and pure-silica zeolite beta would indicate if the conclusions obtained so far, can be extended to clathrasils and multidimensional 12-ring pore zeolites.

To investigate the dynamics of the silanol and water molecules in the zeolites pores, samples of pure-silica zeolites synthesized in D_2O can be analyzed using deuterium NMR spectroscopy. Variable temperature experiments would give information about the motion of these molecules at zeolite synthesis temperatures. Although more difficult, quantitative information about the motion of the organic structure-directing agent may be obtained from deuterium NMR investigation of selectively deuterated organic structure-directing agents.

Some information about the local structure of these defect sites could be obtained from ^{1}H-^{29}Si CP/MAS NMR of zeolite samples prepared with D_2O and deuterated

structure-directing agents. For example, comparison of the relative intensities of Q^3 and Q^4 resonances in samples prepared with trimethyladamantamonium and d^9-trimethyl-adamantamonium may indicate whether the bulky adamantyl group or the methyl groups are closer to the silanol species in the zeolite pores. This kind of information may be critical to understand how the organic and inorganic interact to define the topology of the zeolite that is formed and to design new organic molecules that would give novel molecular sieves and zeolites.